Functional Characterization Of Atxa, The Bacillus Anthracis Virulence Regulator

Troy G. Hammerstrom

FUNCTIONAL CHARACTERIZATION OF ATXA,

THE *BACILLUS ANTHRACIS* VIRULENCE REGULATOR

by

Troy G. Hammerstrom, B.S.

APPROVED:

_____
Supervisory Professor
Theresa M. Koehler, Ph.D.

_____
Edward P. Nikonowicz, Ph.D.

_____
William Margolin, Ph.D.

_____
Peter J. Christie, Ph.D.

_____
Richard G. Brennan, Ph.D.

APPROVED:

_____
Dean, The University of Texas
Health Science Center at Houston
Graduate School of Biomedical Sciences

FUNCTIONAL CHARACTERIZATION OF ATXA,

THE *BACILLUS ANTHRACIS* VIRULENCE REGULATOR

A

DISSERTATION

Presented to the Faculty of

The University of Texas

Health Science Center at Houston

and

The University of Texas

M. D. Anderson Cancer Center

Graduate School of Biomedical Sciences

In Partial Fulfillment

of the Requirements

for the Degree of

DOCTOR OF PHILOSOPHY

by

Troy G. Hammerstrom, B.S.

Houston, Texas

May, 2011

Acknowledgements

A scientific endeavor is like an incredible journey: there is a higher probability of success if you have skilled advisors, loyal companions, and an ever-present guide.

I would like to thank several skilled advisors who have been a valuable resource before and during my journey. First, I must thank my supervisor, Dr. Theresa Koehler who has been a great encourager of my scientific development. Not only has she adapted my ways of writing and presenting, she has been a clear role model as she demonstrates her passion for science and for teaching science at all levels. Her excitement is infectious. Dr. Ed Nikonowicz was a co-mentor for the majority of my work. He brought an outsider's view to many of my results that helped to expand the implications and reveal alternative explanations for my work. Additionally, I would like to thank Drs. William Margolin, Peter Christie, and Richard Brennan. These individuals were committee members throughout my education in the GSBS. They provided key analyses throughout my tenure and continue to push me to think more critically and more deeply to see the full extent of my work. Other faculty members within the Microbiology and Molecular Genetics Department were very supportive of my work and their encouragement was not overlooked.

Outside of my mentors, committee members, and MMG faculty, I have utilized the knowledge and skills of several researchers. Dr. Yousif Shamoo allowed access to equipment in his lab. Drs. William Dubinsky, Richard Cook, and David Engler assisted with analyses of various samples. Drs. Masaya Fujita, Jorg Stulke, and Kevin McIver provided insight about various experiments and proteins that I used within my work.

Many teachers throughout my education have contributed to my scientific knowledge and passion. In third grade, Joan Mendel would never accept anything but perfection and pushed me to work harder. My love for studying life began in ninth grade in Bob Hank's biology class. While studying at Texas A&M University, I learned microbiology from Dr.

Michael Manson, Dr. Rita Moyes, and Dr. Thomas Ficht. Each professor brought a unique perspective to studying bacteria and trained me well to succeed in my Ph.D. studies.

At times people that accompanied me on my journey were both skilled advisors and loyal companions. I have had outstanding colleagues in the Koehler and Nikonowicz labs. Dr. Jennifer Dale and I started graduate school at the same time, and I know that a vast majority of my experiments would not have been successful if I had not discussed a protocol, experimental setup, or result with Jennifer. She is a great thinker and a natural scientist who I will seek out for advice in the future. Dr. Jung Hyoeb Roh overcame two critical obstacles to make my work possible. He developed the protocol to visualize AtxA via Western blot analysis, and he provided the initial observations that AtxA formed a multimer. Maureen Ty, a skilled and inquisitive scientist, produced mutants used in this work and also made sure that I took the time to explain experiments and protocols thoroughly. Dr. Jason Rall constructed the vector used to make the *atxA* mutation, and Dr. Maria Hadjifrangiskou constructed the IPTG-inducible *atxA* plasmid. Dr. Kate Pflughoeft, Malik Raynor, Dr. Cana Ross, Kerrie Thomason, Dr. Michelle Swick, Dr. Lori Horton, Dr. Galia Zaide, and Dr. Jing Cao Pan have impacted me and this dissertation through discussions of our work and critical analysis of my data.

Many friends and family members have helped in my research not through their scientific knowledge but through their questions, encouragement, and love. I thank the Buis, Griffin, Carter, and Jordan families for being great friends and giving me a reason to relax from my experiments. The Abel, Lohmer, and Sherman families have cared about my success in science and often have asked me to explain my research. My parents, Doug and Lindy Hammerstrom, encouraged me from an early age to pursue my education and always continue to work hard and complete the tasks I am given. I learned how to be curious and to never give up learning from my grandparents, Francis and Clarice Speck. I am thankful for my family, especially my late grandmother, Betty Granger, who would always ask how my

work was going. My wife's family, including James and Lucille Davidson, Lorretta Davidson, and Orville Simmang, has been constant in their encouragement through weekend retreats away from the lab to eat amazing food and figure out how to beat the "hard levels" on a new game. James Davidson always believed in me and that I would be successful. I loved the times I got to talk to him and how he treated me like one of his own grandchildren. To my wife, Aimee Hammerstrom, my most loyal and beloved companion, I thank you for your constant love and support and for pushing me to work as hard and to be as smart as you.

Finally, I must acknowledge my ever-present guide. I truly believe that Jesus Christ, God the Father, and the Holy Spirit show me how to be a thoughtful and creative scientist. I look to Him constantly for direction and purpose, and He has never failed to provide for me.

Abstract

FUNCTIONAL CHARACTERIZATION OF ATXA,

THE *BACILLUS ANTHRACIS* VIRULENCE REGULATOR

Publication No._____

Troy G. Hammerstrom, B.S.

Supervisory Professor: Theresa M. Koehler, Ph.D.

Coordinated expression of virulence genes in *Bacillus anthracis* occurs via a multi-faceted signal transduction pathway that is dependent upon the AtxA protein. Intricate control of *atxA* gene transcription and AtxA protein function have become apparent from studies of AtxA-induced synthesis of the anthrax toxin proteins and the poly-D-glutamic acid capsule, two factors with important roles in *B. anthracis* pathogenesis. The amino-terminal region of the AtxA protein contains winged-helix (WH) and helix-turn-helix (HTH) motifs, structural features associated with DNA-binding. Using filter binding assays, I determined that AtxA interacted non-specifically at a low nanomolar affinity with a target promoter (P*lef*) and AtxA-independent promoters. AtxA also contains motifs associated with phosphoenolpyruvate: sugar phosphotransferase system (PTS) regulation. These P̲TS-regulated d̲omains, PRD1 and PRD2, are within the central amino acid sequence. Specific histidines in the PRDs serve as sites of phosphorylation (H199 and H379). Phosphorylation of H199 increases AtxA activity; whereas, H379 phosphorylation decreases AtxA function. For my dissertation, I hypothesized that AtxA binds target promoters to activate transcription and that DNA-binding activity is regulated via structural changes within the PRDs and a carboxy-terminal EIIB-like motif that are induced by phosphorylation and ligand binding. I determined that AtxA has one large protease-inaccessible domain containing the PRDs and the carboxy-terminal end of the protein. These results suggest that AtxA has a domain that is distinct from the putative DNA-binding region of the protein.

My data indicate that AtxA activity is associated with AtxA multimerization. Oligomeric AtxA was detected when co-affinity purification, non-denaturing gel electrophoresis, and bis(maleimido)hexane (BMH) cross-linking techniques were employed. I exploited the specificity of BMH for cysteine residues to show that AtxA was cross-linked at C402, implicating the carboxy-terminal EIIB-like region in protein-protein interactions. In addition, higher amounts of the cross-linked dimeric form of AtxA were observed when cells were cultured in conditions that promote toxin gene expression. Based on the results, I propose that AtxA multimerization requires the EIIB-like motif and multimerization of AtxA positively impacts function.

I investigated the role of the PTS in the function of AtxA and the impact of phosphomimetic residues on AtxA multimerization. *B. anthracis* Enzyme I (EI) and HPr did not facilitate phosphorylation of AtxA *in vitro*. Moreover, markerless deletion of *ptsHI* in *B. anthracis* did not perturb AtxA function. Taken together, these results suggest that proteins other than the PTS phosphorylate AtxA. Point mutations mimicking phosphohistidine (H→D) and non-phosphorylated histidine (H→A) were tested for an impact on AtxA activity and multimerization. AtxA H199D, AtxA H199A, and AtxA H379A displayed multimerization phenotypes similar to that of the native protein, whereas AtxA H379D was not susceptible to BMH cross-linking or co-affinity purification with AtxA-His. These data suggest that phosphorylation of H379 may decrease AtxA activity by preventing AtxA multimerization.

Overall, my data support the following model of AtxA function. AtxA binds to target gene promoters in an oligomeric state. AtxA activity is increased in response to the host-related signal bicarbonate/CO_2 because this signal enhances AtxA multimerization. In contrast, AtxA activity is decreased by phosphorylation at H379 because multimerization is inhibited. Future studies will address the interplay between bicarbonate/CO_2 signaling and phosphorylation on AtxA function.

Table of Contents

List of Figures

List of Tables

Abbreviations

Alo	Anthrolysin O
BCAA	Branched-chain amino acids
BHI	Brain Heart Infusion medium
BMH	Bis(maleimido)hexane cross-linking agent
BN-PAGE	Blue native polyacrylamide gel electrophoresis
bp	Basepair
BSA	Bovine serum albumin
CA	Casamino acids medium
$CACO_3$	Casamino acids medium supplemented with 0.8% sodium bicarbonate
CCA	Carbon Catabolite Activation
CCR	Carbon Catabolite Repression
CMD-1	Conserved Mga Domain-1
Co-AP	Co-Affinity Purification
cre	Catabolite response elements
DTT	Dithiothreitol
EF	Edema Factor
EI	Enzyme I
EI-His	Amino-terminal hexa-histidine tagged Enzyme I
EIIA-D	Enzyme II subunit A, B, C, and/or D
EMSA	Electrophoretic mobility shift assays
FBP	Fructose-1,6-bisphosphate
GAS	Group A *Streptococcus*
HPr	Histidine protein of the PTS
HPr-His	Amino-terminal hexa-histidine tagged HPr

HTH	Helix-turn-helix
IPTG	Isopropyl β-D-1-thiogalactopyranoside
kb	Kilo-basepairs (10^3 basepairs)
LB	Luria-Bertani medium
LF	Lethal Factor
Mb	Mega-basepairs (10^6 basepairs)
OD_{600}	Optical Density at 600 nm
P~His-HPr	HPr phosphorylated at His15 by EI
P-Ser-HPr	HPr phosphorylated at Ser46 by HprK/P
PA	Protective Antigen
PCR-SOEing	Splicing by overlap extension PCR
PDGA	Poly-γ-D-glutamic acid
PEP	Phosphoenolpyruvate
PEPCK	PEP carboxy kinase
P*hs*	*hyper-spank* promoter
Phyre	Protein homology/anology recognition engine
PRD	Phosphoenolpyruvate:sugar phosphotransferase system regulation domain
PTS	Phosphoenolpyruvate:sugar phosphotransferase system
rbs	Ribosome binding site
SDS	sodium dodecyl sulfate
SDS-PAGE	SDS polyacrylamide gel electrophoresis
TCS	Two component systems
WH	Winged Helix-turn-helix
X-gal	5-bromo-4-chloro-indolyl-β-D-galactopyranoside

Chapter I

<u>Introduction</u>

1.1 Gene regulation in response to environmental signals

The ability to respond to niche-specific stimuli is key to thriving in changing environments and a defining characteristic of life. Organisms within all domains of life have various methods to react to niche-specific signals, and a common response is to control gene expression. *Cis-* and *trans*-acting factors can promote or impede transcription of genes encoding proteins that produce a proper response. In bacteria, the process of signal transduction occurs most often via classical two-component systems (TCS) containing a histidine kinase and a response regulator (reviewed in (1). Histidine kinases contain motifs which sense a change in the environment and then transmit the signal to the kinase domain to induce autophosphorylation. The phosphorylated kinase domain promotes phosphorylation of the response regulator which then interacts with promoter elements of specific genes. There are several variations on the theme of TCS. Some systems have multiple inputs. Some use more than two proteins to shuttle phosphate from the sensing protein to the regulator. Sometimes a single protein senses a signal and alters gene expression. The numerous mechanisms used to respond to the environment indicate that understanding the proteins involved in signal transduction is crucial to understanding life.

B. anthracis, the etiological agent of anthrax disease, has two distinct lifestyles that require drastically different gene expression profiles. As a pathogen in mammalian tissue and as a saprophyte associated with rhizospheres, signal transduction is crucial for the bacterium to adapt and thrive in each niche. The work I present in this dissertation focuses on the protein AtxA, which is the linchpin in the transition from a soil-dwelling bacterium to a mammalian pathogen.

1.2 *Bacillus anthracis* and Anthrax Disease

B. anthracis is a non-motile, Gram-positive bacterium and contains a 5.23 Mb chromosome and two large plasmids, pXO1 (182 kb) and pXO2 (96 kb) (2–4). The plasmids

harbor genes necessary for virulence. The structural genes for the anthrax toxins, *pagA* (Protective Antigen, PA), *cya* (Edema Factor, EF), and *lef* (Lethal Factor, LF), are located noncontiguously on pXO1 (Fig. 1-1, (5–7). The capsule biosynthetic operon (*capBCADE)* is located on pXO2 (8).

For many years, it was thought that the plasmids were unique to *B. anthracis*; however, several strains within the *Bacillus cereus* group have been isolated with pXO1- or pXO2-like plasmids (9, 10). In addition to *B. anthracis*, the *B. cereus* group includes *Bacillus thuringiensis*, an insect pathogen, and *B. cereus*, an opportunistic pathogen which can also cause food poisoning. All three of these species normally reside in the soil.

Replication in soil is an under-studied area of the *B. anthracis* infection cycle. Saile and Koehler (11) were the first to show germination of spores in the rhizosphere. Cells were metabolically active as demonstrated by the transfer of genetic material from one strain of *B. anthracis* to another. More recently, two studies provided evidence that *B. anthracis* may reside within earthworm intestines and that bacteriophages play a significant role in genotypic and phenotypic alteration (12, 13).

The first step in the infection process occurs when spores from the environment enter the host. The spores are engulfed primarily by macrophages, although other cell types have been implicated in this process as well (14, 15). Spores are transported to regional lymph nodes where they germinate and produce several different virulence factors. After release, *B. anthracis* spreads rapidly until the victim perishes due to bacteremia (16). Upon death of the host, the bacilli develop into dormant spores and re-enter the local ecosystem. *B. anthracis* spores are highly resistant for long periods, greater than 200 years (17), to environmental insults such as heat, desiccation, and UV light.

The route spores of *B. anthracis* enter the host dictates the symptoms and outcomes of the infected mammal or human. Cutaneous anthrax manifests when spores invade the host through a cut or wound in the skin. A large wound called a black eschar develops at the

site of infection (18, 19).   Gastro-intestinal anthrax occurs when diseased meat or contaminated food products are eaten. The disease is marked with fever, bloody diarrhea, vomiting, and abdominal pain (20). *B. anthracis* is most lethal when spores are inhaled into the lungs.   The victim develops flu-like symptoms which lead to a misdiagnosis of the disease (16, 20).   Infections will result in mortality unless the recommended antibiotics, ciprofloxacin and doxycyline, are administered early during the infection (20, 21).   It is notable to mention that anthrax disease has not been found to be transmitted from one person to another.

1.3 Virulence Determinants of *B. anthracis*

Of the many proteins needed by *B. anthracis* to cause anthrax disease, the two major virulence factors are the anthrax toxin and poly-γ-D glutamic acid (PDGA) capsule. The anthrax toxin proteins are the most abundant proteins secreted from the cell. Toxemia induced via injection of the toxins into an animal or delayed antibiotic treatment of an infection will result in death of the host (22–24). The importance of the PDGA capsule has also been demonstrated. A murine model for anthrax disease succumbs to infection of capsulated, nontoxinogenic strains with a similar dose of spores and survival time as capsulated, toxinogenic strains (25).

The anthrax toxin is an atypical A-B type toxin which contains a single binding (B) moiety, protective antigen (PA, 83 kDa), and two enzymatic (A) proteins, edema factor (EF, 89 kDa) and lethal factor (LF, 90 kDa).   After PA binds to the anthrax toxin receptor on host cell membranes, a furin-like protease cleaves PA to release a 20-kDa fragment (PA_{20}) (26, 27).   The remaining 63-kDa PA polypeptide (PA_{63}) spontaneously forms a seven-member pre-pore structure on the cell membrane (28). The pre-pore, which is capable of binding up to three molecules of EF and/or LF (29), is endocytosed and transported to early endosomes (30).   Upon acidification of the vesicle, PA forms a pore (31) and facilitates EF and LF

translocation into the cytoplasm of the host cell (32). EF functions as a calmodulin-dependent adenylate cyclase to increase cAMP levels in the afflicted cell (33). Elevated levels of cAMP, a potent second messaging molecule, cause changes in neutrophil function and disruptions in the cellular water balance (34). LF is a Zn-dependent metalloprotease which targets and cleaves mitogen-activated protein kinase kinases (35, 36). Degradation of the LF targets results in suppression of proinflammatory cytokines (37) and may induce apoptosis (38).

As a means of evading immune detection, *B. anthracis* constructs a PDGA capsule. The capsule is a polymer of amino acid residues while other bacterial capsules are polysaccharides. The PDGA capsule is found only in *B. anthracis* and a few recently discovered *B. cereus* and *B. thuringiensis* strains (9, 10). The humoral response of the immune system only detects the capsule weakly. This allows the bacteria to proliferate without raising much alarm.

Lesser known virulence factors also play roles in *B. anthracis* pathogenesis. Phospholipases function to cleave the phospholipid head groups from the non-polar tails resulting in destabilization of the plasma membrane and lysis of the cell. Three phospholipases are present in *B. anthracis*, and each has specificity for a different class of phospholipids (39). InhA1, a well-studied metalloprotease, has been shown to cleave host proteins as well as *B. anthracis*-derived products (24, 40–43). Alo, a cholesterol-dependent cytolysin, forms pores in host cell membranes leading to the entrance of Ca^{2+} into the host cytoplasm (44). Strains with gene deletions of these factors have slightly less virulence than a parent strain during the course of infection. Nevertheless, each protein is thought to act in a critical niche or step in pathogenesis (39, 45).
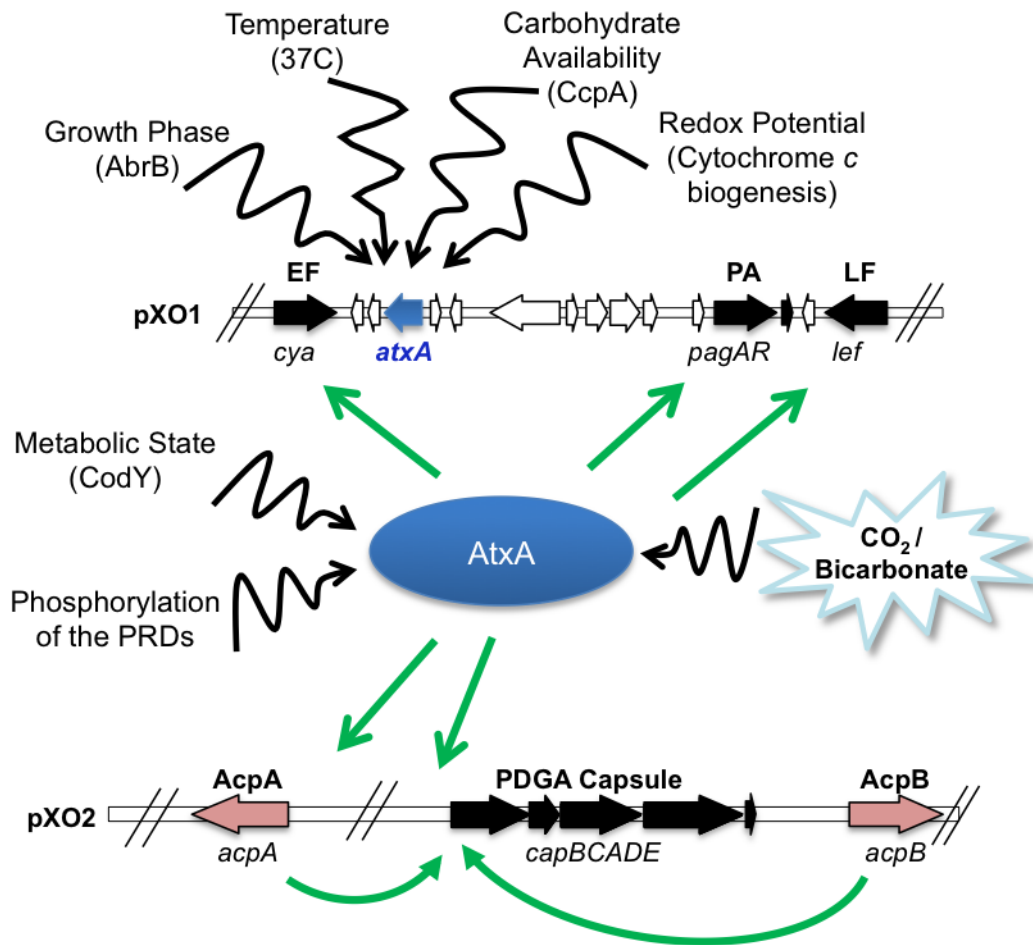
Figure 1-1. Model of virulence gene activation in *B. anthracis*. Transcriptional and post-translational control of AtxA allows *B. anthracis* to coordinate expression of the toxin genes (*cya*, *lef*, and *pagA*) and the poly-D-glutamic acid (PDGA) capsule biosynthetic operon (*capBCADE*). The *atxA* gene (colored blue) is affected positively via temperature and carbohydrate availability and negatively via growth phase cues and redox conditions. Metabolic activity and phosphorylation of the AtxA PRDs result in stabilization and changes in the protein's activity, respectively. The most important signal in the cascade is CO_2/bicarbonate which affects AtxA protein function. Several factors involved in the signal transduction remain unknown (indicated by the winding black arrows). The known players in each pathway are in parentheses. AtxA activates transcription (green arrows) of the toxin genes, *acpA*, *cap* operon, and other genes located on pXO1, pXO2, and the chromosome (not depicted). AcpA and AcpB (colored red) are AtxA-like regulators of the *cap* operon.

1.4 The Anthrax toxin Activator, AtxA

The Anthrax toxin Activator AtxA is required for activation of the virulence genes in *B. anthracis* (Fig. 1-1, (46–48). Deletion of *atxA*, which is located on pXO1, leads to attenuation of virulence in murine models for anthrax disease presumably due to decreased transcription of the anthrax toxin genes and the capsule biosynthetic operon (46, 47, 49–54). Transcript levels of at least 47 genes on the virulence plasmids and the chromosome are changed in a Δ*atxA* strain (55–57). AtxA-dependent promoters do not display any consensus sequence. However, all three toxin genes contain structural similarity (58).

The phenotypes of an *atxA*-null strain indicate that *atxA* is important for virulence and that the function of the protein should be discerned. Based on the sequence of the 475 amino acids within AtxA, it is predicted that AtxA contains five motifs (Fig. 1-2) (59, 60). The 56-kDa, soluble basic protein has two DNA-binding motifs at the amino terminus in the form of winged-helix (WH) and helix-turn-helix (HTH) motifs (51, 59, 60). Two phosphoenolpyruvate: carbohydrate phosphotransferase system (PTS) regulation domains (PRDs) are encoded after the DNA-binding region. The last 90 amino acids are similar to an Enzyme IIB (EIIB) motif of the PTS (60).

AtxA function is affected by phosphorylation of the PRDs while a metabolic state regulator impacts AtxA protein amount. The PRDs within AtxA are phosphorylated at H199 and H379 (59). Using H→A and H→D mutations in AtxA to mimic the non-phosphorylated and phosphorylated states, respectively, Tsvetanova *et al*. suggest that a phosphohistidine at position 199 increases AtxA activity while H379 phosphorylation decreases protein function. The activity of AtxA is decreased when AtxA is phosphorylated at both residues. CodY is a pleiotropic regulator which represses genes during early exponential phase of growth when metabolic activity is high (61). In a Δ*codY* strain, AtxA protein amount is decreased severely. Transcription and translation rates are unaffected in this mutant; therefore CodY regulates AtxA indirectly via a post-translational mechanism (62).
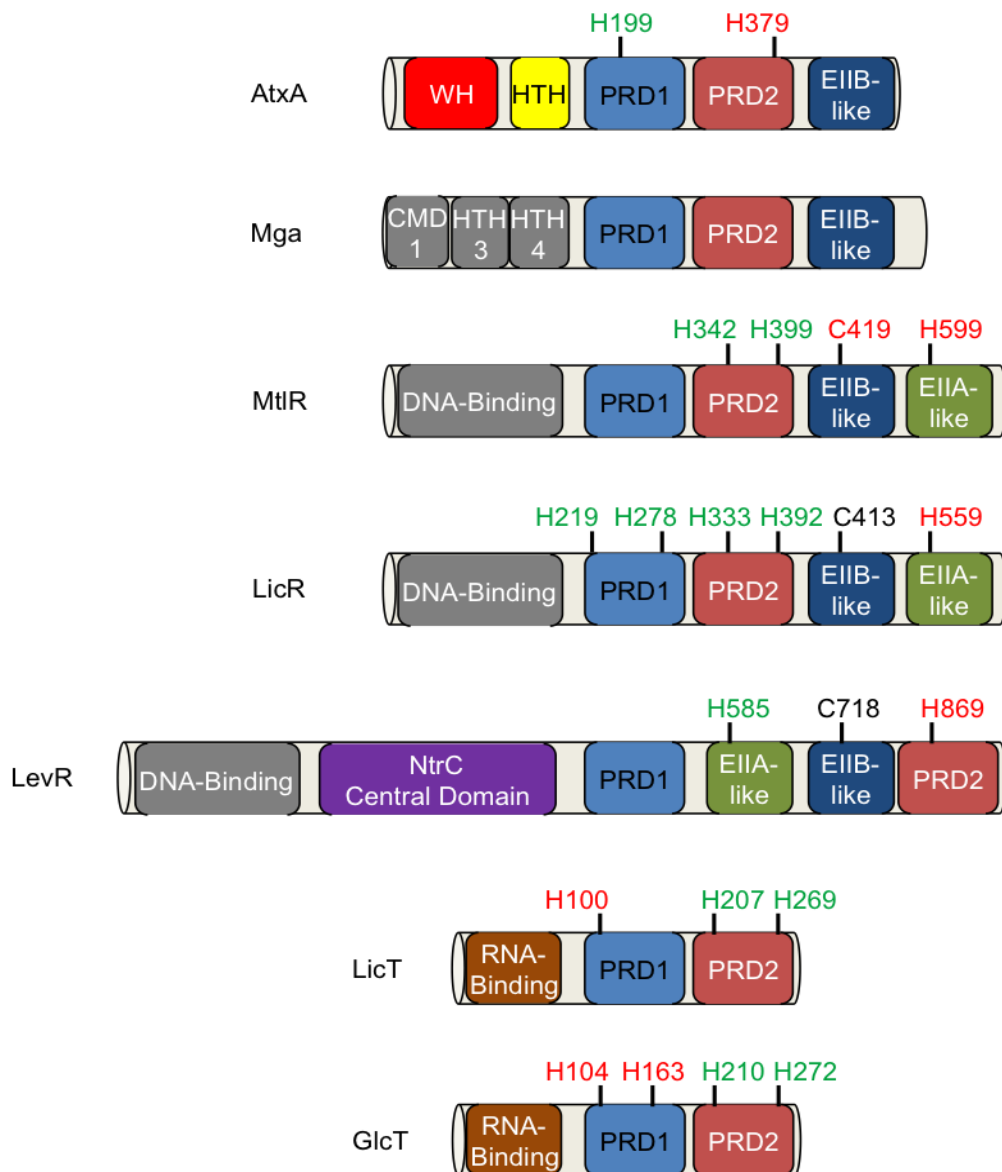
Figure 1-2. Comparison of AtxA and PRD-containing proteins. AtxA contains five putative motifs: a winged helix-turn-helix (WH), a helix-turn-helix (HTH), two PTS regulation domains (PRDs), and an Enzyme IIB-like (EIIB-like) motif. PRD-containing proteins are shown as a comparison to AtxA. Mga contains a conserved Mga domain (CMD-1) and two HTH motifs upstream of the PRDs and EIIB-like motif. MtlR and LicR are similar to AtxA and Mga; however, MtlR and LicR encode an Enzyme IIA-like (EIIA-like) motif. Another variation is seen in LevR. It has the same domains as MtlR and LicR, except there is an NtrC Central Domain and the PRDs are separated by the EIIA-like and EIIB-like motifs. LicT and GlcT are antiterminators; they contain RNA-binding motifs and two PRDs. Several other PRD-containing proteins have been discovered (not depicted). Phosphorylated histidines are labeled for each protein. Phosphorylation sites that lead to increased function of the protein are colored green, whereas the red residues indicate sites which decrease the protein's activity.

Environmental signals and *trans*-acting factors, other than CodY, affect *atxA* transcription predominantly at the P1 promoter 99 nucleotides upstream of *atxA* (49). A second weaker promoter (P2) is located approximately 750 nucleotides in front of the translational start site (63). The environmental signals impacting *atxA* are temperature, redox state, and carbohydrate availability (64–66). Increased transcription of *atxA* occurs at 37° C versus 28° C and in the presence of glucose and not glycerol. In agreement, carbon catabolite activation (CCA) is present, since mutation of the *ccpA*, encoding the c̲atabolite c̲ontrol p̲rotein A̲, leads to a decrease in *atxA* transcription (66). Cytochrome *c* is involved in sensing the redox state of the cell. An increased amount of *atxA* is detected when cytochrome *c*-deficient *B. anthracis* mutants are cultured in non-toxin inducing conditions (65). AbrB, a transition state regulatory protein, binds upstream of the P1 transcriptional start site of *atxA* and down-regulates *atxA* during exponential phase of batch culture growth (67, 68).

Several signals affect virulence of *B. anthracis*; however, CO_2/bicarbonate appears to be the most critical host-associated factor needed for AtxA-dependent virulence gene expression (Fig. 1-1). Virulence genes are transcribed optimally when *B. anthracis* is cultured in a buffered medium in the presence of bicarbonate and 5% or greater CO_2 (47, 49, 50, 69–71). Previous work demonstrated that the CO_2/bicarbonate-dependent induction of the toxin genes was abrogated in an *atxA*-null mutant (47). This pointed to *atxA* as the mediator for the CO_2/bicarbonate signal, but the small molecule does not affect transcription rate of *atxA* or stability of the AtxA protein (25, 47, 54, 72).

1.5 Regulation of PRD-containing proteins and CcpA via the Phosphoenolpyruvate: carbohydrate phosphotransferase system

The role of the PRDs, CcpA, and CodY in AtxA expression and function indicates that the metabolic state of *B. anthracis* affects virulence gene regulation. The

phosphoenolpyruvate: carbohydrate phosphotransferase system (PTS) is the major carbohydrate import and utilization machine within bacteria (Fig. 1-3, (73). CcpA activity and regulation of PRDs is controlled by the PTS.

The primary task of the PTS is to recycle phosphate from the end of glycolysis to carbohydrates as they enter the cell. The PTS is composed of two general enzymes, Enzyme I (EI) and HPr, and sugar-specific Enzyme II (EII) complexes. PTS-dependent carbohydrates are recognized and transported via one of four EII superfamilies: the glucose-fructose-lactose superfamily, the ascorbate-galactitol superfamily, the mannose family, and the dihydroxyacetone family. EII complexes consist of A, B, C, and in some cases D motifs/proteins and may be one protein with multiple domains (EIIABC) or divided into up to four proteins containing each motif separately or in tandem (i.e. EIIA and EIICB) (73).

The phosphotransfer begins as EI catalyzes the conversion of phosphoenolpyruvate (PEP) to pyruvate resulting in EI phosphorylated at a conserved histidine. EI~P transfers the chemical group to HPr at H15 (*Bacillus subtilis* numbering), which subsequently phosphorylates EIIA. EIIA~P phosphorylates EIIB which transfers its phosphate to carbohydrate molecules crossing the cell membrane via the EIIC(D) complex. The phosphorylated sugar serves as a substrate in glycolysis or other catabolic pathways (73).

It is significant to note that the PTS also functions to regulate gene expression based on available sugars. HPr is the main player in carbon catabolite repression (CCR) and carbon catabolite activation (CCA) in low-G+C Gram-positive bacteria, such as *B. anthracis* (Fig. 1-3). In addition to EI-dependent phosphorylation of HPr at H15 (P~His-HPr), the HPr kinase/phosphorylase (HprK/P) phosphorylates HPr at S46 (P-Ser-HPr). EI activity is affected by the PEP/pyruvate ratio; whereas, HprK/P modifies HPr in an ATP-dependent manner in response to high levels of fructose-1,6-bisphosphate. Two methods of HPr-dependent signaling relevant to this work include activation of the catabolite control protein (CcpA) and phosphorylation of PTS regulation domains (PRDs) (73).
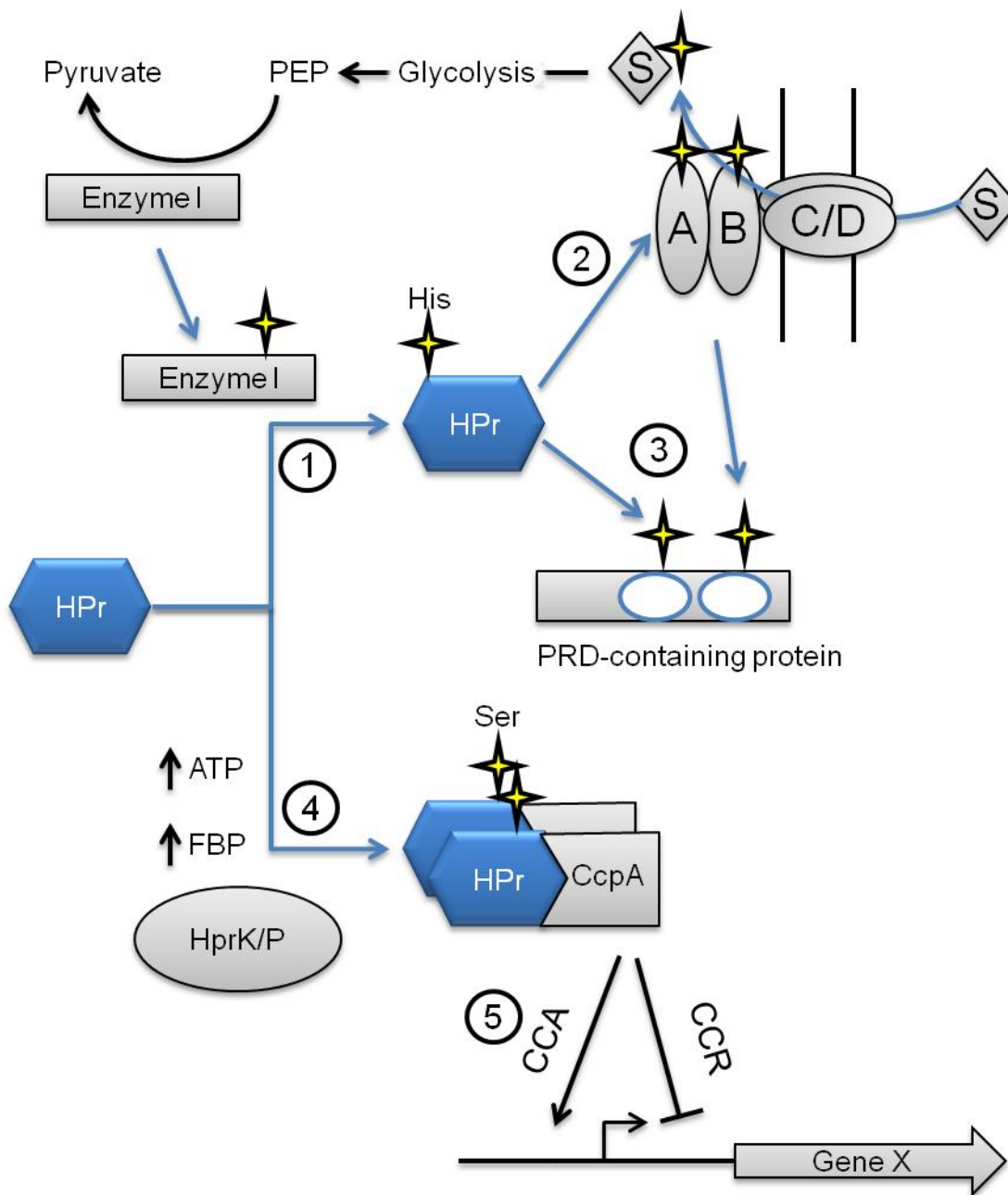
Figure 1-3. HPr-dependent processes related to carbohydrate metabolism.

Figure 1-3. HPr-dependent processes related to carbohydrate metabolism. HPr is phosphorylated by Enzyme I (EI) or HprK/P. EI converts PEP to pyruvate when PEP concentrations are high. The reaction produces a phosphorylated EI. (1) EI~P phosphorylates HPr at His15. (2) EIIA is one target of P~His-HPr. P~EIIA phosphorylates EIIB, which in turn phosphorylates the sugar (S) transported via EIIC/D. (3) PRD-containing proteins are phosphorylated by P~His-HPr to induce activity whereas EIIA- or EIIB-dependent phosphorylation decreases activity. PRD-containing proteins function as transcriptional antiterminators or activators. P~His-HPr has other targets not depicted. (4) Ser46 of HPr is phosphorylated by HprK/P when high levels of ATP and fructose-bis-1,6-phosphate (FBP) are present. P-Ser-HPr forms a heterotetramer with CcpA, and (5) the complex binds to promoters to induce carbon catabolite activation (CCA) or repression (CCR). Blue arrows represent a transfer of phosphate. Black arrows indicate other processes.

CcpA, a *B. subtilis* DNA binding protein within the LacI/GalR family of transcriptional regulators, induces CCA and CCR after interacting with P-Ser-HPr or an HPr-like protein called Crh (reviewed in (74). Similar to HPr, Crh can be phosphorylated at S46. Heterotetramers of CcpA/P-Ser-HPr or CcpA/P-Ser-Crh bind to catabolite response elements (*cre*) located in promoter regions. If a *cre* is upstream of a transcriptional start site, CcpA/P-Ser-HPr will activate the promoter upon binding. Conversely, when the *cre* is downstream of the transcriptional start, CcpA/P-Ser-HPr acts as a repressor to decrease transcription of the gene. The CcpA/P-Ser-HPr regulon includes ~10% of the *B. subtilis* genome, and in several pathogenic bacteria, CcpA plays a role in virulence (75). Deletion of *ccpA* in *B. anthracis* causes a decrease in the transcription of *atxA* (66). Transcription of *mga*, the regulator of early virulence traits in group A *Streptococcus* (GAS), is affected by *ccpA* (76).

PRD-containing proteins typically function as transcriptional activators or antiterminators. The *B. subtilis* protein LicT is the prototypical PRD-containing protein. It contains an amino-terminal RNA-binding motif followed by two PRDs (Fig. 1-2). LicT antiterminates transcription of genes needed to import and metabolize β-glucosides (77). The effect of the PTS on PRD-containing proteins is varied for each regulator and can be different based on the sites phosphorylated via P~His-HPr and a specific class of EIIA and/or EIIB (Fig. 1-3). In LicT, HPr phosphorylates H207 and H269 within PRD2 and H100 in PRD1 is phosphorylated by BglP, the β-glucosides-specific EIIBCA complex (78). Structural studies have shown that the HPr-dependent phosphorylation of PRD2 promotes dimer formation causing an increase LicT activity (79). In contrast, phosphorylation of PRD1 decreases activity by destabilizing the dimeric form (80). Based on the study of LicT and other PRD-containing antiterminators, PRDs have three main properties: (i) PRDs contain 5 α-helices, (ii) histidine residues within the PRDs are phosphorylated via proteins in the PTS, and (iii) phosphorylation of the PRDs leads to structural changes affecting the activation state of the protein.

Other PRD-containing proteins function as transcriptional activators. LicR and MtlR contain DNA-binding motifs at the amino-terminus, followed by two PRDs, an EIIB-like motif and an EIIA-like motif (Fig 1-2, ((81, 82)). Slight variations on the motif organization also exist since LevR contains an NtrC central domain and has its PRDs separated by EIIA-like and EIIB-like motifs (83). Like LicT, the PRDs within these proteins are phosphorylated; however, EIIB-like and EIIA-like motifs can be phosphorylated as well (73). Modification of MtlR, a regulator of mannitol utilization found in *B. subtilis* and *Geobacillus stearothermophilus*, is the best understood of the PRD-containing transcriptional activators (82, 84, 85). PRD2 of MtlR contains two histidines that are phosphorylated by HPr. The Mtl-specific EIIA (EIIA^{Mtl}) phosphorylates MtlR at a conserved cysteine in the EIIB-like motif, and the EIIB^{Mtl} domain (within the EIICB^{Mtl} protein) is responsible for phosphorylating H599 in the EIIA-like motif of MtlR (82). Phosphorylation of PRD2 induces DNA binding by MtlR while phosphorylation of the EIIB-like or EIIA-like motif is antagonistic (84).

1.6 AtxA homologues in Gram positive low G+C pathogens

Recently, PRDs were discovered in several virulence gene regulators: Mga in GAS; AtxA, AcpA, and AcpB in *B. anthracis*; and the Mga-like protein and EbpR in *Enterococcus faecalis* (59, 86–88). These proteins contain amino-terminal DNA-binding motifs, internal PRDs, and a carboxy-terminal EIIB-like motif and regulate virulence-associated genes (Fig. 1-2, (86). This small family of proteins could have functional and structural similarity.

The most-studied of the PRD-containing virulence regulators is Mga (86). Originally described as the regulator of the *emm* gene, Mga controls approximately 10% of the GAS genome during exponential phase of growth (89). *In vitro* electrophoretic mobility shift assays (EMSAs) show Mga binding specifically to several GAS promoters (90). Mga has three amino-terminal features that affect DNA binding and gene activation. One major HTH (HTH-4, residues 107-126) and one minor HTH (HTH-3, residues 53-72) are thought to

interact with DNA specifically (91).   In addition, a small motif called the conserved Mga domain-1 (CMD-1) is required for Mga-dependent activation of promoters (92).   Recently, Mga has been shown to contain an EIIB-like motif and to be phosphorylated via HPr and EI (McIver, personal communication).   Phosphorylation of H204 and H270 decreases Mga activity, whereas phosphorylation of H324 increases the function of the protein.

The Anthrax capsule Activator (AcpA) and AcpB, a homologue of AcpA, are encoded on pXO2 of *B. anthracis* and are part of the AtxA/Mga family.   The proteins have high similarity to each other (62%) and to AtxA (AcpA-AtxA, 50%; AcpB-AtxA, 50%; Drysdale, 2004).   The capsule biosynthesis operon is regulated at the transcriptional level via AtxA, AcpA, and AcpB (Fig. 1-1, (93, 94)).   In a laboratory-derived, genetically-complete strain of *B. anthracis*, *atxA* and either *acpA* or *acpB* are necessary for PDGA capsule synthesis.   Single deletions of *acpA* or *acpB* resulted in an insignificant decrease in capsule production. AcpA and AcpB may appear to be functionally redundant; however, a Δ*acpB* strain is slightly attenuated compared to the parent and Δ*acpA* strains (25).   AtxA increases expression of *acpA* twenty-fold at one of its two promoters, and the other promoter is activated at a low constitutive level.   In addition to an *atxA*-independent promoter directly upstream of *acpB*, its transcript level is thought to be enhanced by read-through transcription from the *cap* operon (95).

The only structural information about an AtxA/Mga family member was obtained when researchers at the Argonne National Laboratory solved the X-ray crystal structure of an Mga-like protein from *E. faecalis* (PDB entry 3SQN,(88)).   No functional or genetic data is available for this protein, except that it crystallized as a dimer.   The structure shows the EIIB-like motif from one monomer is encircled by the DNA-binding motif and PRDs of the other monomer (Fig 1-4).   Interestingly, another AtxA/Mga-like protein, EbpR, is present in *E. faecalis* and regulates pilus biogenesis and biofilm formation (87).   Similar to AtxA, EbpR function is increased in buffered medium containing bicarbonate and CO_2 (96).
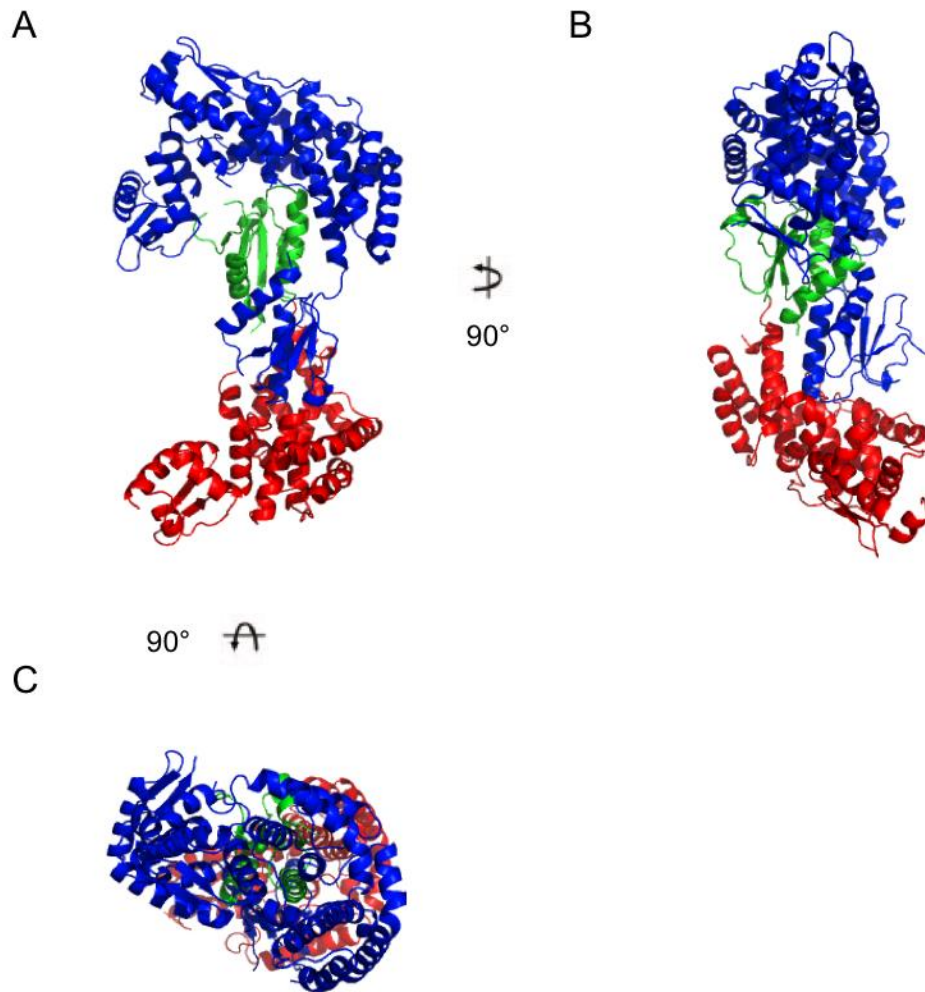
Figure 1-4. Crystal structure of the Mga-like protein of *E. faecalis*. The cartoon structure of the Mga-like protein homodimer (3sqn PDB file) is shown. Subunit A is colored blue. The DNA-binding elements and PRDs of Subunit B are red and the EIIB-like motif is green. Three representations of the structure are shown with different rotations around the y- or x-axis.

1.7 Gaps in knowledge and significance of this work

Studies of AtxA protein function in *B. anthracis* will reveal the mechanism used to control virulence gene expression in response to environmental signaling. Moreover, the knowledge of the specific system used by *B. anthracis* will increase our overall understanding of signal transduction and microbial pathogenesis.

B. anthracis is a model bacterial pathogen. Few bacteria require both intracellular and extracellular mechanisms of immune evasion and survival. The organism utilizes toxins and a capsule like other pathogens, yet the virulence traits within *B. anthracis* have several unique features. The genome contains a chromosome and two large virulence plasmids which encode for the virulence factors. Regulators on all three genetic elements can influence gene expression on the other DNA molecules. The processes of spore formation and germination allow for studies related to the development and morphogenesis of organisms. Finally, powerful biochemical and genetic tools, many developed in the related species *B. subtilis*, are available when working with *B. anthracis*.

Activation of *B. anthracis* virulence requires AtxA; however, it is not understood how AtxA functions to regulate virulence genes. For my thesis work, I hypothesize that AtxA binds target promoters to activate transcription when structural changes within the PRDs and EIIB-like motif are induced by phosphorylation and/or ligand binding. WH and HTH motifs indicate DNA-binding activity though specific binding of DNA has not been shown (51, 60). Tsvetanova *et al.* (59) demonstrated that AtxA is phosphorylated and suggested the PTS is involved in phosphorylation. The effect of phosphorylation and the proteins responsible have not been identified. AtxA function is strongly induced in the presence of CO_2/bicarbonate, but the molecular mechanism for the impact of this signal on protein function has not been discerned.

Chapter II

<u>Materials and Methods</u>

2.1 Culture conditions

"*B. anthracis* strains were cultured at 37° C in Luria-Bertani (LB) medium (97), Brain Heart Infusion (BHI) medium(98) or Casamino Acid (CA) medium (99). LB broth cultures were shaken in air. CA broth cultures were shaken in air or in 5% atmospheric CO_2. For CA cultures incubated in elevated CO_2, 0.8% sodium bicarbonate was added to the medium ($CACO_3$) (100). Cells from stationary phase cultures were transferred into fresh medium ($CACO_3$, unless noted otherwise) to an initial optical density at 600nm (OD_{600}) of approximately 0.08. Cultures were incubated for 7 h and the OD_{600} was determined hourly. Generally, cultures reached early-exponential phase (OD_{600} 0.20 to 0.35) at 2 h and stationary phase (OD_{600} 1.2 to 1.7) at 4 h. For strains harboring *atxA* controlled by the hyper-spank promoter (P*hs*) (101), expression was induced with 30-50 µM isopropyl β-D-thiogalactoside (IPTG) at 2 h and cells were harvested at 4 h.

"Antibiotics were used when appropriate in the following concentrations: spectinomycin (50 µg ml^{-1} for *E. coli* and 100 µg ml^{-1} for *B. anthracis*), erythromycin (150 µg ml^{-1} for *E. coli* and 5 µg ml^{-1} for *B. anthracis*), and carbenicillin (100 µg ml^{-1} for *E. coli*). Antibiotics and other chemicals were purchased from Fisher Scientific (Fairlawn, NJ) or Sigma-Aldrich (St. Louis, MO) unless indicated otherwise." (102)

2.2 Strain Construction

"*B. anthracis* strains and plasmids are shown in Table 2-1. All *B. anthracis* mutants were derived from the parent strain ANR-1 (<u>A</u>mes <u>n</u>on-<u>r</u>everting), a pXO1+ pXO2- isolate originally obtained from Ames (pXO1+ pXO2+) (103). *E. coli* strains JM109, TG1, and GM2163 were employed as hosts for cloning plasmids. Amplification, manipulation, and isolation of plasmid DNA were performed according to general practices. Non-methylated plasmid DNA was obtained from *E. coli*

Table 2.1 *B. anthracis* strains and plasmids

Name	Description	Reference
Strains		
ANR-1	Parent strain, pXO1+, pXO2-	(103)
UT375	*lef* promoter–*lacZ* fusion (P*lef-lacZ*) at native *lef* locus	This work
UT376	*lef* promoter–*lacZ* fusion (P*lef-lacZ*) at native *lef* locus, *atxA*-null	This work
UT405	ANR-1, *ptsHI*-null	This work
UT408	*lef* promoter–*lacZ* fusion (P*lef-lacZ*) at native *lef* locus, *ptsHI*-null	This work
Plasmids		
pHT304-18z	Low-copy vector harboring a promoter-less *lacZ*; Erm^R	(104)
pUTE657	Expression vector derived from pDR111 and pBC16 with IPTG-inducible P*hyper-spank*; Spec^{R}Amp^R	(105)
pUTE658	pUTE657 - derived expression vector for AtxA; the *atxA* ribosome binding site and coding region controlled by P*hyper-spank*	This work
pUTE843	pHT304-18z - derived reporter vector for *atxA*; -72 to +99 of the *atxA* promoter (relative to the P1 transcriptional start) is upstream of *lacZ*	(106)
pUTE991	pUTE658 - derived expression vector for AtxA-His (hexa-histidine tag on the C-terminus of AtxA)	This work
pUTE992	pUTE658 - derived expression vector for AtxA-FLAG (FLAG tag on the C-terminus of AtxA)	This work
pUTE1013	pUTE657 - derived expression vector for GFP-FLAG (FLAG tag on the C-terminus of GFP); the *gfpmut3a* ribosome binding site, coding region, and sequence encoding FLAG controlled by P*hyper-spank*	This work
pUTE1018-FLAG	pUTE657 - derived expression vector for AtxA$_{1-164}$-FLAG (FLAG tag on the C-terminus); the *atxA* ribosome binding site, coding region, and sequence encoding FLAG controlled by P*hyper-spank*	This work
pUTE1019-FLAG	pUTE657 - derived expression vector for AtxA$_{1-385}$-FLAG (FLAG tag on the C-terminus); the *atxA* ribosome binding site, coding region, and sequence encoding FLAG controlled by P*hyper-spank*	This work
pUTE1020-GFP-FLAG	pUTE657 - derived expression vector for AtxA$_{167-385}$-GFP-FLAG (GFP-FLAG tag on the C-terminus); the *atxA* ribosome binding site, coding region, and sequence encoding GFP-FLAG controlled by P*hyper-spank*	This work
pUTE1021-GFP-FLAG	pUTE657 - derived expression vector for AtxA$_{167-475}$-GFP-FLAG (GFP-FLAG tag on the C-terminus); the *atxA* ribosome binding site, coding region, and sequence encoding GFP-FLAG controlled by P*hyper-spank*	This work

Table 2.1 *B. anthracis* strains and plasmids (continued)

Name	Description	Reference
pUTE1022-FLAG	pUTE657 - derived expression vector for AtxA$_{385-475}$-FLAG (FLAG tag on the C-terminus); the *atxA* ribosome binding site, coding region, and sequence encoding FLAG controlled by P*hyper-spank*	This work
pUTE1022-GFP-FLAG	pUTE657 - derived expression vector for AtxA$_{385-475}$-GFP-FLAG (GFP-FLAG tag on the C-terminus); the *atxA* ribosome binding site, coding region, and sequence encoding FLAG controlled by P*hyper-spank*	This work
pUTE1032	pUTE657 - derived expression vector for His-HPr (hexa-histidine tag on the N-terminus of HPr); the *ptsH* ribosome binding site, sequence encoding the His tag, and *ptsH* coding region controlled by P*hyper-spank*	This work
pUTE1034	pUTE657 - derived expression vector for HPr and EI; the *ptsH* ribosome binding site, *ptsH* coding region, *ptsI* ribosome binding site, and *ptsI* coding region controlled by P*hyper-spank*	This work
pUTE1040	pUTE657 - derived expression vector for His-EI (hexa-histidine tag on the N-terminus of EI); the *ptsI* ribosome binding site, sequence encoding the His tag, and *ptsI* coding region controlled by P*hyper-spank*	This work

GM2163 for electroporation into *B. anthracis* (47, 107).

"All gene deletions were inserted using derivatives of pHY304, a temperature-sensitive *E. coli* – *B. anthracis* shuttle vector harboring an erythromycin-resistance gene (108). To construct UT375, in which the *lef* coding sequence on pXO1 was replaced by a promoterless β-galactosidase gene (*lacZ*), the polymerase chain reaction (PCR) and primers TH126 and TH127 (Table 2-2) were used to amplify a 797-bp DNA fragment corresponding to sequence from -686 to +111 relative to the *lef* transcriptional start site (*lef$_{up}$*) (49). The PCR product was cloned into pHT304-18z (109) using *Pst*I and *BamH*I restriction enzyme sites upstream of the plasmid-borne *lacZ*. Subsequently, a 854-bp DNA sequence corresponding to sequences +2510 to +3363 (*lef$_{down}$*) was amplified using primers TH128 and TH129 and cloned into the *Kpn*I and *EcoR*I sites of pHT304-18z containing *lef$_{up}$*. The *lef$_{up}$-lacZ-lef$_{down}$* segment of DNA was removed via digestion with *Xho*I and *EcoR*I and cloned in pHY304. Integration of the plasmid was performed according to methods described previously (105). Briefly, *B. anthracis* containing the plasmid was cultured at 41° C (the temperature non-permissive for pHY304 replication) in the presence of erythromycin to select for isolates in which the plasmid inserted into the *lef* locus via homologous recombination. Subsequently, cultures were passaged multiple times at 30° C in the absence of antibiotic to allow excision of the pHY304 derivative from the *lef* locus. Single colony isolates were tested using PCR and sequencing for replacement of the *lef* coding sequence with the promoterless β-galactosidase gene.

"To generate UT376, a markerless *atxA*-deletion mutant of UT375, DNA fragments corresponding to approximately 1 kb upstream of the *atxA* translational start (-1009 to +99 from the P1 transcriptional start site) and 1 kb downstream of the *atxA* stop codon (+1528 to +2517) were amplified using primers JR170-171 and

Table 2.2 Primers used in this dissertation

Name	Brief Description	Sequence (5' to 3')
TH126	P*lef-lacZ* insertion	GACTCTGCAGCTCGAGTATGCAGTGAGGCTCTTATGATT
TH127	P*lef-lacZ* insertion	GATAGGATCCATAAAGACGGGACCACTCAAAG
TH128	P*lef-lacZ* insertion	CAGTGGTACCGGGACCAGCCATTATGAAGCAAC
TH129	P*lef-lacZ* insertion	GGAAGAATTCAAGATGAAGATCGACAAAATGGCTC
JR170	*atxA* markerless deletion	GGCCGCGGAGAGCCGCATTAAACT
JR171	*atxA* markerless deletion	GGGCATGTCTATAATTGATTCTCCTTTCCTG
JR172	*atxA* markerless deletion	GAGAATCAATTATAGACATGCCCTTTAAATATTTGTTTAATGACAC
JR173	*atxA* markerless deletion	GGCTCGAGCGCTTGTCTCACAATCTCATC
TH235	*ptsHI* markerless deletion	GAGATCTAGACTAGTAGCACTTGGTGGTAAAG
TH244	*ptsHI* markerless deletion	CAGCCTCGAGTTCATACGGAAGCTTTATCGCAC
TH245	*ptsHI* markerless deletion	CGACTCAGGTTTTTTTATTAATTACATGATAATTTATCTCC
TH246	*ptsHI* markerless deletion	GGAGATAAATTATCATGTAATTAATAAAAAAACCTGAGTCG
TH191	*atxA* rbs (*Sal*I)	GGTAGTCGACAGGAAAGGAGAATCAATTATAGACATGC
TH192	*atxA* stop codon (*Sph*I)	CCTTGCATGCTTATATTATCTTTTTGATTTCATG
TH198	*atxA* codon 475 + FLAG + stop (*Sph*I)	GGGCATGCTATTTATCATCATCATCTTTATAATCTATTATCTTTTTGATTTCATGAAAAT
TH199	*atxA* codon 475 + His6 + stop (*Sph*I)	GGGCATGCTAGTGGTGGTGGTGGTGGTGTATTATCTTTTTGATTTCATGAAAAT
TH254	*atxA* rbs + codon 167 (*Sal*I)	CCAAGTCGACAGGAAAGGAGAATCAATTATAGACATGTATTGGCCGTTTCCCTATATTAA
TH247	*atxA* rbs + codon 385 (*Sal*I)	CCAAGTCGACAGGAAAGGAGAATCAATTATAGACATGCTATTTAAAAATAACCCG
TH257	*atxA* codon 164 + FLAG + stop codon (*Sph*I)	GGGCATGCTATTTATCATCATCATCTTTATAATCTGGAATATTGCAATATAACC
TH260	*atxA* codon 385 + FLAG + stop codon (*Sph*I)	GGGCATGCTATTTATCATCATCATCTTTATAATCCATACGTTGAGTTTCAAAATGCATTG
TH267	*atxA* codon 385 + *gfp-mut3a* start (Forward)	CAATGCATTTTGAAACTCAACGTATGATGAGTAAAGGAGAAGAACTTTTCAC
TH268	*atxA* codon 385 + *gfp-mut3a* start (Reverse)	GTGAAAAGTTCTTCTCCTTTACTCATCATACGTTGAGTTTCAAAATGCATTG
TH212	*atxA* codon 475 + *gfp-mut3a* start (Forward)	GATTTTCATGAAATCAAAAAGATAATAATGAGTAAAGGAGAAGAACTTTTCAC
TH213	*atxA* codon 475 + *gfp-mut3a* start (Reverse)	GTGAAAAGTTCTTCTCCTTTACTCATTATTATCTTTTTGATTTCATGAAAATC
TH228	*atxA* C96S	CTAAATCTTCAAATTAGTGAAGAACTTGTATTC
TH229	*atxA* C96S	GAATACAAGTTCTTCACTAATTTGAAGATTTAG
TH216	*atxA* C161S	ATGTTAAGGTTATATAGTAATATTCCAAATGAT
TH217	*atxA* C161S	ATCATTTGGAATATTACTATATAACCTTAACAT
TH218	*atxA* C202S	TCAAAACACAAATTGAGTGTGTTGTTCGCTATA
TH219	*atxA* C202S	TATAGCGAACAACACACTCAATTTGTGTTTTGA

Table 2.2 Primers used in this dissertation (continued)

Name	Brief Description	Sequence (5' to 3')
TH230	*atxA* C356S	AATACAATTCAAGAA<u>AGT</u>ATTAGTAATTTAAAC
TH231	*atxA* C356S	GTTTAAATTACTAAT<u>ACT</u>TTCTTGAATTGTATT
TH222	*atxA* C370S	TACTCCCATTTCGAC<u>AGT</u>TATGAAATTTCATTA
TH223	*atxA* C370S	TAATGAAATTTCATA<u>ACT</u>GTCGAAATGGGAGTA
TH224	*atxA* C402S	TACACCTCACAAGGA<u>AGT</u>ATACATCGAGAG
TH225	*atxA* C402S	CTCTCGATGTATA<u>ACT</u>TCCTTGTGAGGTGTA
TH183	*atxA* H199A	CAAATGTACACCTATTCAAAA<u>GCC</u>AAATTGTGTGTG
TH184	*atxA* H199A	CACACACAATTT<u>GGC</u>TTTTGAATAGGTGTACATTTG
TH22	*atxA* H199D	CAAATGTACACCTATTCAAAA<u>GAC</u>AAATTGTGTGTG
TH23	*atxA* H199D	CACACACAATTT<u>GTC</u>TTTTGAATAGGTGTACATTTG
TH185	*atxA* H379A	CATTATTAACAATG<u>GC</u>TTTTGAAACTCAACGTATGC
TH186	*atxA* H379A	GCATACGTTGAGTTTCAAAA<u>GC</u>CATTGTTAATAATG
TH24	*atxA* H379D	CATTATTAACAATG<u>GA</u>TTTTGAAACTCAACGTATGC
TH25	*atxA* H379D	GCATACGTTGAGTTTCAAAA<u>TC</u>CATTGTTAATAATG
TH193	*gfp-mut3a* rbs (*Sal*I)	GCGCGTCGACCTCTAGATTTAAGAAGGAGATATAC
TH234	*gfp-mut3a* stop codon + FLAG (*Sph*I)	GGGCATGCTATTTATCATCATCATCTTTATAATCTTTGTATAGTTCATCCATGCCATG
MT10	*ptsH* rbs (*Sal*I)	GGTAGTCGACATTTAAAGGAGATAAATTATCATG
TH286	*ptsH* His6 + 5' end of ORF	GCACACCACCACCACCACCACGAAAAAATCTTTAAAGTAACTAGCG
TH287	*ptsH* rbs + His6	GTGGTGGTGGTGGTGTGCCATGATAATTTATCTCCTTTAAATGTC
TH288	*ptsH* stop codon (*Sph*I)	ATGCATGCTTATTCTCCTAATCCTTCG
MT12	*ptsI* rbs (*Sal*I)	GGTAGTCGACAACGAAGGATTAGGAGAATAATG
TH289	*ptsI* His6 + codon 2	GCACACCACCACCACCACCACACTCTTAACATTCAAGGG
TH290	*ptsI* rbs + His6	GTGGTGGTGGTGGTGTGCCATTATTCTCCTAATCCTTCGTTGTC
MT13	*ptsI* stop codon (*Sph*I)	GGGCATGCATCGACTCAGGTTTTTTTATTAATTA
TH195	pUTE657 sequencing primer (upstream)	GAACGTTGCTCGAGGGTAAATG
TH196	pUTE657 sequencing primer (downstream)	GGTACGTACGATCTTTCAGCC

Abbreviations: rbs, ribosome binding site; His6, hexa-histidine tag; ORF, open reading frame Restriction enzymes are listed in parentheses. If the primer encodes a point mutation, the mutagenic codon is underlined.

JR172-173, respectively (Table 2-2), fused via splicing by overlapping extension PCR (PCR-SOE) (110), and inserted into pHY304 using the *Sac*II and *Xho*I restriction enzyme sites. *B. anthracis* containing the P*lef-lacZ* reporter (UT375) was transformed with the *atxA* deletion construct. The strain was cultured as described above and an isolate deleted for *atxA* was confirmed using PCR and sequencing." (102)

The vector used to remove *ptsHI* from the *B. anthracis* chromosome contained sequences homologous to the regions upstream of *ptsH* and downstream of *ptsI*. Primers TH235 and TH245 facilitated amplification of a 869-nt sequence upstream of the *ptsH* (GBAA_4268) start codon while TH246 and TH244 were used to amplify a 873-nt region downstream of the *ptsI* (GBAA_4267) stop codon. The products were fused via PCR-SOE and cloned into pHY304 using the *Xba*I and *Xho*I restriction enzyme sites. The plasmid containing the *ptsHI* flanking regions was electroporated into ANR-1 and UT375 to produce the *ptsHI*-null strains (UT405 and UT408, respectively) using the methods described above for gene deletion.

"I cloned the *atxA* coding region into pUTE657 (105), which carries the IPTG-inducible promoter P*hyper-spank* (P*hs*) from pDR111 (101) and the origin of replication from pBC16. The *atxA* gene was amplified using TH191 and TH192 (Table 2-2) to add a *Sal*I site 5' of the ribosome binding site (rbs, +76 from P1) and a *Sph*I site after the translational stop codon. The resulting plasmid (pUTE658) contains *atxA* controlled by P*hs*.

"I used a comparable strategy to clone the *gfp-mut3a* sequence (111) into pUTE657, yielding pUTE1013. Using TH193 and TH234 (Table 2-2), the *gfp-mut3a* sequence was PCR amplified from pAD123 (112) to include the ribosome binding site and to add a C-terminal FLAG tag to *gfp-mut3a*." (102)

I constructed *B. anthracis* strains carrying P*hs*–controlled *atxA* alleles on pUTE657 to allow expression of carboxy-terminal epitope-tagged parent and mutant AtxA proteins. Mutant alleles were generated using PCR-SOE and appropriate oligonucleotide primers (Table 2-2). For carboxy-terminal epitope tags (FLAG and hexa-His), primers were designed to encode the desired tag at the 3' end of *atxA* prior to the stop codon. To create 5' deletions of *atxA*, oligonucleotides fused the rbs of *atxA* to codon 167 or 385 (TH254 or TH247). For 3' deletions of *atxA*, a FLAG-tag and stop codon were inserted after the 164th or 385th codon (TH257 or TH260). AtxA-GFP-FLAG fusions were created using PCR-SOE to connect the 385th (TH267 and TH268) or 475th codons (TH212 and TH213) of *atxA* to the *gfp-mut3a* sequence containing a carboxy-terminal FLAG tag. Each of the *atxA* alleles was cloned into the *Sal*I and *Sph*I sites of pUTE657. In total, I produced six vectors (AtxA truncations): pUTE1018-FLAG (AtxA$_{1-164}$-FLAG), pUTE1019-FLAG (AtxA$_{1-385}$-FLAG), pUTE1020-GFP-FLAG (AtxA$_{167-385}$-GFP-FLAG), pUTE1021-GFP-FLAG (AtxA$_{167-475}$-GFP-FLAG), pUTE1022-FLAG (AtxA$_{385-475}$-FLAG), and pUTE1022-GFP-FLAG (AtxA$_{385-475}$-GFP-FLAG) (Table 2-1).

To express proteins within *B. anthracis*, I inserted genes of interest into the pUTE657 vector. The *ptsHI* genes were amplified using MT10 and MT13 and subsequently cloned into the *Sal*I and *Sph*I sites of pUTE657. The resulting vector (pUTE1034, Table 2-1), was used as a template to generate an amino-terminal hexa-His tagged HPr in pUTE657 (pUTE1032). Using a primer upstream of P*hs* on pUTE657 (TH195) and TH286, I added the hexa-His tag after the rbs and start codon of *ptsH*. Using PCR-SOE the product was combined with sequences representing the entire coding region, minus the start codon, of *ptsH* (TH287 and TH288). Similarly, the *ptsI* open reading frame was cloned into pUTE657. Oligonucleotides MT12 and MT13 amplified the region and contained the enzyme restriction sites to clone the sequence into pUTE657. The construct served as the template to create an amino-terminal fusion of the His6 tag and *ptsI*. The rbs and start codon were added to the hexa-His tag using TH195 and TH289. The remaining *ptsI* sequence was amplified using TH290 and

MT13. The two DNA products were connected using PCR-SOE. The vector encoding the His-tagged EI is pUTE1040.

2.3 AtxA-His purification

"The recombinant epitope-tagged protein AtxA-His was purified from *B. anthracis* using affinity chromatography. *B. anthracis* UT376 (pUTE658) was cultured in 2-L baffled flasks containing 750 ml CACO$_3$. Following induction with 50 µM IPTG, cells were harvested using centrifugation at 6200 x g for 10 min at 4° C. Cells were resuspended in 3 ml Binding Buffer (5 mM imidazole, 0.5 M NaCl, 5 mM β-mercaptoethanol, 20 mM Tris pH 7.2,) supplemented with 1X EDTA-free Complete proteinase inhibitor (Roche, Indianapolis, IN), 1 mM MgCl$_2$, and 10 units DNASe I (Ambion, Inc., Austin, TX). Cells were lysed via three passages through a French Pressure Cell Press (SLM Instruments, Inc., Urbana, IL) and soluble material was obtained following centrifugation at 30,000 x g for 20 min at 4° C. Lysates were added to 1 ml NTA-Ni resin (Qiagen, Hilden, Germany) in Binding Buffer (total volume of 10 ml) and the suspension was mixed gently for 2 h at 4° C. The resin was washed in batch three times with 4 ml of Binding Buffer and once with 4 ml of Wash Buffer 1 (40 mM imidazole pH 7.9, 1.0 M NaCl, 20 mM Tris pH 7.2, 5 mM β-mercaptoethanol). The resin was transferred to a gravity column and washed sequentially with (1) 10 ml Wash Buffer 1, (2) 1.5 ml Wash Buffer – High Salt (40 mM imidazole pH 7.9, 1.5 M NaCl, 20 mM Tris pH 7.2, 5 mM β-mercaptoethanol), (3) 2.5 ml Wash Buffer 1, (4) 1.5 ml Wash Buffer 2 (75 mM imidazole pH 7.9, 1.0 M NaCl, 20 mM Tris pH 7.2, 5mM β-mercaptoethanol), and (5) 2.5 ml Wash Buffer 1. Upon addition of 7.5 ml Elution Buffer (20 mM Tris pH 7.2, 800 mM imidazole pH 7.9, 500 mM NaCl, 5 mM β-mercaptoethanol), 250 µl fractions were collected in 1.5-ml tubes containing 250 µl Collection Buffer (20 mM Tris pH 7.2, 150 mM NaCl, 10% glycerol,

5 mM EDTA, 5 mM β-mercaptoethanol). Protein concentration and purity of the fractions were assessed using the Bradford reagent (Bio-Rad, Hercules, CA) and SDS-PAGE with Coomassie staining (1% coomassie brilliant blue, 10% acetic acid, 40% methanol). Fractions containing AtxA-His were pooled and dialyzed in 400 mM NaCl, 5% glycerol, 20 mM Tris pH 7.2, and 5 mM dithiothreitol (DTT)." (102)

2.4 α-AtxA Antibody and AtxA Western blots

"Antiserum for Western blotting was raised in rabbits (Cocalico Biologicals, Inc., Reamstown, PA). AtxA-His, purified from *E. coli* using a method similar to that described above, was injected into rabbits and serum was collected on day 56. To remove non-specific antibodies, the serum was adsorbed to an immobilized *E. coli* lysate (Thermo Scientific) using the manufacturer's protocol. IgG in the serum was purified using Pierce Nab Spin Columns (Thermo Scientific).

"B. *anthracis* cell lysates for Western blotting analysis were obtained from cultures at early stationary phase (OD_{600} = 1.2 to 1.7). Culture samples (4 ml) were centrifuged as described above. After washing cells two times in KTE-PIC (10 mM Tris-HCl pH 8.0, 100 mM KCl, 10% ethylene glycol, and EDTA-free Complete proteinase inhibitor), cells were resuspended in KTE-PIC to a final volume of 850 µl and transferred to a 1.5-ml screw-cap tube containing 400 µl 0.1 mm Zirconia/Silica Beads (BioSpec Products, Bartlesville, OK). The samples were lysed mechanically for 2 min using a Mini BeadBeater (BioSpec Products). After centrifugation, soluble material was mixed with SDS loading buffer (final concentration of loading buffer was 5% glycerol, 100 mM DTT, 2% SDS, 40 mM Tris-Cl pH 6.8), boiled, and subjected to sodium dodecyl sulfate (SDS) polyacrylamide gel electrophoresis (SDS-PAGE).

"Prior to protein transfer, gels were equilibrated in CAPS Buffer (10 mM CAPS pH 11.0, 10% methanol). Using a Hoefer transfer unit (Hoefer, Inc., Holliston, MA)

containing CAPS Buffer, proteins were transferred to Immobilon-P membrane (Millipore, Billerica, MA) at 50V at 4° C for 1.5 to 2 h. Membranes were blocked with TBS-T (20 mM Tris base, 137 mM NaCl, 0.1% Tween 20 [pH 7.6]) containing 5% non-fat dry milk. Membranes were subsequently treated with primary antibodies (α-AtxA, α-RNA polymerase β subunit [Santa Cruz Biotechnology, Santa Cruz, CA], α-THE His [Genscript, Piscataway, NJ], and α-FLAG M2 [Sigma Aldrich]) in TBS-T. After washing with TBS-T, membranes were finally treated with the corresponding secondary antibody (goat α-rabbit–HRP conjugate or goat α-mouse-HRP conjugate [Bio-Rad]). Blots were developed using the SuperSignal West Dura Chemiluminescent Substrate (Thermo Scientific). For re-probing, membranes were stripped using Restore Western Blot Stripping Buffer (Thermo Fisher) or 62.5 mM Tris pH 6.8 containing 2% SDS and 100 mM β-mercaptoethanol." (102)

2.5 Limited Proteolysis

AtxA-His was cleaved with trypsin and chymotrypsin. 30 µg AtxA-His was combined with 0.3 µg trypsin or chymotrypsin in 100 mM Tris-Cl pH 8.5, 1 mM $CaCl_2$. The digestion reaction was incubated at 25° C for 4 h and quenched by adding 190 mM Tris-Cl pH 6.8, 4.3 M β-mercaptoethanol, 6% SDS, 3 mM PMSF and boiling for 3 min. AtxA-His fragments were separated via electrophoresis through 16% polyacrylamide-SDS gels and detected with Coomassie stain. The 40-kDa band was excised from the gel and digested to completion with trypsin. The polypeptide fragments were identified via mass spectrometry in the laboratory of William Dubinsky at the University of Texas Health Science Center – Houston. A similar experiment was performed except the proteins were transferred to a PVDF membrane in 10 mM Tris Base, 100 mM glycine, 10% methanol. I stained the membrane with 0.1% Coomassie, 40% methanol, and 10% acetic acid and destained with 40% methanol. The amino-terminus of the major cleavage product was identified via Edman

Degradation and N-terminal sequencing by Richard Cook at the Baylor College of Medicine Protein Chemistry Core Facility.

2.6 Filter Binding Assay

The affinity of AtxA-His for ^{32}P-labeled DNA probes was determined using a filter binding assay similar to established protocols (113). Promoter regions of the *lef* (167 bp), *bla*1 (267 bp), and *papR* (169 bp) genes were digested from pUTE749, pUTE756, and pUTE757, respectively (58), using *Xba*I and *Sal*I. The probes were dephosphorylated during a reaction with calf intestinal alkaline phosphatase, PNK-treated to label with γ-^{32}P-ATP, and isolated with Micro Bio-Spin 30 Chromatography columns (Bio-Rad) according to the product manuals.

The DNA probes (3 pM) and purified AtxA-His (0.01 nM, 0.1 nM, 0.3 nM, 1 nM, 2 nM, 5 nM, 10 nM, 20 nM, 50 nM, 100 nM, 300 nM, and 1000 nM) were diluted in 10 mM Tris-Cl pH 7.5, 150 mM KCl, 5 mM MgCl$_2$, 5 mM DTT, 3% glycerol, and 0.1 mg ml^{-1} bovine serum albumin (BSA). In a 96-well plate, 220 μl reactions were prepared in triplicate. Protein and DNA solutions were incubated at room temperature for 30 min. A nitrocellulose filter membrane was pre-wetted in 150 mM KCl, 10 mM Tris-Cl pH 7.5, 5 mM MgCl$_2$, and 3% glycerol and placed within a 96-well vacuum manifold. Aliquots of 150 μl of the reaction were applied to the filter. Subsequently, the filter was dried at 37° C and protein-^{32}P-labeled DNA complexes were detected via phosphor-imaging screen (Fujifilm, Tokyo, Japan). The images were scanned via a STORM imager (Amersham Pharmacia Biotech, Piscataway, NJ) and the intensity of each sample was quantified via ImageQuant software (Amersham Pharmacia Biotech). The signal intensity minus the background of triplicate samples was averaged and then normalized to the sample containing 1000 nM AtxA-His.

When varying the KCl concentration or pH, the experiment was performed as described except with minor modifications. Only 0.2 nM, 20 nM or 200 nM AtxA-His was

assayed in each condition. The membranes were pre-wetted with buffer containing the lowest salt concentration or lowest pH. Before applying the samples to the filter, the wells of the vacuum manifold were rinsed with buffer of the corresponding sample.

2.7 BN-PAGE assay

"To perform Blue Native polyacrylamide gel electrophoresis (BN-PAGE), protein samples mixed with NativePAGE Sample Buffer containing 5% G-250 Sample Additive were electrophoresed using NativePAGE Novex 4-16% Bis-Tris Gels in the XCell *Surelock* Mini-Cell electrophoresis unit according to the manufacturer's instructions (Invitrogen, Carlsbad, CA). Electrophoresed proteins were transferred to PVDF at 20V overnight at 4° C. Blots were fixed with 8% acetic acid for 15 min prior to probing with α–AtxA antibody as described above." (102)

2.8 Co-affinity purification

"*B. anthracis* UT376 containing vectors encoding AtxA-His (pUTE991), AtxA-FLAG (pUTE992), or GFP-FLAG (pUTE1013) were cultured independently. Three pools, containing 20 ml of each culture, were collected: UT376 (pUTE991) and UT376 (pUTE1013); UT376 (pUTE991) and UT376 (pUTE992); and UT376 (pUTE992) and UT376 (pUTE1013). The cells were washed with 10 ml Binding Buffer containing EDTA-free Complete proteinase inhibitor (BB-PIC). Pellets were flash frozen in an ethanol-dry ice bath and stored at -80° C.

"To create cleared soluble cell lysates, samples were thawed in an ice bath, resuspended in 2.5 ml BB-PIC, and transferred to two 1.5-ml screw cap tubes, each containing 500 μl 0.1 mm Zirconia/Silica beads. The samples were lysed mechanically for 1 min using a Mini BeadBeater, placed on ice for 5 min, and then subjected to an additional 1 min of bead beating. Following centrifugation at 10,000 x

31

g for 5 min at 4° C, the soluble material was incubated at 37° C for 20 min. NTA-Ni resin (70 µl) was added and the samples were incubated at 4° C for 2 h. The resin was transferred to spin filters (EMB Chemicals, Darmstadt, Germany) and several 500-µl washes were performed in the following sequence: 2x Binding Buffer, 2x Wash Buffer 1, 1x Wash Buffer-High Salt, 2x Wash Buffer 1, 1x Wash Buffer 2, and 2x Wash Buffer 1. Proteins were eluted from the column using 125 µl Elution Buffer and then denatured with SDS loading buffer. Samples were probed with α-AtxA, α-His, and α-FLAG antibodies using Western blotting." (102)

2.9 BMH Cross-linking

"Protein cross-linking was performed as described elsewhere (114). Briefly, cultures containing UT376 (pUTE658) were induced with 30 µM IPTG for 2 h. Cells were washed twice with 5 ml phosphate-buffered saline (PBS) containing 10 mM EDTA and adjusted to pH 7.2. Cells were then resuspended in 1 ml PBS 10 mM EDTA pH 7.2 and lysed.   For each experiment, 250 µl of cleared soluble cell lysate, representing 5 ml of culture, was mixed with 5 µl of 20 mM bis(maleimido)hexane (BMH, Thermo Scientific, prepared freshly in DMSO) and incubated at 4° C for 2 h with end-over-end mixing. Control reactions lacking BMH contained the DMSO solvent only. Reactions were quenched by adding 40 mM cysteine, vortexing for 10 min, and boiling in the presence of 1X SDS loading buffer containing 100 mM DTT. The samples were analyzed on 4-15% polyacrylamide SDS gels (Bio-Rad) and AtxA was detected via Western blotting. ImageJ software (115) was used to determine relative intensities of cross-reactive bands.

"AtxA-His for cross-linking experiments was affinity purified using NTA-Ni resin and washes were performed with solutions made without β-mercaptoethanol. AtxA-

His was eluted from the resin, and subjected to BMH cross-linking as described above." (102)

2.10 Purification of EI, HPr, and PEPCK

EI-His and HPr-His were isolated separately from *B. anthracis* following previously published methods (116, 117). Two 2-L baffled flasks containing 500 ml LB medium inoculated with an eight-hour culture of ANR-1(pUTE1032) or ANR-1(pUTE1040) were incubated at 37° C. During late exponential phase of growth (OD$_{600}$ = 0.6 – 0.8), the cultures were induced with 0.5 mM IPTG at for four hours. Cell pellets were frozen after harvesting via filtration onto a nitrocellulose membrane (0.22 µm pore-size) and centrifugation at 6200 x g for 10 min at 4° C. Each cell pellet was resuspended in 10 ml Buffer A-PIC (20 mM Tris-Cl pH 8.0, 100 mM NaCl, 5% glycerol, 30 mM imidazole pH 7.9, 1X EDTA-free Complete proteinase inhibitor cocktail) supplemented with 1 mM MgCl$_2$ and 10 units DNAse I. Cells were lysed via three passages through a French Pressure Cell Press and soluble material was obtained following centrifugation at 30,000 x g for 20 min at 4° C. Lysates were added to 1 ml NTA-Ni resin in Buffer A-PIC (total volume of 10 ml) and the suspension was mixed gently for 2 h at 4° C. The resin was washed in batch three times with 4 ml of Buffer A-PIC. The resin was transferred to a gravity column and washed with 5 ml Buffer A-PIC. Upon addition of 5 ml Buffer E (20 mM Tris-Cl pH 8.0, 100 mM NaCl, 5% glycerol, 200 mM imidazole pH 7.9), 500 µl fractions were collected. Protein concentration and purity of the fractions were assessed using the Bradford reagent and SDS-PAGE with Coomassie staining. Fractions containing EI-His or HPr-His were pooled, concentrated, and desalted using Microcon centrifugal concentrators (Millipore). The proteins were stored at 4° C in 50 mM Tris-Cl pH 7.4, 5 mM MgCl$_2$, 5% Glycerol.

PEP carboxykinase (His-PEPCK) was expressed and purified from the *E. coli* strain C41(DE3) harboring plasmid pKSM879 (gift from K. McIver, University of Maryland). A

colony of the strain was used to inoculate three 2-L baffled flasks each containing 500 ml ZYP-5052 autoinduction medium (118). The cells were cultured at 37° C for 24 hours. After harvesting cells via centrifugation (10 min, 6200 x g, 4° C), the cell pellet was washed twice with 50 ml 100 mM NaH_2PO_4 pH 8.0 and stored at -80° C. The cell pellet was resuspended in 35 ml Buffer 1 (20 mM imidazole, 20 mM NaH_2PO_4, 500 mM NaCl, pH 7.4) containing Complete EDTA-free proteinase inhibitor and cell membranes were ruptured during five passages through a French Pressure Cell. The sample was centrifuged at 6200 x g at 4° C for 10 min. The soluble material was transferred to a new tube and centrifuged for 20 min at 20,000 x g and 4° C before applying to 2 ml NTA-Ni resin prewashed with Buffer 1. After binding for 1 h at 4° C, the resin was washed in batch using 8 ml Buffer 1. The resin was transferred to a gravity-flow column and subsequently washed with 25 ml Buffer 1. PEPCK was eluted from the resin with 10 ml Buffer 2 (500 mM imidazole, 20 mM NaH_2PO_4, 500 mM NaCl, pH 7.4). 20 µl Ni chelation buffer (250 mM EDTA, 50 mM NaH_2PO_4) was added per ml fraction and fractions containing His-PEPCK were dialyzed four times against 1 L Buffer 3 (20 mM Tris-Cl pH 7.4, 1 mM EDTA, 100 mM KCl). The induction and purification yielded 100 mg His-PEPCK.

2.11 Synthesis of ^{32}P-PEP

^{32}P-PEP was synthesized and isolated according to methods established previously (119) using γ-^{32}P-ATP (PerkinElmer, Waltham, Massachusetts) and PEPCK. 0.5 ml reactions containing 50 mM HEPES pH 7.5, 12.5 mM KF, 5 mM $MgCl_2$, 1 mM oxaloacetate, 500 µg PEPCK, 50 µM γ-^{32}P-ATP (2 mCi ml^{-1}, 10 Ci mmol^{-1}) were incubated for 5 min at room temperature (21° C). The reaction was diluted 10-fold with ddH_2O, and the newly synthesized ^{32}P-PEP was isolated via anion exchange chromatography using AG-1-X8 Bicarbonate resin. The hydroxide form of the AG-1-X8 resin (BioRad) was converted to the bicarbonate form according to the product manual. The PEP reaction was added to 2 ml of

resin and ^{32}P-PEP was eluted using a step-wise gradient consisting of 5 ml 0.3 M, 0.4 M, 0.6 M, and 0.7 M triethylammonium bicarbonate. ^{32}P-PEP was present in fractions containing 0.6 M and 0.7 M triethylammonium. The fractions were concentrated 5 fold via vacuum centrifugation in a vacufuge (Eppendorf, Hamburg, Germany).

2.12 *In vitro* Phosphotransfer Assay

Phosphotransfer assays were conducted using purified EI-His, HPr-His, and AtxA-His. Reactions contained 3 µg EI-His, 1.6 µg HPr-His, 2 µg AtxA-His in a total volume of 30 µl buffer (50 mM Tris-Cl pH 7.4, 5 mM MgCl$_2$). ^{32}P-PEP (0.5 µCi, 10 Ci mmol^{-1}) was added to a final concentration of 10 µM and the solutions were incubated for 30 min at 37° C. Reactions were quenched by adding SDS loading buffer (final concentration of loading buffer was 5% glycerol, 100 mM DTT, 2% SDS, 40 mM Tris-Cl pH 7.4). Samples were subjected to SDS-PAGE (12% poly-acrylamide SDS gel). The gels were dried and exposed to phosphor-imaging screen to detect ^{32}P-labeled protein. The screens were scanned using a STORM 840 scanner and analyzed with ImageJ software.

Chapter III

Analysis of the domains and DNA binding properties of AtxA, the virulence gene regulator of _B. anthracis_.

3.1 Introduction

B. anthracis virulence gene regulation requires AtxA, a protein encoded on the extrachromosomal virulence plasmid pXO1. In *atxA* mutant strains, toxin gene expression and capsule biosynthesis, the major *B. anthracis* virulence traits, are decreased severely and the organism is attenuated (46, 47, 49–54). The molecular function of AtxA is unknown; however, a model has been proposed that AtxA contains two functional regions (60). The amino-terminus of AtxA is predicted to bind DNA promoters via two putative DNA-binding elements. DNA-binding activity of AtxA is controlled via structural changes occurring within a regulatory region containing the carboxy-terminal PRDs and EIIB-like motifs (AtxA motifs are introduced in section 1.4).

The amino acid sequence of AtxA indicates that two types of helix-turn-helix motifs are present within the putative DNA-binding region: a winged helix-turn-helix (WH) and a classical helix-turn-helix (HTH). HTH motifs are the most common DNA-binding modules used in bacteria (120). Consisting of approximately 20 amino acids, HTH motifs contain two α-helices separated by a four-residue loop creating a 120° turn (121). The second helix is the recognition helix which binds the major groove of DNA forming base-specific contacts (122). Mutations in the recognition helix can disrupt DNA binding without altering the stability of the protein (91). The prototypical WH is arranged H1-S1-H2-H3-S2-W1-S3-W2. The HTH in the WH is H2 and H3, while the wings (W1 and W2) are loops which form between and after anti-parallel β sheets (S2 and S3) (123). The wings can contact the phosphate backbone or make specific hydrogen bonds to the DNA. There are examples of the wings facilitating protein-protein interactions (124, 125). Interestingly, WH motifs are known to undergo disorder-to-order shifts when small molecule cofactors are present (126). The classical HTH within AtxA has strong similarity to HTH-4 of Mga (see section 1.6 for an introduction to Mga). Mga HTH-4 binds specifically to DNA probes in electrophoretic

mobility shift assays (90, 91). Even with two putative DNA-binding motifs, AtxA has not been shown to bind specifically to target promoters.

Most DNA-binding proteins bind to a specific nucleotide sequence; however, a few proteins bind to unique structural elements within the DNA (127). The toxin gene promoters display no sequence similarity. Hadjifrangiskou and Koehler (58) determined the minimal functional promoters for the toxin genes, *pagA*, *lef*, and *cya*. No consensus sites were detected within these regions which ranged from 137 to 168 bp in length; however, the A+T content was significantly higher for the toxin gene promoters (79-85%) than the *B. anthracis* genome (64.6%, (4)). Considering high proportions of A+T bases indicate a high level of DNA curvature, Hadjifrangiskou and Koehler provided *in vitro* and *in silico* evidence that the *pagA*, *lef*, and *cya* promoters form 90° bends and distinct kinks. Given this information, AtxA may bind to a structural feature within the DNA and not a specific sequence.

One way to study protein-DNA interaction and the function of individual motifs within a protein is to investigate the domain organization of a protein via limited proteolysis and express each domain or motif independently. LicT, a *B. subtilis* protein containing an RNA binding motif and two PRDs, was studied using limited proteolysis and protein truncations. Data from limited proteolysis experiments suggested there are two major domains within the protein (128). When the motifs were expressed in isolation, each one was capable of maintaining some functional activity. The PRDs formed a homodimer and the RNA binding motif bound its RNA target sequence (129).

In this chapter, I describe a system for over-expression of AtxA in *B. anthracis* that allowed me to uncouple transcriptional control of *atxA* expression from *in vivo* studies of protein function. I present results from limited proteolysis experiments suggesting protease-resistant domains. The activity of truncated versions of AtxA, missing one or more motifs, in parent and *atxA*-null strains is assessed. Lastly, I determine the DNA binding affinity of AtxA and measure the effects of KCl concentration and pH on the degree of DNA binding.

3.2 Results

3.2.1 Induction of AtxA in *B. anthracis*

To study AtxA protein function *in vivo*, it is desirable to over-express the protein within *B. anthracis.* The *atxA* gene is subject to complex transcriptional control (Fig. 1-1). Moreover, the amount of AtxA in each cell is low (approximately 250 proteins per cell, Raynor and Koehler unpublished results). To overcome these complications, I developed an expression system that allows controlled induction of *atxA* expression resulting in specific levels of AtxA protein. The induced protein may be purified and used for *in vitro* analyses or utilized *in vivo* to answer questions regarding the function of AtxA. The inducible system was used in several experiments throughout my dissertation. Here I describe the expression pattern of AtxA when IPTG is titrated into cell cultures. I also demonstrate that the protein is functional when over-expressed.

I cloned the *atxA* gene downstream of the IPTG-inducible *hyper-spank* promoter (P*hs*) on a low-copy plasmid (pUTE657) and determined the amount of AtxA protein and activity gained in *B. anthracis.* P*hs* contains 2 *lacO* sequences that can bind the plasmid-encoded LacI repressor. IPTG binds to LacI to relieve the repression and allow transcription of the downstream gene. Using P*hs-gfp*, I determined that there was little variation in the amount of GFP expression within each cell in the culture indicating that IPTG activates transcription uniformly (data not shown). The plasmid containing P*hs-atxA* (pUTE658) was transformed into an *atxA*-null mutant of the ANR-1 strain harboring a P*lef-lacZ* transcriptional fusion (UT376). During early exponential growth in toxin-inducing medium (CACO$_3$), I added 10-60 μM IPTG to induce expression of *atxA*. Samples for AtxA Western blots and AtxA activity assays were collected at the transition to stationary phase (Fig. 3-1A). AtxA activity, defined by the amount of β-galactosidase activity resulting from expression of the P*lef-lacZ* reporter, increased in an IPTG dose-dependent manner (Fig. 3-1B). The AtxA activity in cultures induced with 10 μM IPTG was similar to the parent strain in which AtxA was
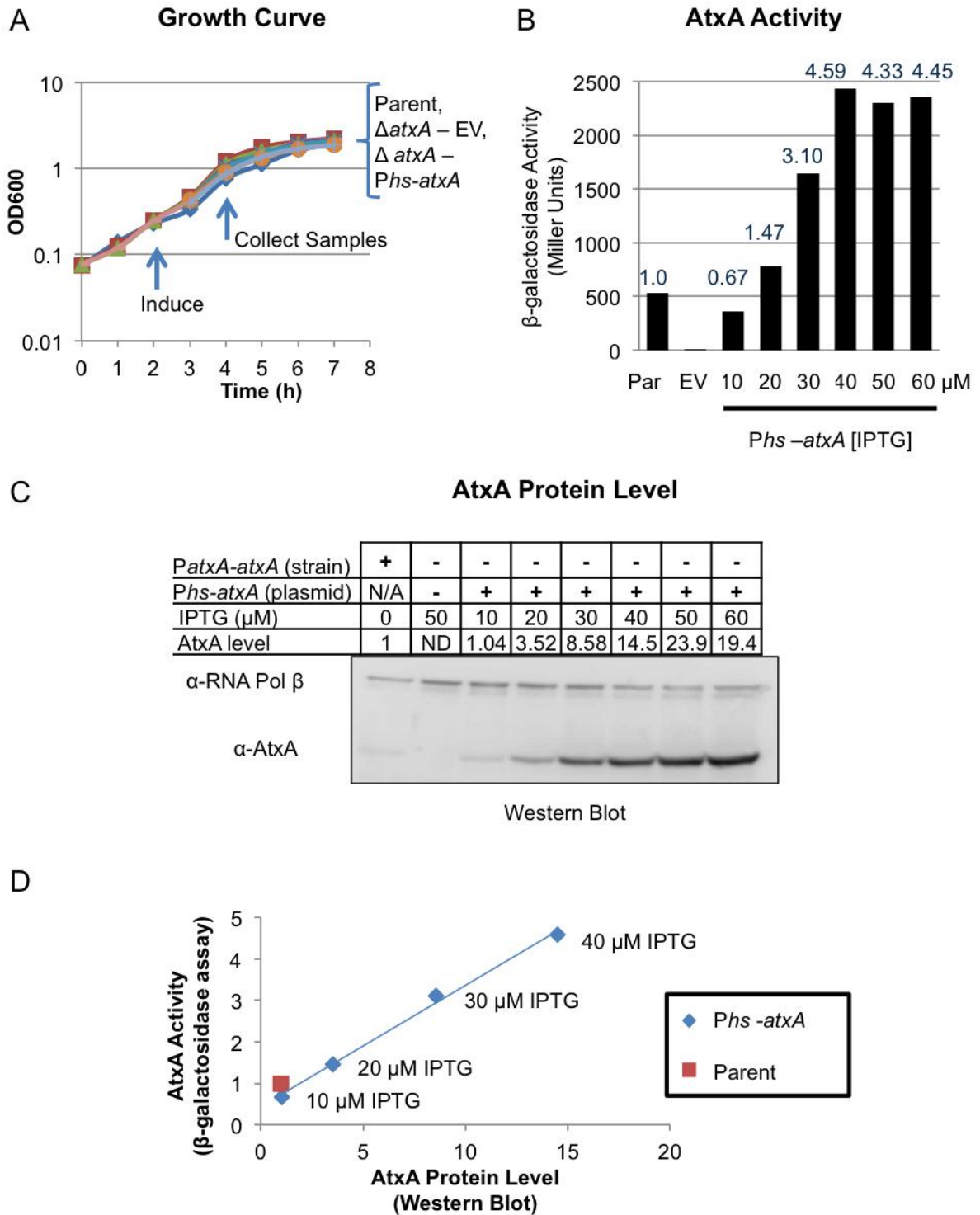
Figure 3-1. AtxA activity and protein amount after induction with IPTG.

Figure 3-1. AtxA activity and protein amount after induction with IPTG. A. In an *atxA-null strain* (UT376), production of AtxA (P*hs-atxA*, pUTE658) was induced (arrow, 2 h; OD_{600} 0.23 – 0.25) using 10 - 60 μM IPTG during growth in $CACO_3$. The parent strain (UT375) contained *atxA* at its native locus. The empty vector sample (EV) was derived from UT376 (pUTE657) that lacks *atxA.* Samples were obtained at the transition to stationary phase (arrow; 4 h; OD_{600} 1.2–1.7). B. The β -galactosidase activity of *B. anthracis* mutants harboring the P*lef-lacZ* reporter and IPTG-inducible *atxA* alleles was determined as described previously (130), and results from a representative experiment are shown.   The histograms represent the Miller Units. Values, normalized to the parent strain, are shown above each sample. C. AtxA and RNA Polymerase β subunit in soluble cell lysates were detected via immunoblotting. The AtxA levels indicated were normalized relative to the corresponding RNA polymerase β level.   D. The AtxA Protein Level of each sample was plotted in respect to the AtxA Activity. The concentration of IPTG in each culture is present next to each data point. The line of best fit is shown (R^2 = 0.9959).

produced from its native promoter. Inducing with 40 µM IPTG produced 4.59-fold more

activity, the highest amount of activity detected. Interestingly, AtxA activity did not increase

further when 50 or 60 µM IPTG was added even though the amount of AtxA protein changed.

AtxA protein levels increased upon IPTG addition (Fig. 3-1C). Induction of P*hs-atxA*

with 10 µM IPTG resulted in AtxA levels equal to the parent strain. Cells produced 23.9

times more AtxA than the parent strain when induced with 50 µM IPTG. In other

experiments, cells induced with 1 mM IPTG produced approximately 50-fold excess AtxA;

however the cells stopped replicating after adding IPTG (data not shown).

I plotted AtxA protein levels versus AtxA activity and saw a linear relationship

between these two parameters within a defined region (10 – 40 µM IPTG, Fig. 3-1D). These

results demonstrated that the steady state level of AtxA can be increased 25-fold above the

native level and that the induced AtxA is active.

3.2.2 AtxA contains two large domains

Domain organization of the five putative motifs of AtxA is poorly understood. The

structure of AtxA was probed using limited proteolysis, a facile method to detect well-folded

protein domains (131). Proteolytic enzymes cut proteins in regions where the protease-

specific sequences are solvent-accessible and flexible. Tightly-folded domains are resistant

to cleavage, whereas loops between the domains are sensitive.

I digested purified AtxA-His with trypsin and chymotrypsin. AtxA-His was induced in

E. coli and purified to greater than 90% homogeneity. Trypsin cuts after lysine or arginine

residues, and chymotrypsin cleaves primarily after aromatic amino acids. To prevent

complete digestion of AtxA, I incubated AtxA with a low concentration of protease. Both

proteases released one major product, an approximately 40-kDa fragment of AtxA (Fig. 3-

2A). The tryptic protein fragment was identified via mass spectrometry and amino-terminal
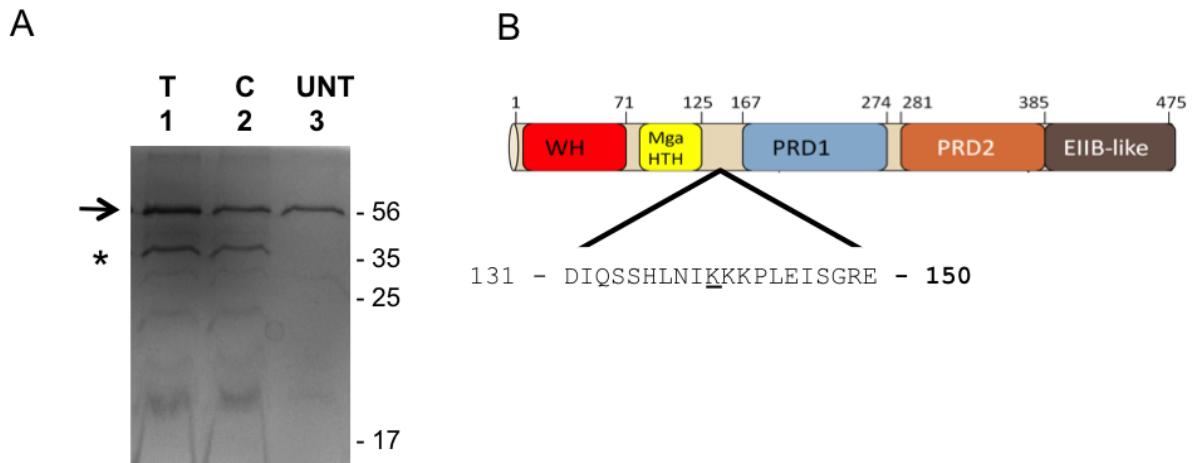
Figure 3-2. AtxA contains one major protease cleavage site. Affinity-purified AtxA-His was subjected to limited proteolysis with trypsin (T) and chymotrypsin (C) for 4h at 25° C. A. Coomassie-stained SDS-PAGE displays the major cleavage product (*). Full-length AtxA (arrow) is present in all samples, including the untreated control (UNT). B. Using amino-terminal sequencing, the dominant cleavage site after trypsin digest was identified as K140 (underlined).

sequencing as the last 335 amino acids of AtxA-His (AtxA$_{141-475}$, Fig. 3-2B). The major site of cleavage for chymotrypsin was not identified; however it may be Y129, L136, L143, or F155. These data suggested that AtxA contains two domains. The first domain encompassed the putative DNA-binding elements (AtxA$_{1-125}$), while the second consisted of the PRDs and EIIB-like motif (AtxA$_{167-475}$). The 41 amino acids between the domains (AtxA$_{126-166}$) may be a flexible, linker region.

3.2.3 The function of individual motifs of AtxA

The results from the limited proteolysis experiments guided the construction of several truncated versions of AtxA. As depicted in Fig. 3-3A, the AtxA truncations lack one or more motifs. I incorporated a carboxy-terminal FLAG or GFP-FLAG tag on each derivative of AtxA cloned into the IPTG-inducible vector pUTE657. FLAG-tagged proteins were distinct from AtxA when using the α-FLAG antibody. GFP-FLAG added 29 kDa and increased the stability of the truncated versions of AtxA. GFP also permitted the use of fluorescence microscopy to confirm expression of the protein.

The fragments of *atxA* were expressed in a parent strain and an *atxA* mutant containing the P*lef-lacZ* reporter (UT375 and UT376, respectively). After induction with 50 or 100 µM IPTG, the proteins were soluble within the cell and present at levels similar to full-length AtxA (data not shown). The AtxA protein derivatives were not functional in an *atxA*-null strain as no protein provided P*lef-lacZ* activity greater than the empty vector control (Fig. 3-3B). These results suggest that all the motifs were necessary for AtxA to function properly. The activity of native AtxA was not affected by the protein fragments with the exception of AtxA$_{167-385}$–GFP-FLAG and AtxA$_{167-475}$–GFP-FLAG (Fig. 3-3C). Only 40% of the parent strain activity was detected during expression of these protein fragments, which include the PRDs. The data suggest that AtxA$_{167-385}$–GFP-FLAG and AtxA$_{167-475}$–GFP-FLAG may be dominant negative and function to titrate a signal from AtxA. An alternate explanation is that the
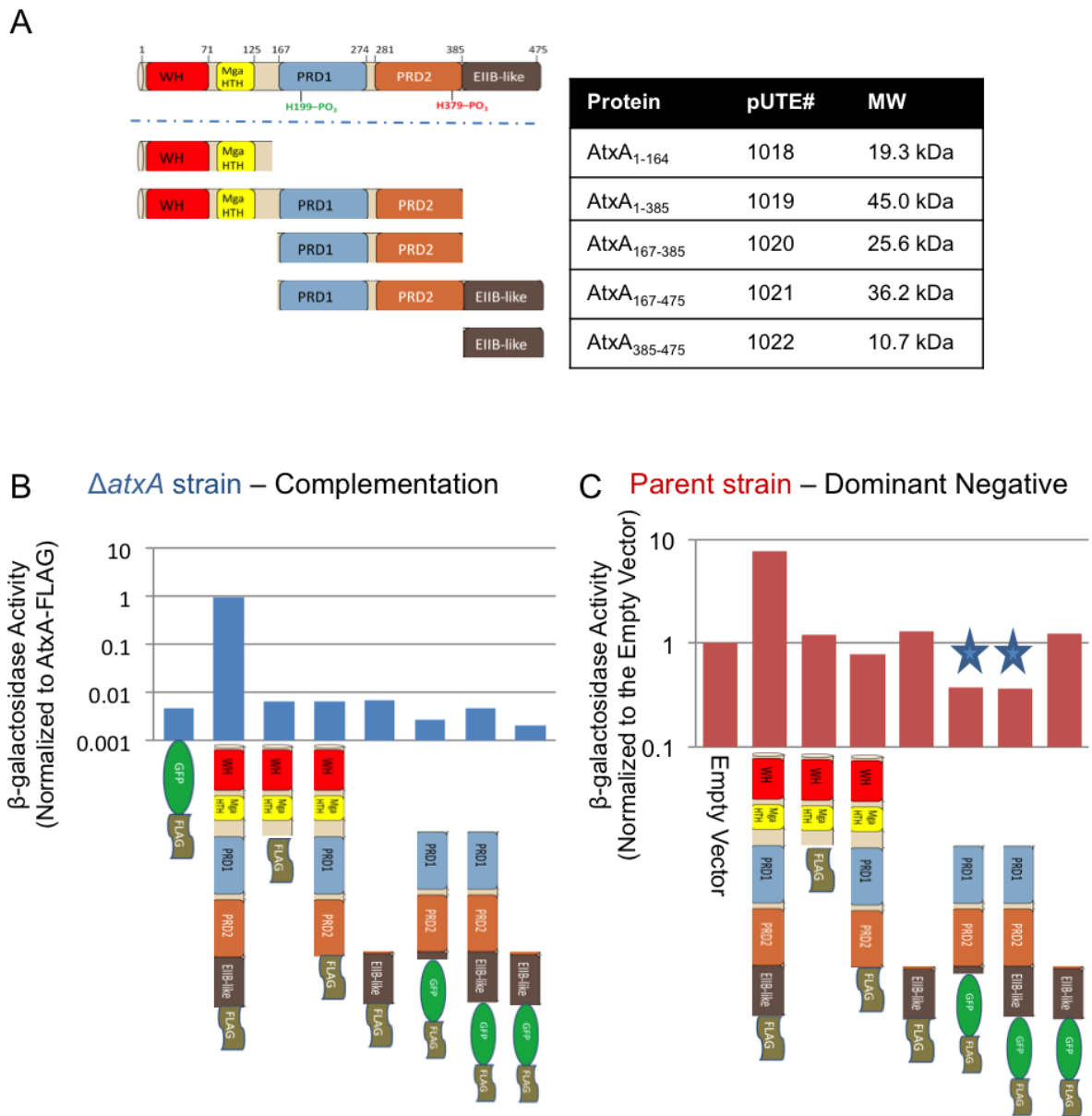
Figure 3-3. AtxA activity of the AtxA motifs *in vivo*. A. AtxA contains five putative motifs as shown in the schematic. Five truncated AtxA proteins (containing one or more of the motifs fused to FLAG or GFP-FLAG tags on the carboxy-terminus) were placed under the control of the IPTG-inducible P*hs* (pUTE657) to make pUTE1018-1022. B. and C. The *atxA*-null and parent strains harboring P*lef-lacZ* (UT376 and UT375, respectively) and the AtxA truncations were cultured in $CACO_3$. Cultures were induced during early exponential phase and samples were collected at the transition to stationary phase for β-galactosidase activity assays. Graphs show the β-galactosidase activity normalized to the AtxA-FLAG sample (B, Δ*atxA* strain) or to the empty vector (C, Parent strain). Note the change in scale of the y-axes. Cartoons below each bar represent the tagged AtxA fragment induced in each sample. AtxA$_{167-385}$–GFP-FLAG and AtxA$_{167-475}$–GFP-FLAG decrease native AtxA activity (blue stars).

45

fragments prevent full-length AtxA from functioning via protein-protein contacts. Notably, AtxA$_{1-385}$–FLAG and AtxA$_{385-475}$–GFP-FLAG did not diminish AtxA activity. Each of these AtxA protein truncations contains the PRDs, the EIIB-like motif, or the GFP-FLAG fusion; therefore, the reason for the dominant negative phenotype is unknown. These data provide an initial analysis of the function of each AtxA region.

3.2.4 AtxA binds DNA non-specifically

WH and HTH motifs indicate that AtxA binds to specific promoter elements; however, there does not appear to be a consensus sequence within the promoters of the AtxA-regulated toxin genes *pagA*, *lef*, and *cya* (58). To investigate if AtxA interacts directly and specifically with DNA, I conducted *in vitro* DNA-binding using filter binding assays. A constant amount of ^{32}P-labeled DNA and increasing concentrations of AtxA-His were mixed in Tris buffer containing 150 mM KCl at pH 7.5. The protein, which was purified from *E. coli*, was bound to a nitrocellulose membrane, and the AtxA-DNA association equaled the intensity of the radioactive signal. For DNA probes, I used a promoter from an AtxA-regulated toxin gene (P*lef*), promoters from *B. anthracis* genes that are AtxA-independent (P*bla1* and P*papR*), and sequence from an *E. coli* expression vector (pET23d). The binding curves indicated that AtxA binds to all probes with high affinity and no specificity (Fig. 3-4). The dissociation constant (Kd) of the AtxA-DNA interaction is below 1 nM. A low nanomolar Kd is significant and suggests that AtxA binds DNA *in vivo*.

In order to determine if the interaction between AtxA and DNA is facilitated by ionic interactions, I performed DNA binding assays with different pH or KCl concentrations. AtxA bound less effectively to the *lef* promoter and a segment of pET23d as the KCl concentration increased from 22 mM to 300 mM (Fig. 3-5A). 22 mM KCl promoted the greatest amount of AtxA-DNA interaction. 300 mM KCl abolished AtxA binding to DNA. Lowering the pH from 7.5 to 6.8 increased the amount of DNA bound by 20 nM AtxA (Fig. 3-5B). AtxA-DNA
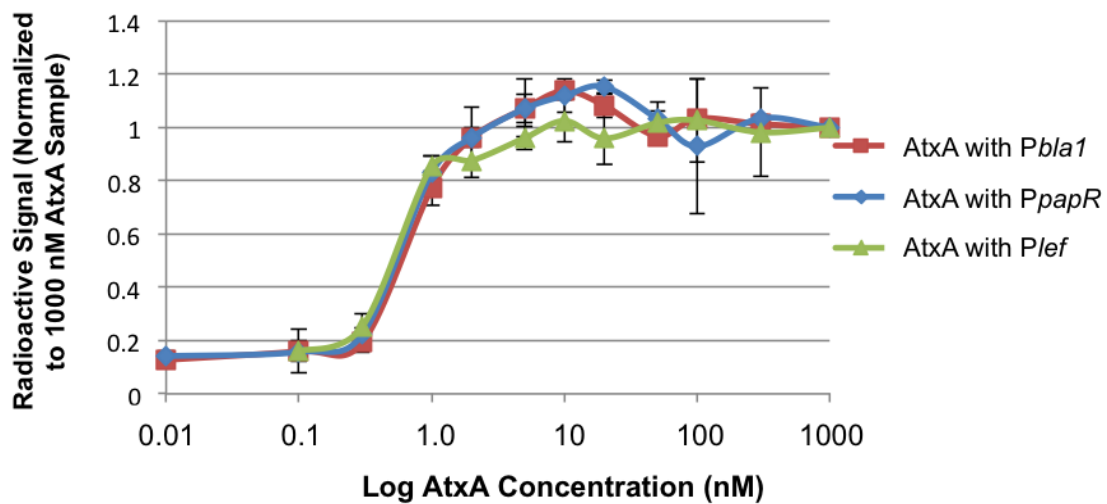
Figure 3-4. AtxA binds DNA non-specifically with high affinity. Filter Binding Assays were used to probe the interaction between affinity-purified AtxA-His and non-specific control promoter sequences (P*bla1*, 267 bp, and P*papR*, 169 bp) or an AtxA-dependent promoter (P*lef*, 167 bp). A six-log range of protein concentration was used with a constant amount of ^{32}P-labeled DNA (0.3 nM) in 150 mM KCl, 10 mM Tris-Cl, 5 mM $MgCl_2$, 5 mM DTT, 3% glycerol, 0.1 mg/ml BSA, pH 7.5. The radioactive signal from triplicate reactions was averaged and normalized to the sample containing 1000 nM AtxA. Error bars represent ±1 SD.

interaction did not change when the pH was increased from 7.5 to 8.5 or 9.1. Altering the KCl concentration or pH did not result in specific DNA binding. AtxA bound to the target and control promoters with similar affinities. These data indicate that an AtxA-DNA interaction is dependent on the KCl concentration; however, increasing pH of the solution above 7.5 did not have a great effect.

3.3 Discussion

In this chapter, I have described the IPTG-inducible system for AtxA expression in *B. anthracis*, analysis of the domain organization and motifs of AtxA, and an initial characterization of the DNA binding properties of AtxA.

Expression of *atxA* using a heterologous promoter led to a 25-fold higher AtxA concentration and a 4.5-fold increase in P*lef-lacZ* expression. Preliminary experiments performed by others in our laboratory indicate that there are as few as 250 AtxA molecules per cell when AtxA is expressed from its native promoter (unpublished 2010). The low level of AtxA makes it challenging to detect the protein in *B. anthracis* cells. Controlling AtxA via an IPTG-inducible promoter allows over-expression of AtxA-His for purification, production of mutant forms of AtxA (point mutations and truncated versions), and induction of AtxA in conditions that do not favor AtxA activity.

The relationship between AtxA protein level and AtxA activity suggests that AtxA is limiting for *lef* expression. Induction of AtxA with 10 µM IPTG produced native levels of AtxA protein and activity, and a slight increase in IPTG concentration led to increased AtxA and P*lef-lacZ* expression. Control experiments showed that IPTG did not induce expression of the toxin genes in the parent strain (lacks P*hs-atxA*). Therefore, elevated P*lef-lacZ* upon the addition of IPTG to cells containing the P*hs-atxA* was due to higher AtxA protein levels. If AtxA was not limiting, increased AtxA protein would not lead to higher *lef* transcript levels.
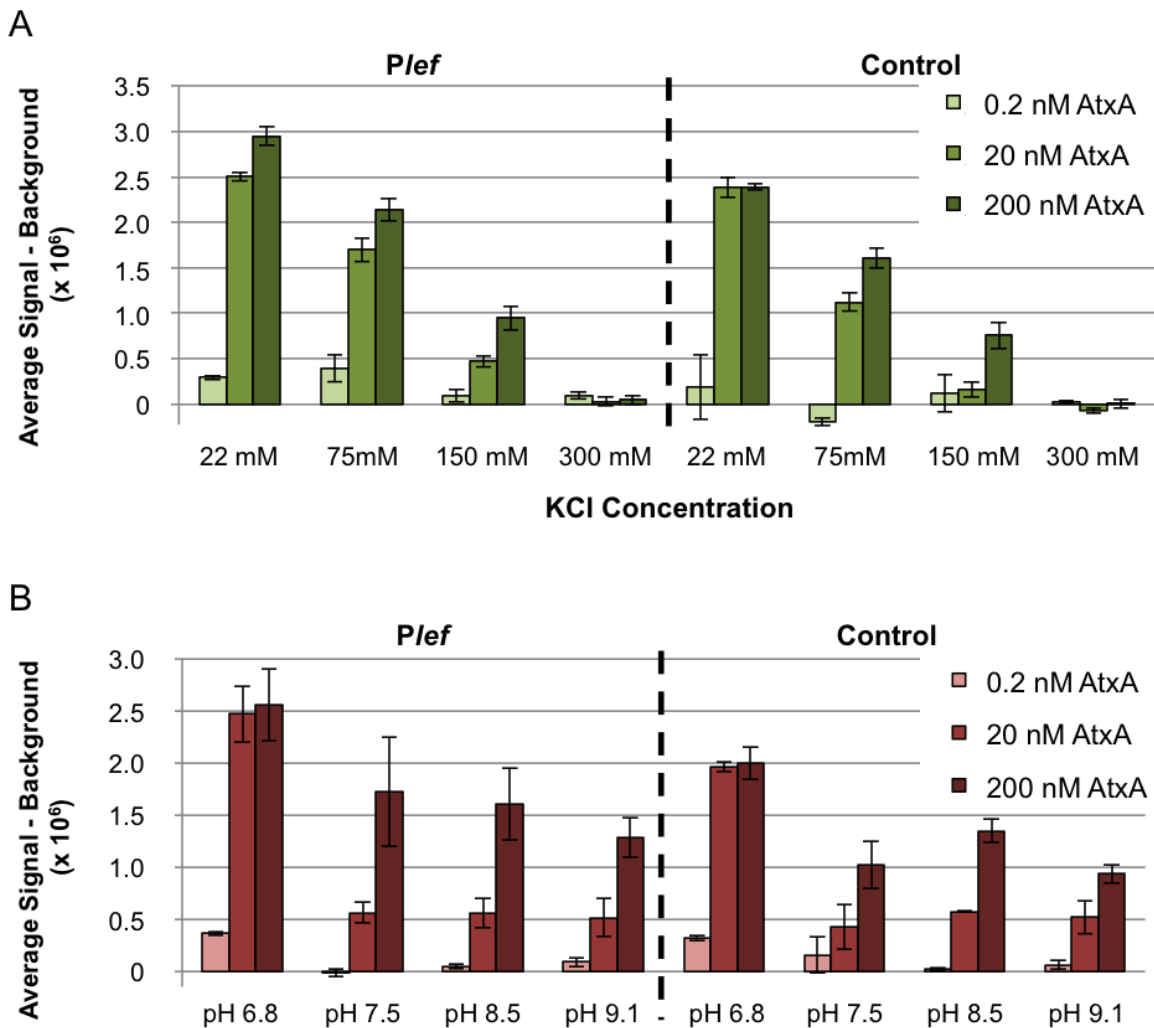
Figure 3-5. AtxA-DNA binding is sensitive to KCl concentration but not to pH. Affinity-purified AtxA-His and P*lef* (167 bp) or a control DNA probe (179bp of the plasmid pET23d) were subjected to Filter Binding Assays. 0.2 nM, 20 nM, or 200 nM AtxA was mixed with a standard amount of ^{32}P-labeled DNA (0.3 nM) in 150 mM KCl, 10 mM Tris-Cl, 5 mM $MgCl_2$, 5 mM DTT, 3% glycerol, 0.1 mg/ml BSA, pH 7.5. A. The concentration of KCl was changed to 22 mM, 75 mM, 150 mM, or 300 mM. B. AtxA-DNA interactions were probed in a Tris buffer at pH 6.8, 7.5, 8.5 or 9.1. Each column represents the average radioactive signal minus the background signal (DNA alone) of an experiment done in duplicate. Error bars represent ±1 SD.

Although AtxA may be a limiting factor for toxin gene expression under native conditions, the data also suggest that AtxA does not act independently. Soluble AtxA protein levels increased from 14.5 to 23.9 times the parent concentration between 40 and 50 µM IPTG; however, AtxA activity plateaued when cells were induced with 40, 50, or 60 µM IPTG. If AtxA acted independently, then I would expect AtxA activity to be highest in cultures induced with 50 µM IPTG. I was not able to determine the identity of the limiting factor in the process when AtxA activity is at its maximum. Two possible explanations are that P*lef-lacZ* transcription rate may be at its maximum or the cellular amount of a post-translational signal, ligand, or binding protein may have been exhausted.

The IPTG-inducible promoter allows the study of the AtxA motifs by expressing truncated forms of AtxA. As I describe in the introduction (section 1.7), I favor a model in which AtxA contains two functional domains. The amino-terminal region appears to bind DNA, and the remainder of the protein regulates the DNA binding activity. Limited proteolysis supports this model: the final 335 amino acids of AtxA are resistant to digest with trypsin or chymotrypsin. Due to the numerous trypsin cut sites (58 in total, 39 downstream of the dominant site of digestion K140), AtxA is expected to be completely digested during an extended reaction. The 40-kDa product could only be present if that region of the protein was a well-folded domain where trypsin could not cleave.

The protease-resistant AtxA fragment contains two PRDs and an EIIB-like motif. When I expressed these motifs fused to a carboxy-terminal GFP-FLAG tag (AtxA$_{167-475}$–GFP-FLAG) in an *atxA*-null strain, little *lef* expression was detected from the P*lef-lacZ* reporter. In the parent strain, AtxA$_{167-475}$–GFP-FLAG decreased the amount of AtxA activity by 60%. AtxA$_{167-385}$–GFP-FLAG, which contains only the PRDs, displayed a similar phenotype. These data suggested that while the PRDs were not capable of complementing *atxA*, they were able to produce a dominant negative phenotype in the parent strain.

Why were the PRDs able to cause a decrease in toxin gene expression in the parent strain? One possible explanation is that the PRDs (with or without the EIIB motif) could complex with AtxA or another protein. In Chapter 4, I describe experiments which indicate that AtxA forms a homomultimer *in vivo,* and I propose that the EIIB-like motif facilitates AtxA-AtxA interactions. A second explanation for the dominant negative phenotype is that a signal was titrated from AtxA by $AtxA_{167-385}$–GFP-FLAG and $AtxA_{167-475}$–GFP-FLAG. The protein(s) that phosphorylate H199 and H379 may modify the protein fragments instead of full length AtxA. In this scenario, the PRDs would serve as phosphate sinks. Future experiments are needed to understand fully why $AtxA_{167-385}$–GFP-FLAG and $AtxA_{167-475}$–GFP-FLAG caused a dominant negative phenotype. One confounding factor is that $AtxA_{1-385}$, containing the DNA binding motifs and the PRDs, did not reduce the activity of AtxA in the parent strain. I speculate that $AtxA_{1-385}$ does not exhibit a dominant negative phenotype because the DNA-binding motifs disrupt the protein-protein interaction and/or ligand binding.

Included in $AtxA_{1-138}$ are the amino-terminal WH and/or HTH which are predicted to bind DNA. The protein fragment failed to complement an *atxA*-null strain suggesting that the motifs require the rest of the protein to function properly. Alternatively, the truncation could have been misfolded. Although it is unknown if $AtxA_{1-138}$ binds DNA *in vivo*, the protein can be tested using the filter binding assay.

Purified AtxA-His bound without sequence specificity to DNA with sub-nanomolar affinity in a filter binding assay. The binding affinity of the AtxA-DNA interaction is quite significant as other specific DNA binding proteins have affinities less than 10 nM (132, 133). Mga and MtlR are proteins with motifs similar to AtxA and bind specifically to DNA. MtlR binds to five regions spanning 45 bp upstream of the -35 consensus sequence within a target promoter (84). The DNA binding affinity of MtlR changes from 3.4 nM to 1300 nM depending on the phosphorylation state of MtlR. Similar to MtlR, Mga specifically binds to several promoters and protects a 45 bp region adjacent to the -35 consensus sequences of the *emm*

and *scpA6* genes (90). The studies with MtlR and Mga suggest that specific conditions within the experiment (pH or salt) or mutated versions of AtxA can be determined to promote specific DNA binding.

I altered the salt concentration and pH of the experiment and determined that the DNA binding affinity of AtxA decreased as the KCl concentration increased. Changing the ionic strength of the buffer may have interfered with AtxA contacts on the phosphate backbone of the DNA. Protein-phosphate interactions are DNA sequence-independent by nature, because any positively charged amino acid can interact with the anionic phosphate. However, several DNA-binding proteins contact the phosphate backbone to increase the stability of the protein-DNA complex (126). My results show that disrupting the ionic interactions between AtxA and DNA has a major effect on the binding properties of AtxA.

On the other hand, changing the pH of the reaction did not have a severe effect. The affinity of AtxA to DNA increased at pH 6.8. A dose-dependent binding curve was established independent of the pH (from 6.8 to 9.1). This was surprising, since changing the pH will change the net charge of AtxA. The isoelectric point (pI) of AtxA is predicted to be 9.3. The net charge of AtxA is ~14 at pH 6.8, ~12 at pH 7.5, ~ 7 at pH 8.5, and ~3 at pH 9.1. The pI of the DNA binding region of AtxA (residues 1-164) is 9.73; therefore the net charge of the region would be slightly greater than full length AtxA. These results suggest that there are sequence-specific sites of AtxA-DNA interaction.

The filter binding assays have shown that AtxA has a high affinity for DNA and that the AtxA-DNA affinity can be altered with KCl, but not pH. However, AtxA bound to DNA non-specifically in this assay. As you will see in the coming chapters, AtxA forms a multimeric structure in specific growth conditions (elevated CO_2/bicarbonate) and phosphorylation of AtxA affects the activity of AtxA. Could a ligand or post-translational modification be needed for AtxA to interact to only its target promoters? Future experiments

should use AtxA point mutations that mimic phosphorylation and utilize buffer conditions that

contain potential AtxA ligands.

Chapter IV

The _B. anthracis_ virulence regulator AtxA: oligomeric state,

function, and CO$_2$-signaling

4.1 Introduction

Regulation of protein function can occur in the form of modulation between a non-active state and an active form of the protein. In several cases, the transition between each state is mediated via post-translational modification and/or ligand binding which induce changes to the protein structure. Protein multimerization may result from the altered structure. Understanding the forms of a protein *in vivo* provides clues to the function of the protein and the mechanism(s) needed to activate the protein. For example, dimerization of the PRD-containing proteins, LicT and BglG, is affected by phosphorylation (79, 80, 128, 134). LicT, when phosphorylated within PRD2, forms a homodimer due to stabilization of the complex via salt bridges forming between the phosphohistidine residues and two arginines (135). Conversely, phosphorylation of PRD1 prevents dimerization via electrostatic repulsion between the phosphohistidines and a glutamic acid residue. The regulation of the form and function of LicT provides the impetus for me to study the multimeric state of AtxA, the PRD-containing virulence gene regulator of *B. anthracis*.

"The molecular basis for AtxA function as a positive regulator of B. anthracis virulence genes has not been established. As described in section 1.4, the amino acid sequence of AtxA reveals a number of motifs associated with potential functional domains. The amino terminal region of the protein contains adjacent winged helix and helix-turn-helix (HTH) motifs. The central region of the AtxA amino acid sequence reveals motifs suggesting two phosphoenolpyruvate:carbohydrate phospho-transferase system (PTS) regulation domains (PRDs). PRDs are generally found in bacterial proteins that function to activate or anti-terminate transcription of genes involved in the metabolism of specific carbohydrates (73). Transcriptional profiling studies have not revealed AtxA targets associated with catabolism (57), but Tsvetanova et al. (59) reported that phosphorylation of specific histidine residues, H199 and H379, each within a PRD, impacts AtxA activity.

"A key host-related signal associated with AtxA-regulated gene expression is CO_2/bicarbonate. Growth of *B. anthracis* in 5% or greater atmospheric CO_2 in buffered medium results in elevated transcription of the toxin, capsule, and other AtxA-regulated genes (47, 49, 50, 69–71). Some studies suggest that the CO_2/bicarbonate effect on toxin genes occurs in an *atxA*-dependent manner (47, 54, 64, 72), yet the signal does not appear to significantly affect steady state levels of *atxA* transcript or AtxA protein (64, 95). Moreover, a protein-ligand relationship between CO_2/bicarbonate and AtxA has not been established, nor have additional proteins associated with AtxA function been identified.

"In this chapter I provide data indicating that AtxA exists in a homo-oligomeric state and that AtxA-AtxA contacts occur within a previously uncharacterized carboxy-terminal EIIB-like motif. I also show a correlation between growth in elevated CO_2/bicarbonate, the steady state level of AtxA multimer, and AtxA activity." (102)

4.2 Results

4.2.1 AtxA activity *in vivo*

"AtxA is a cytoplasmic protein with a predicted MW of 55.6 kDa (46). Some functional domains have been postulated (59, 60); however, the structure of AtxA has not been solved. Moreover, the multimeric state of AtxA *in vivo* and whether AtxA associates with other *B. anthracis* proteins, have not been discerned.

"Expression of the *atxA* gene is highly regulated. Therefore, to investigate AtxA form and function *in vivo*, I developed a system to control AtxA protein levels and quantitatively assess AtxA activity in *B. anthracis*. Alleles of *atxA* encoding native, mutant, and C-terminal epitope-tagged versions of the protein were cloned such that expression was under control of the IPTG-inducible hyper-spank promoter on a low copy number plasmid, pUTE657. Recombinant epitope-tagged proteins, AtxA-His and

AtxA-FLAG, facilitated immuno-detection and purification from *B. anthracis*. AtxA positively controls transcription of multiple genes in *B. anthracis*, although a direct interaction of the AtxA protein with promoters of target genes has not been demonstrated. One of the genes most strongly regulated by AtxA is *lef*, encoding the lethal factor protein, a component of the anthrax toxin (57). Plasmids bearing IPTG-inducible *atxA* alleles were introduced into a *B. anthracis* strain (UT376) which harbors a markerless deletion of *atxA* and a transcriptional reporter, P*lef-lacZ*, at the native *lef* locus on pXO1. AtxA activity was quantified by measuring β-galactosidase activity following IPTG induction of the *atxA* alleles.

"Strains were cultured in $CACO_3$ in a 5% CO_2 atmosphere, conditions shown previously to be conducive for *atxA*-controlled toxin gene expression (49). Figure 4-1 shows relative AtxA levels and activities in *B. anthracis* cultures expressing native AtxA, AtxA-His and AtxA-FLAG. RNA polymerase β subunit was used as a loading control. Induction with 30 μM IPTG yielded levels of epitope-tagged proteins that were comparable to untagged AtxA (Fig. 4-1A), indicating that protein stability was unaltered by the C-terminal His- and FLAG-tags. The cultures also displayed similar levels of β-galactosidase activity (Fig. 4-1B), indicating that the recombinant proteins do not exhibit altered function. The amount of induced AtxA is 8.5-fold greater than the level of AtxA expressed from its native promoter on pXO1 and results in 3-fold more β-galactosidase activity (data not shown). Notably, expression of the P*lef-lacZ* fusion in the *atxA*-null strain containing the empty vector (pUTE657) was barely detectable, confirming previous reports that transcriptional control of the *lef* gene is highly dependent upon AtxA (46, 49)." (102)
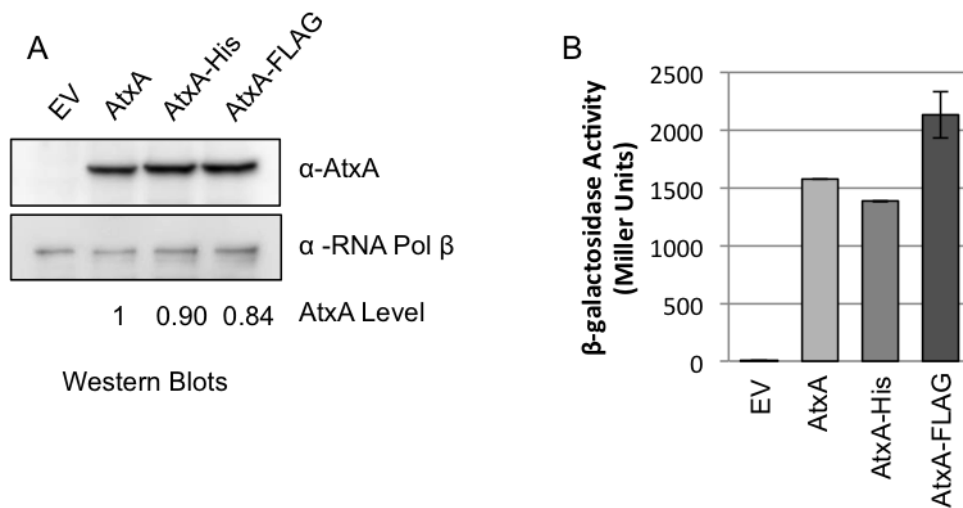
Figure 4-1. *In vivo* activity of AtxA-His and AtxA-FLAG. In an atxA-null strain (UT376), production of AtxA (pUTE658), AtxA-His (pUTE991) and AtxA-FLAG (pUTE992) was induced using 30 µM IPTG during growth in CACO3. The empty vector sample (EV) was derived from UT376 (pUTE657) that lacks atxA. Samples were obtained at the transition to stationary phase (4 h; OD600 1.2–1.7). A. AtxA and RNA Polymerase β subunit in soluble cell lysates were detected via immunoblotting. The AtxA levels indicated were normalized relative to the corresponding RNA polymerase β level. B. The β -galactosidase activity of B. anthracis mutants harboring the Plef-lacZ reporter and IPTG-inducible atxA alleles was determined as described previously (130). Error bars represent ±1 SD.

4.2.2 Multimerization of AtxA

"*In vivo* AtxA – protein interactions are of interest because DNA-binding proteins and proteins containing PRDs often function as dimers (79, 80, 126, 128, 134). Furthermore, some investigations have suggested that an additional factor is required for AtxA function (47, 59). To explore possible protein-protein interactions, I subjected lysates from *B. anthracis* strains producing native AtxA to Blue Native PAGE (BN-PAGE) to determine the migration pattern of AtxA in native conditions. Electrophoresed proteins were transferred to membranes and probed with α-AtxA antibody. The mobility of immuno-reactive bands relative to molecular weight markers suggested that AtxA was in a complex (Fig. 4-2A).

"To test for stable interactions between AtxA and other cytosolic proteins, I subjected cell lysates of *B. anthracis* cells producing AtxA-His to affinity purification using NTA-Ni resin. Purified AtxA-His was analyzed using BN-PAGE and denaturing PAGE. Western hybridization using α-AtxA serum revealed three major bands migrating at approximately 110 kDa, 225 kDa, and > 225 kDa and a minor band migrating at approximately 60 kDa (Fig. 4-2A). In contrast, Coomassie staining after SDS-PAGE revealed only one band in the AtxA-His eluate and its gel mobility was consistent with the size of an AtxA-His monomer (56 kDa) (Fig 4-2B). Since no other proteins were detected in the AtxA-His eluate via SDS-PAGE and the protein mobilized as multiple species on BN-PAGE, these results suggested that AtxA forms multiple homomeric complexes in cell lysates.

"To detect association of two or more monomers of AtxA, I combined culture lysates of *B. anthracis* strains producing AtxA-His or AtxA-FLAG and used affinity chromatography to purify AtxA-His. A lysate from a *B. anthracis* strain producing GFP-FLAG was used as a control. Lysates were derived from pools of cultures containing (1) AtxA-His and GFP-FLAG, (2) AtxA-His and AtxA-FLAG, and (3) AtxA-
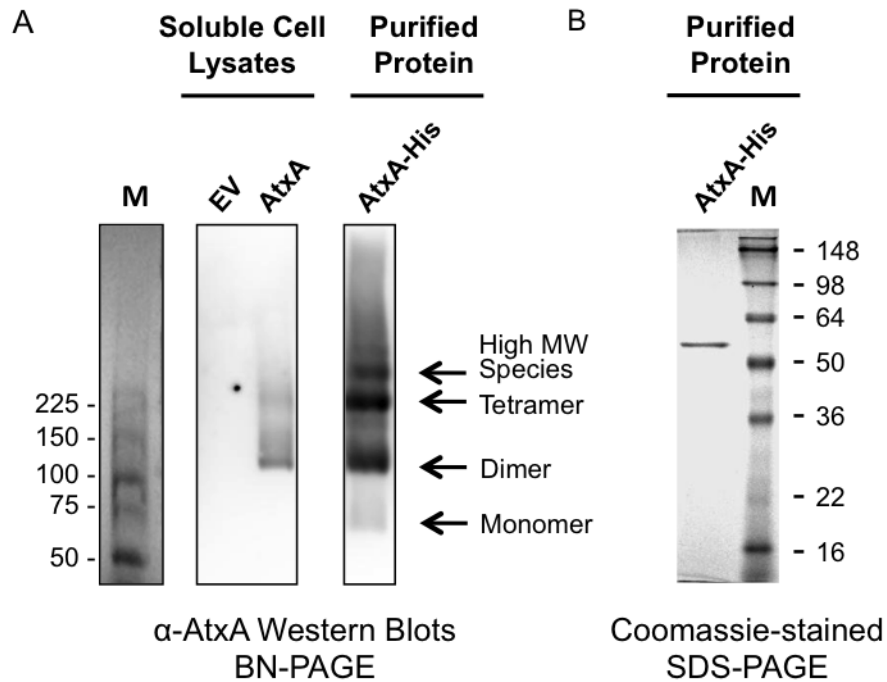
Figure 4-2. Oligomeric states of AtxA. (A) Lysates from *B. anthracis* strains UT376 (pUTE657) and UT376 (pUTE658), containing an empty vector (EV) and IPTG-inducible *atxA* respectively, and affinity-purified AtxA-His were electrophoresed on BN polyacrylamide gels. AtxA protein was detected using Western blotting. M = molecular weight markers (ProSieve Unstained Protein Marker, VWR). (B) Affinity purified AtxA-His from *B. anthracis* UT376 (pUTE991) was subjected to SDS-PAGE and stained with Coomassie. M = molecular weight markers (SeeBlue Plus2 Pre-Stained Standard, Invitrogen).

FLAG and GFP-FLAG. Proteins were captured using NTA-Ni resin, eluted with imidazole, and detected by Western blotting. As shown in Figure 4-3 (lanes 1-3), prior to affinity purification each tagged protein was detected in the appropriate pools. Eluates from NTA-Ni resin are shown in lanes 4-6. AtxA-FLAG was detected in the eluate only when combined with AtxA-His (lane 5). GFP-FLAG served as a negative control to ensure that non-specific proteins were washed from the NTA-Ni resin and that the His and FLAG tags did not interact. These results demonstrate that AtxA-His and AtxA-FLAG form a stable complex *in vitro*. Considering these data and the results from BN-PAGE, I conclude that AtxA self-associates to form dimers, tetramers, and higher MW species." (102)

4.2.3 Role of the carboxy-terminal region of AtxA in multimerization

"To further explore the properties of AtxA multimerization, I tested for the ability of the cross-linking reagent BMH to covalently fix AtxA complexes in cell lysates. BMH reacts specifically and irreversibly to link cysteine residues within 13Å. AtxA has cysteine residues at positions 96, 161, 202, 356, 370, and 402 (Fig. 4-5A). A cell lysate from an IPTG-induced culture expressing AtxA was treated with BMH, subjected to SDS-PAGE, and probed for AtxA via Western blot (Fig. 4-4). Two bands were detected slightly above the 98-kDa marker when the lysate was treated with BMH (lane 6), while a single band near the 50-kDa marker was detected in an untreated lysate (lane 2). The predicted molecular weight of AtxA is 55.6 kDa; therefore, the approximately 100-kDa bands may represent two AtxA proteins joined via BMH. The appearance of the doublet band indicates two separate AtxA complexes present in the cross-linked lysate. To investigate the composition of the protein complexes, I affinity purified AtxA-His from an *atxA*-null strain and subjected the protein to BMH cross-linking. The migration pattern of cross-linked, purified AtxA-
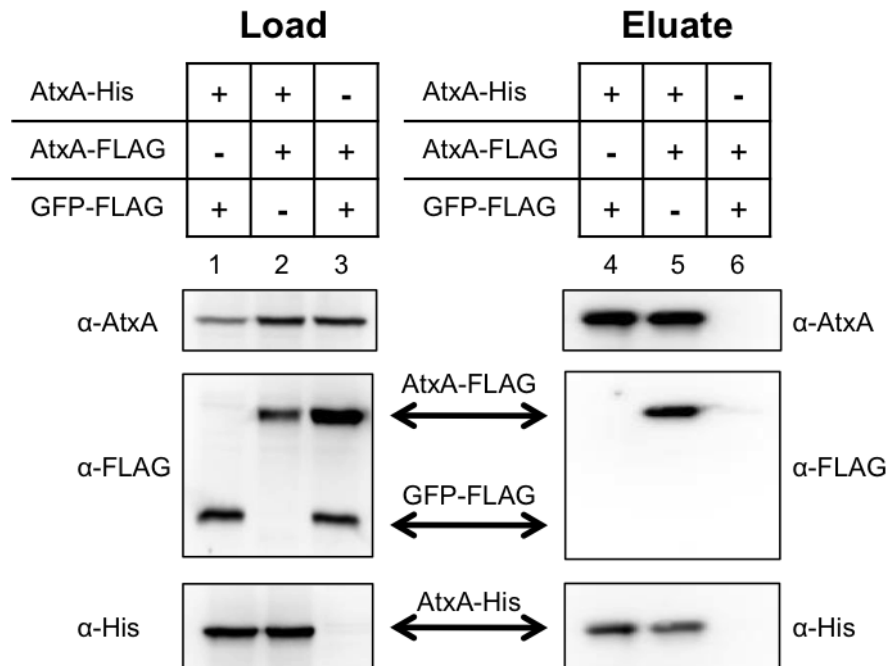
Figure 4-3. Specific binding of AtxA-His to AtxA-FLAG. Lysates from *B. anthracis atxA*-null strains (UT376) containing AtxA-His (pUTE991), AtxA-FLAG (pUTE992), or GFP-FLAG (pUTE1013) induced with 30 µM IPTG were subjected to co-affinity purification using NTA-Ni resin. Western blots probed with α-AtxA, α-FLAG, and α-His antibodies were performed on soluble cell lysates (Load, lanes 1-3) and purified proteins (Eluate, lanes 4-6).
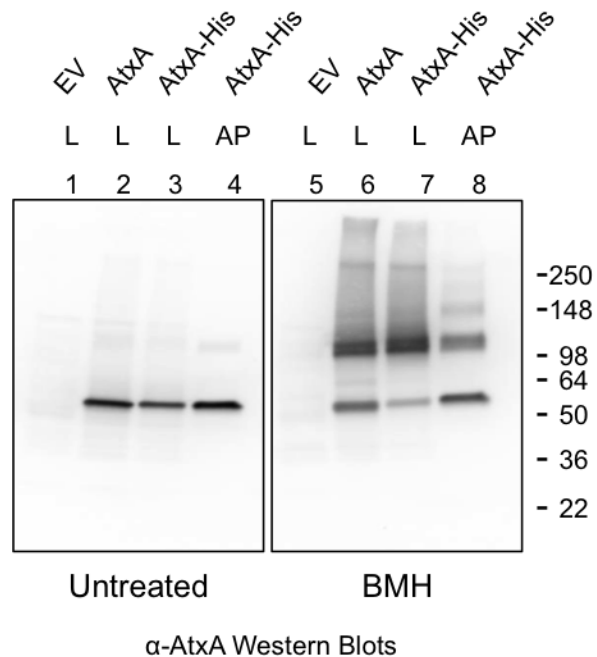
Figure 4-4. Fixation of AtxA complexes with a cysteine-reactive cross-linking agent.
Cultures of the *atxA*-null strain UT376 containing pUTE658 (encoding AtxA) or pUTE991 (encoding AtxA-His) were induced with 40 µM IPTG. Cell lysates or affinity-purified AtxA-His were treated with the cross-linking agent BMH. SDS-PAGE (4-15%) and Western blots with AtxA-specific antibody were used to detect various forms of AtxA. EV = empty vector, L = cell lysate, and AP = affinity-purified. Molecular weights of the protein standards are listed (SeeBlue Plus2, Invitrogen).

His was similar to that observed for AtxA and AtxA-His cross-linked in cell lysates (Fig. 4-4, lanes 6-8); a doublet band migrated near the 98-kDa molecular weight marker. I conclude that the doublet does not result from AtxA linked to another protein. Rather, the doublet suggests at least two conformational states of the dimeric AtxA complex.

"BMH-mediated cross-linking of AtxA proteins allowed me to test for region(s) at the interface of AtxA multimers. I created strains harboring distinct *atxA* Cys→Ser alleles (Fig. 4-5A). Mutant AtxA proteins were expressed in the *atxA*-null background and cell lysates were reacted with BMH. The presence of the dimer band in lysates containing mutated AtxA (Fig. 4-5B) indicates that these proteins are capable of multimerization and are cross-linked with BMH. The lysate containing AtxA C402S differed significantly from lysates containing other AtxA mutants. The AtxA C402S sample contained a relatively low level of cross-linked protein and a high level of the apparent monomer. This result suggests that C402 is the major site of BMH crosslinking, but some other Cys residue(s) can participate in cross-linking.

"To determine if the dominant BMH cross-link occurs between C402 of two AtxA monomers, AtxA C402S-FLAG was expressed in the parent strain of *B. anthracis*, which also expresses native AtxA from the *atxA* locus on pXO1. I reasoned that if BMH utilizes C402 on both proteins then, after cross-linking, FLAG-reactive protein would be detected as a monomer band (55 kDa) and not as a dimer containing AtxA C402S-FLAG and AtxA. Following BMH cross-linking, the native AtxA plus AtxA C402S-FLAG sample contained a high level of monomer when examined in Western blots probed with α-FLAG antibody (Fig. 4-5C, lane 5) similar to the sample containing only AtxA C402S (Fig. 4-5B, lane 8). In contrast, samples containing native AtxA plus Cys→Ser AtxA mutant proteins (C202S and C370S) or native AtxA plus AtxA-FLAG showed high levels of cross-linked protein reacting with α-FLAG antibody
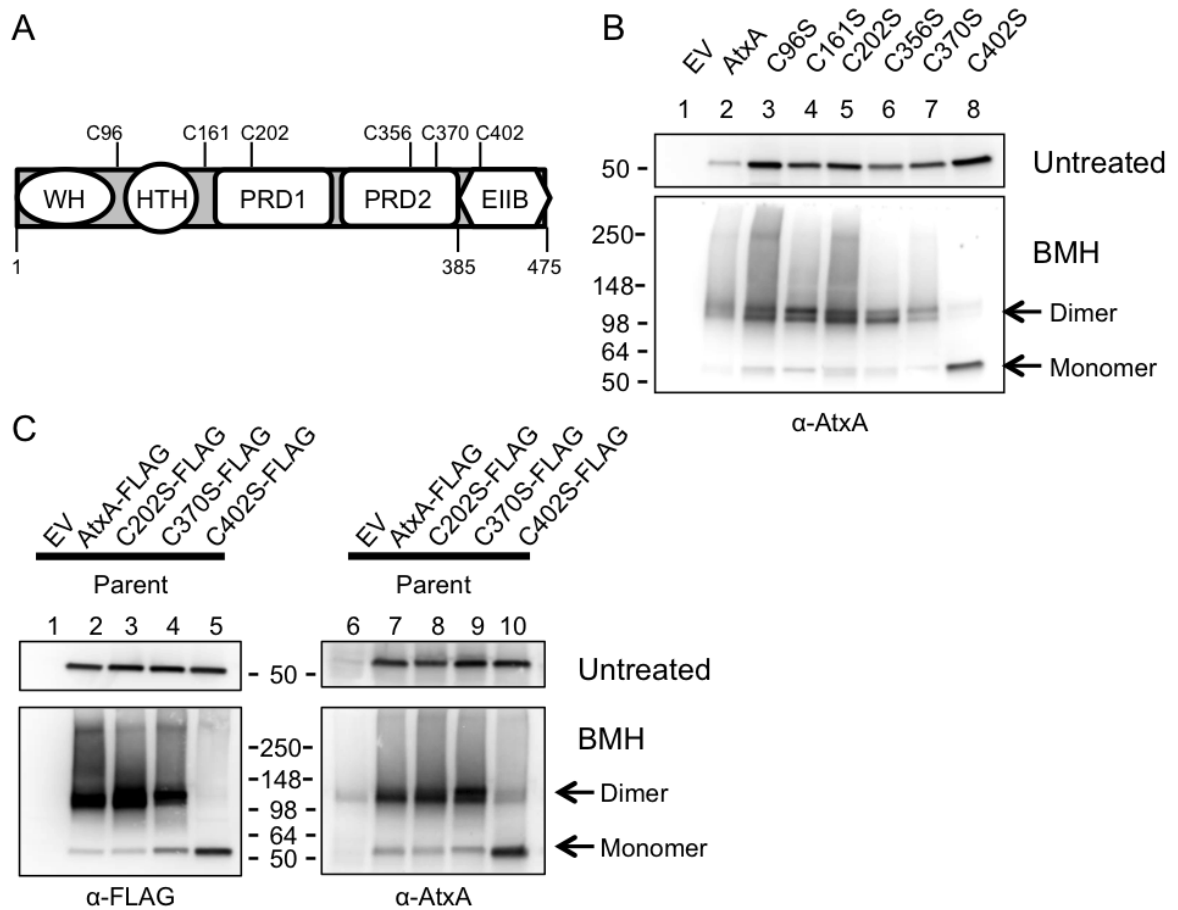
Figure 4-5. Determination of the site of BMH cross-linking. (A) The AtxA protein, which contains six cysteine residues, has five putative motifs: a winged helix-turn-helix (WH), a Mga-like helix-turn-helix (HTH), two phosphotransferase regulation domains (PRD1 and PRD2), and an Enzyme IIB-like motif (EIIB). (B) Following induction with 30 μM IPTG, cells from cultures of *atxA*-null strains (UT376) containing pUTE658-derived *atxA* point mutants were lysed and treated with BMH. SDS-PAGE (4-15%) and Western blots with AtxA-specific antibody were used to detect various forms of AtxA. (C) A similar experiment was performed using derivatives of the parent strain (UT375) expressing *atxA* from its native locus and pUTE992-derived FLAG-tagged versions of AtxA or the AtxA point mutants. Westerns were probed with α-FLAG and α-AtxA antibodies. EV = empty vector. Molecular weights of the protein standards are as indicated (SeeBlue Plus2, Invitrogen).

(Fig. 4-5C, lanes 2-4). Further, when the same samples were probed with α-AtxA antibody, dimer bands representing cross-linked AtxA (tagged and native) were present in all samples (lanes 6-10). Dimer bands detected in the AtxA C402S-FLAG plus AtxA sample probed with α-AtxA (lane 10) likely represent native AtxA because dimer bands were not detected when the same sample was probed with α-FLAG antibody (lane 5). The relatively low level of cross-linked protein in the sample containing only native AtxA (lane 6) and the sample containing native AtxA plus AtxA C402S-FLAG (lane 10) reflect low level AtxA expression from the native *atxA* locus. Induction of the tagged proteins (lanes 2-5 and 7-10) resulted in approximately 8.5-fold more tagged protein compared to native AtxA (Untreated lanes and data not shown). These results indicate that the major BMH cross-linked species is formed using C402 on two AtxA monomers.

"To verify that AtxA C402S can form a complex with AtxA despite being defective for BMH cross-linking, I performed a co-affinity purification experiment using AtxA C402S-FLAG mixed with AtxA-His. After eluting protein from NTA-Ni resin, AtxA C402S-FLAG was present in the sample with AtxA-His, indicating that AtxA C402S has normal multimerization properties (Fig. 4-6). Taken together, these data demonstrate that BMH utilizes C402 to cross-link two AtxA proteins and suggests that the carboxy-terminus of AtxA is involved in oligomerization.

"Assessment of the carboxy-terminal 91-amino acid sequence of AtxA using the Conserved Domains Database (136) and Protein Homology/Analogy Recognition Engine (Phyre, (137)), predicted that this region of AtxA is similar to an EIIB motif of the PTS, as depicted in Figure 4-5A. EIIB domains typically function enzymatically to phosphorylate carbohydrates after the sugars cross the cell membrane via an EIIC domain or protein. I performed cross-linking experiments using full length AtxA, $AtxA_{1-385}$ (deletion of the EIIB-like motif), and $AtxA_{385-475}$ (only the EIIB-like motif) to
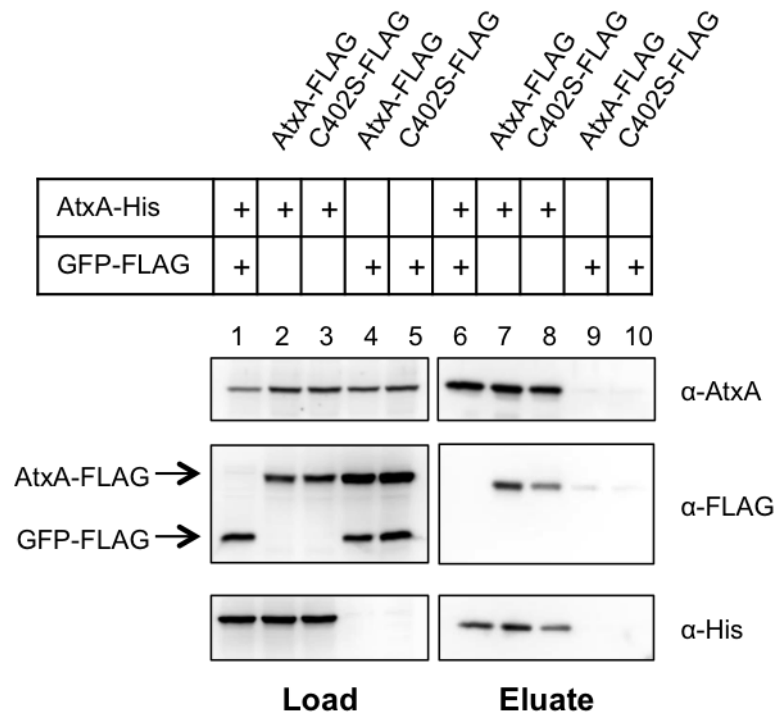
Figure 4-6. AtxA C402S does not have a multimerization defect. Lysates from the *B. anthracis atxA*-null strain UT376 expressing AtxA-His (pUTE991), GFP-FLAG (pUTE1013), AtxA-FLAG (pUTE992), or AtxA C402S-FLAG (pUTE992 C402S) were subjected to co-affinity purification using NTA-Ni resin. Samples were treated as described in Fig. 4-3.

determine if the EIIB-like region of AtxA is involved in AtxA oligomerization. Cell lysates containing full-length and truncated FLAG-tagged proteins synthesized in parent and *atxA*-null backgrounds were subjected to BMH cross-linking. Bands corresponding to 56-kD, 40-kD, and 11-kD monomers of AtxA-FLAG, AtxA$_{1-385}$-FLAG and AtxA$_{385-475}$-FLAG, respectively, were observed in untreated lysates probed with α-FLAG antibody (Fig. 4-7 lanes 2-4 and 6-8). The BMH-treated samples displayed the typical dimer bands (100 kDa) for AtxA-FLAG (lanes 10 and 14). The migration of AtxA$_{1-385}$-FLAG was not altered after cross-linking; only a 40-kDa band was present (lanes 11 and 15). This result is consistent with the requirement of C402 for cross-linking. The several FLAG-reactive bands present in lanes 12 and 16 represent multiple protein complexes containing AtxA$_{385-475}$-FLAG and unidentified proteins. The large α-FLAG-reactive cross-linking products do not represent AtxA cross-linked to AtxA$_{385-475}$-FLAG because the banding patterns of AtxA$_{385-475}$-FLAG in the parent (lane 12) and *atxA*-null strain (lane 16) were identical. These data indicate that the EIIB-like region of AtxA is involved in AtxA oligomerization and suggest that the EIIB-like domain in the absence of other regions of the AtxA protein displays less specificity for AtxA, interacting with several other proteins in cell lysates. It is notable that the truncated AtxA proteins do not exhibit AtxA activity. *B. anthracis* UT376 mutants producing AtxA$_{1-385}$, AtxA$_{1-385}$-FLAG, AtxA$_{385-475}$, or AtxA$_{385-475}$-FLAG show no expression of the P*lef-lacZ* fusion (data not shown)." (102)

4.2.4 Relationship between CO$_2$/bicarbonate, AtxA multimerization and function

"AtxA-dependent transcription of *lef* and other genes is enhanced during growth in buffered media in 5% CO$_2$, relative to growth in air (46, 49, 50, 71). To address relationships between the CO$_2$/bicarbonate signal, the oligomeric state of AtxA, and AtxA function *in vivo*, I compared AtxA multimerization and activity using
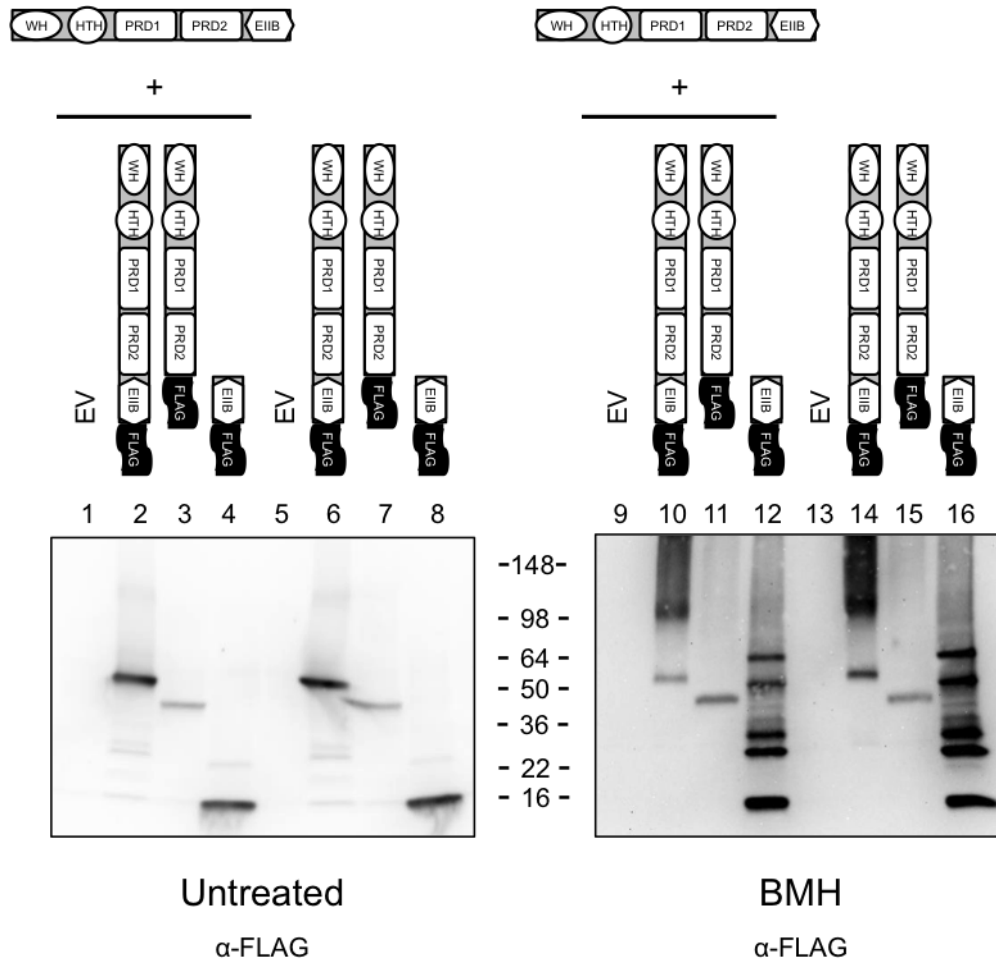
Figure 4-7. Multimerization of AtxA$_{385-475}$. Cell lysates of parent (UT375) and *atxA*-null strains (UT376) containing AtxA-FLAG (pUTE992), AtxA$_{1-385}$-FLAG (pUTE1019-FLAG), and AtxA$_{385-475}$-FLAG (pUTE1022-FLAG) induced using 30 - 50 µM IPTG were treated with the cross-linking agent BMH. SDS-PAGE (4-20%) and Western blots with FLAG-specific antibody were used to detect various forms of AtxA. EV = empty vector. Molecular weights of the protein standards are listed (SeeBlue Plus2, Invitrogen).

cells cultured in CA medium with or without CO_2/bicarbonate. Growth rates and IPTG-induced AtxA levels were similar for *B. anthracis* UT376 (pUTE658) cultures grown with or without added CO_2/bicarbonate (data not shown). For each culture, AtxA function was assessed as β-galactosidase activity resulting from expression of the P*lef-lacZ* reporter gene, and cell lysates were subjected to BMH-mediated cross-linking to determine the levels of AtxA dimer. A representative experiment is shown in Figure 4-8. The AtxA dimer/monomer ratio was approximately 2-fold greater in cells cultured with elevated CO_2/bicarbonate. The increased dimer level correlated with increased AtxA activity. The affect of the CO_2/bicarbonate signal on the AtxA dimer/monomer ratio and AtxA activity was consistent in multiple experiments. These results show that the CO_2/bicarbonate signal shifts the dimer/monomer equilibrium of AtxA toward the dimeric state and this shift is associated with enhanced protein function."(102)

4.3 Discussion

"I have determined that AtxA forms a multimeric protein complex independent of other proteins, and that the level of homodimeric AtxA is increased relative to monomeric AtxA in cells cultured in conditions conducive for function. My experiments employing the BMH cross-linking reagent allow me to discern features of the AtxA multimer. BMH is specific for reduced, solvent-accessible cysteines located within 13 Å. I determined that C402 is the major site of cross-linking between two AtxA proteins, suggesting that C402 is likely surface exposed and in proximity to the corresponding amino acid in an AtxA dimer. Since BMH cross-linking requires reduced cysteines, the C402 residues of associated AtxA proteins do not form a disulfide bond. Moreover, a C402S mutant forms multimers that are indistinguishable from those formed by the native protein. My data indicate that C402 is located in a region of AtxA that forms protein-protein contacts, yet C402 is not required for the protein-protein interactions.
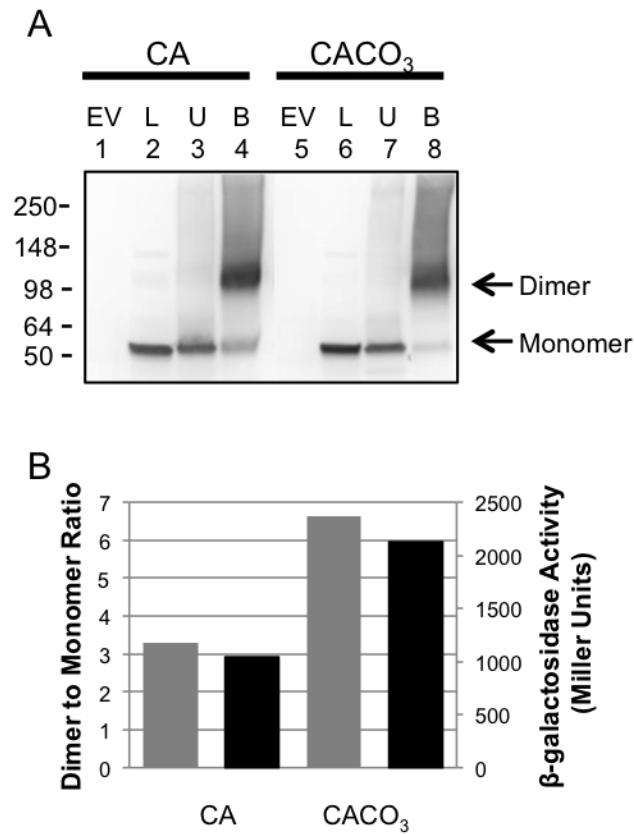
Figure 4-8. The CO$_2$/bicarbonate effect on AtxA multimerization and activity. UT376 (pUTE658), an *atxA*-null strain harboring the native *atxA* gene driven by an IPTG-inducible promoter and the P*lef-lacZ* transcriptional fusion (as a reporter for AtxA activity) was cultured in CA in air and in CACO$_3$ in a 5% CO$_2$ atmosphere. Cells were collected two hours after induction with IPTG. (A) SDS-PAGE (4-15%) and Western blots with AtxA-specific antibody were used to detect various forms of AtxA. EV = empty vector (pUTE657), L = cell lysate, U = untreated samples, B = BMH treated samples. (B) Intensities of bands corresponding to the AtxA dimer and monomer were measured using ImageJ. Dimer/monomer ratios are shown as gray bars. β-galactosidase activities, resulting from expression of the P*lef-lacZ* reporter, are shown as black bars.

"The Protein Homology/Analogy Recognition Engine "Phyre" (137) is a homology-based, fold-recognition tool that provides three-dimensional structure predictions based on sequence similarity to proteins with known structures. Phyre reveals similarity between $AtxA_{385-475}$, containing C402, and EIIB motifs of PTS proteins, leading me to propose a function for the carboxy-terminus of AtxA. As part of the PTS, EIIB proteins are the penultimate proteins in the phosphotransfer from phosphoenol-pyruvate (PEP) to imported carbohydrates (73). Within the PTS, Enzyme II (EII) complexes, consisting of EIIA, EIIB, and EIIC(D), recognize and transport specific carbohydrates. After EI-dependent phosphorylation of HPr, the phosphate is transferred EIIA. EIIA~P phosphorylates EIIB at a conserved cysteine residue within the P-loop, a flexible loop between β-strand 1 and α-helix 1 (138). The phosphocysteine of EIIB transfers its phosphate to carbohydrate molecules crossing the cell membrane via the EIIC(D) complex. The carboxy-terminus of AtxA is similar to GatB, an *E. coli* protein that is a member of the glucitol/galacitol family of EIIB proteins (139). NMR studies of GatB with its cognate EIIA (GatA) reveal regions of GatB – GatA interaction. It is thought that the GatB-GatA interface, which includes the P-loop, is also recognized by the corresponding EIIC protein, GatC (140).

"Interaction of GatB with two different proteins suggests involvement of EIIB-like motifs in protein-protein binding. In experiments when $AtxA_{385-475}$-FLAG is induced in an *atxA*-null strain or the parent strain containing AtxA, I detect four prominent α-FLAG-reactive products in cross-linked cell lysates. In contrast, when full-length AtxA-FLAG is induced in either strain, cross-linked lysates contain only one α-FLAG-reactive product, which corresponds to an AtxA-AtxA dimer. The presence of multiple cross-linked products in the $AtxA_{385-475}$ sample suggests that the EIIB-like motif in the absence of other AtxA domains loses some specificity for protein-protein interactions. These data lead me to propose that the EIIB-like motif is involved in the

AtxA-AtxA interaction, yet one or more motifs within residues 1-385 of AtxA are required to confer specificity to the AtxA-AtxA interaction and to exclude interactions of the AtxA EIIB-like domain with other proteins.

"The presence of an EIIB-like motif adjacent to PRDs is not unique to AtxA (see Fig. 1-2). EIIB-like domains are found in certain other regulators, including the transcriptional activators LicR, MtlR, CelR, ManR and LevR (73, 82, 141). Yet, unlike AtxA, these other regulators also contain EIIA-like motifs and the regulators control a small number of genes encoding proteins associated with use of a specific carbohydrate or group of carbohydrates. For example, in *Streptococcus mutans* CelR regulates the production of proteins required for cellobiose catabolism (142), and MtlR induces expression of the *mtl* operon when *Bacillus subitilis* is in the presence of mannitol (84, 143). In contrast, AtxA is a virulence gene regulator that affects transcription of multiple genes on the chromosome and virulence plasmids within *B. anthracis*, none of which are known to be associated with catabolism (57).

"Interestingly, a cysteine residue within the EIIB-like motif in the MtlR protein of *B. subtilis* was recently shown to be phosphorylated (82). MtlR activity decreases when P~EIIA^{Mtl} phosphorylates MtlR at C419, the conserved cysteine within the P-loop of the EIIB-like motif. In the Phyre-produced model of the EIIB-like motif of AtxA, C402 is located in the P-loop, but the residue is not at the position typically observed for the conserved phosphocysteine in EIIB proteins of the PTS or for the EIIB-like motif in MtlR and LicT. Moreover, current data do not support phosphorylation of AtxA at this site. Phosphorylated C402 would have prevented cross-linking by BMH in my experiments. Also, Tsvetanova *et al*. (59), reported that phosphorylation of AtxA occurs only within the PRDs at residues H199 and H379. $^{32}PO_4$-labelled AtxA was immunoprecipitated from *B. anthracis* cell lysates, but no radio-labelled AtxA was evident in a H199A / H379A mutant.

"Phosphorylation of AtxA may impact the multimeric state of the protein. Phosphorylation can stabilize or disrupt dimerization of the PRD-containing antiterminator proteins LicT and BglG (79, 80, 128, 134). Dimer contacts within the PRDs of LicT are confined to α-helices 2, 3, and 5 in each PRD, and the helices are arranged in an anti-parallel orientation (135). Considering reports concerning LicT and BglG, it is possible that the AtxA PRDs are involved in multimerization. The Phyre-predicted structure of the PRDs of AtxA positions C202 in α-2 of PRD1, C356 in α-4 of PRD2, and C370 in α-5 of PRD2, yet in my studies, C202, C356, and C370 were not required for cross-linking of AtxA proteins by BMH. It is possible that these cysteine residues are in regions that function in multimerization. However, the sulfhydryl groups are inaccessible to BMH because they are buried in the interior of AtxA, oxidized into a disulfide bond, or are greater than 13 Å from another cysteine. More work needs to be performed to determine the protein-protein contacts existing throughout the AtxA protein and to assess potential effects of phosphorylation on multimerization of AtxA (See Ch. 5).

"My findings show for the first time a link between AtxA multimerization, function and an important signal for virulence gene synthesis by *B. anthracis*. Increased synthesis of PDGA capsule and the anthrax toxin proteins during culture of *B. anthracis* in the presence of elevated CO_2/bicarbonate was first reported more than sixty years ago. Yet, the mechanism by which this physiologically relevant signal affects expression of these critical virulence factors has remained largely unknown. In work presented here, I have determined that *B. anthracis* cultures grown in elevated CO_2/bicarbonate contain higher levels of the AtxA dimer than cultures grown in air. Conditions that enhance dimerization also promote AtxA target gene expression. The positive correlation between CO_2/bicarbonate level, the presence of AtxA dimers, and AtxA activity links the signal to AtxA structure and function.

"Many questions remain regarding the mechanism by which CO_2/bicarbonate affects AtxA function. Genetic and biochemical searches have not revealed any cellular factors that might bridge the link between the CO_2/bicarbonate signal and the AtxA protein. I speculate that AtxA may bind to bicarbonate or CO_2 directly. To my knowledge, only one bacterial regulatory protein has been shown to require bicarbonate to stably interact with target promoter sequences. RegA, an AraC/XylS-like regulator found in *Citrobacter rodentium*, binds to bicarbonate via an amino-terminal motif (144). According to the model proposed by Yang *et al.* (145), the binding of bicarbonate to RegA facilitates interaction of its carboxy-terminal DNA binding motif with target sequences. AtxA does not bear apparent sequence homology to RegA, although a binding pocket may not be obvious. Multiple bicarbonate-binding proteins, with varying bicarbonate binding sites and diverse functions have been reported, including proteins associated with photosynthesis and menaquione biosynthesis (146, 147). Direct association of bicarbonate with AtxA multimers is currently under investigation.

"Finally, my experiments were designed to detect stable protein-protein complexes. I do not exclude the possibility of other AtxA-protein interactions. Considering that specific DNA-binding activity has not been demonstrated for purified AtxA protein, it is possible that an additional protein interacts with AtxA to allow specific DNA-binding. Moreover, a specific multimeric and/or phosphorylated form of AtxA may be required to observe this activity. Although it has been suggested that AtxA phosphorylation occurs via the HPr enzyme of the PTS, the kinase has not been identified experimentally. It is likely that the enzyme responsible for phosphorylation of AtxA makes transient protein-protein contacts and thus would not be identified by the approaches used here.

"My working model is that formation of an AtxA homo-dimer is required for virulence gene activation. Future studies will focus on potential relationships between phosphorylation, multimerization, and function of AtxA." (102)

Chapter V

The *B. anthracis* phosphoenolpyruvate:sugar phosphotransferase system (PTS) regulates expression, not function, of AtxA, the virulence gene regulator.

5.1 Introduction

The phosphoenolpyruvate: sugar dependent phosphotransferase system (PTS) serves as a central processing circuit, allowing bacteria to adapt to changing conditions in the local environment (73). The PTS directs carbon catabolite repression (CCR) and carbon catabolite activation (CCA) which affect genes involved in metabolism and bacterial pathogenesis (74, 148). Moreover, the PTS phosphorylates proteins as the primary mechanism to modify metabolism.

CCA and CCR and PTS-dependent phosphorylation are intersecting pathways that converge with the protein HPr. In *Bacillus subtilis*, HPr, the second of the two general enzymes in the PTS (EI and HPr), is phosphorylated by two proteins ((74), see Fig. 1-3). H15 of HPr (P~His-HPr) is phosphorylated by EI following catalysis of phosphoenolpyruvate (PEP) to pyruvate. To generate P-Ser-HPr, S46 of HPr is phosphorylated by HprK/P in an ATP-dependent fashion when cellular levels of fructose-1,6-bisphosphate (FBP) are high (> 5 mM). Some carbohydrates promote phosphorylation on H15 and S46 in the same molecule of HPr (HPr-P2). A bacterium's carbon source dictates the proportion of P~His-HPr, P-Ser-HPr, and HPr-P2 in the cell (149). P~His-HPr phosphorylates several different types of proteins, whereas P-Ser-HPr specifically interacts with CcpA to induce CCA and CCR.

P~His-HPr is responsible for phosphorylating EIIA (73), GlpK (150, 151), and PRD-containing antiterminators and activators (73). The phosphorylated proteins promote catabolism of a specific sugar (EIIA and GlpK) or increase the transcription of genes needed for sugar catabolism (PRD-containing proteins). P~His-HPr phosphorylates two histidines within PRD2 of LicT, a *B. subtilis* antiterminator protein controlling genes involved in the metabolism of β-glucosides (77, 152, 153). Once phosphorylated, LicT homodimerizes and prevents transcriptional termination of the *lic* operon (79).

P-Ser-HPr forms a heterotetramer with CcpA, the master regulator of CCA and CCR within low G+C Gram-positive bacteria (74). The complex binds to promoter elements (*cre*

sites) to repress (CCR) or activate (CCA) transcription (154). In *B. subtilis*, ~10% of the genome is regulated via CcpA/P-Ser-HPr (155). Glucose is one of a few carbohydrates that increase the intracellular concentration of FBP leading to increased HprK/P phosphorylation of HPr (149). The CcpA regulon includes genes associated with pathogenesis of *Listeria monocytogenes*, *Streptococcus pyogenes*, and *Bacillus anthracis* (66, 76, 156).

Recent discoveries implicate P~His-HPr and P-Ser-HPr in the regulation of virulence in *B. anthracis*, the causative agent of anthrax disease. Transcriptional activation of virulence genes occurs via AtxA, a PRD-containing protein encoded on the large plasmid pXO1 (46, 47). P~His-HPr of the PTS has been suggested to phosphorylate a histidine within the PRDs of AtxA (59, 157). Moreover, the CcpA/P-Ser-HPr complex indirectly promotes transcription of *atxA* (66).

P~His-HPr may phosphorylate AtxA on H199 and indirectly provide the phosphate needed for another protein to phosphorylate H379. According to the current model for AtxA function, phosphorylation of AtxA at H199 increases AtxA activity whereas at H379 it reduces the function of the protein (59). Using point mutations mimicking the phosphorylated and non-phosphorylated states (H→D and H→A, respectively), Tsvetanova *et al.* (59) assessed the function of AtxA point mutations using a *pagA-lacZ* reporter fusion in the heterologous host *B. subtilis*. AtxA H199D had the highest activity though it produced only 1.3 times the activity of AtxA, whereas expression of *pagA-lacZ* via AtxA H199A was reduced sixfold. AtxA H379D displayed the lowest function as it induced little or no expression of the reporter fusion. In contrast, AtxA H379A had similar activity as the wild type protein. To confirm the data from the *B. subtilis* reporter, the authors detected PA protein in culture supernates from *B. anthracis* strains expressing the mutated proteins. Significantly, *in vivo* ^{32}P-labeled AtxA was immunoprecipitated from *B. anthracis* cell lysates; however, the bacteria were cultured in a medium that does not promote high levels of AtxA activity. AtxA H199A and AtxA

H379A were phosphorylated as well; however, AtxA H199A/H379A, the double mutant, was not labeled. These data indicated that AtxA was phosphorylated at H199 and H379.

There is some evidence that the PTS represses AtxA function via phosphorylation of H199 and/or H379 (59). A *B. subtilis* mutant lacking HPr and EI via a deletion in *ptsHI* produces twofold higher AtxA activity than the *B. subtilis* parent strain. *B. subtilis* cultured in medium supplemented with glucose was delayed in *pagA-lacZ* expression. These data supported a model that AtxA is phosphorylated via a mechanism involving P~His-HPr (59, 157). In contrast, when *B. anthracis*, the native host of AtxA, was cultured in medium containing glucose, more toxin gene and *atxA* expression were detected than in medium lacking the carbohydrate. The observation that *atxA* and toxin gene expression increase in glucose-containing medium indicated that *atxA* was subject to CCA. The result from *B. subtilis*, the heterologous host, indicated that *atxA* was repressed in glucose-containing medium; however, *atxA* gene expression was stimulated by glucose in *B. anthracis* (66).

The glucose-effect on *atxA* expression in *B. anthracis* is mediated by CcpA. After determining that AtxA protein function was unaffected by glucose, Chiang *et al.* (66) demonstrated that a *B. anthracis* Δ*ccpA* mutant reduced the amount of *atxA* and toxin gene transcripts similar to cultures without glucose. However, there is not a *cre* site near the *atxA* promoter and purified CcpA was not able to bind to the *atxA* promoter; therefore, the mechanism of CcpA-dependent regulation of *atxA* has not been elucidated. It is proposed that CcpA and P-Ser-HPr cooperatively activate the *atxA* promoter in an indirect manner (66); however, there is no conclusive link between HPr and *atxA* transcription.

Since CcpA/P-Ser-HPr regulates transcription of specific genes and P~His-HPr may phosphorylate PRD-containing proteins, I hypothesize that the PTS regulates *B. anthracis* virulence in two ways. CcpA/P-Ser-HPr may activate transcription of *atxA* while P~His-HPr phosphorylates AtxA. In work presented in this chapter, I present experiments which provide support for HPr function in *atxA* transcription; however, my data show that the PTS does not

affect AtxA protein function. Because the kinase of AtxA is unknown, I investigated the multimeric properties of phosphomimetic versions of AtxA to determine if the mutant proteins follow the model of PRD-containing proteins.

5.2 Results

5.2.1 EI and HPr do not phosphorylate AtxA *in vitro*.

Previously, it was shown that the PRDs within AtxA were phosphorylated *in vivo* potentially via the PTS (59). As shown with LicT and MtlR (84, 153), PRD-containing proteins can be phosphorylated *in vitro* when combined with EI, HPr, and ^{32}P-PEP. Given the presence of PRDs within AtxA, I hypothesized that HPr phosphorylates AtxA.

To address this question, I attempted an *in vitro* phosphotransferase experiment. AtxA containing a carboxy-terminal hexa-histidine tag (AtxA-His) was purified from *B. anthracis* to yield highly purified, soluble protein (see Fig. 4-2B). Expression of hexa-histidine-tagged versions of HPr and EI was induced via the IPTG-inducible P*hs* in *B. anthracis*, and the proteins were purified via NTA-Ni affinity chromatography. EI-His, HPr-His, and AtxA-His were incubated with ^{32}P-PEP and subjected to SDS-PAGE. A phosphor-image of the experiment displayed phosphorylated EI-His and HPr-His (Fig. 5-1A, lanes 1, 4, 5, and 7). An unidentified protein was also present in lanes 1, 4, 5, and 7. I presume that the protein was a fragment of EI. HPr-His and AtxA-His were not phosphorylated when they were alone or incubated together (lanes 2, 3, and 6). Moreover, AtxA-His was not phosphorylated by EI-His and HPr-His (lane 7). All three proteins were detected via immunoblot analysis using α-His antibody (Fig. 5-1B). The lack of AtxA phosphorylation was surprising, because HPr has been demonstrated to phosphorylate several PRD-proteins during *in vitro* reactions (82, 84, 153, 158–160). The results suggest that EI and HPr do not transfer phosphate directly to AtxA.

81
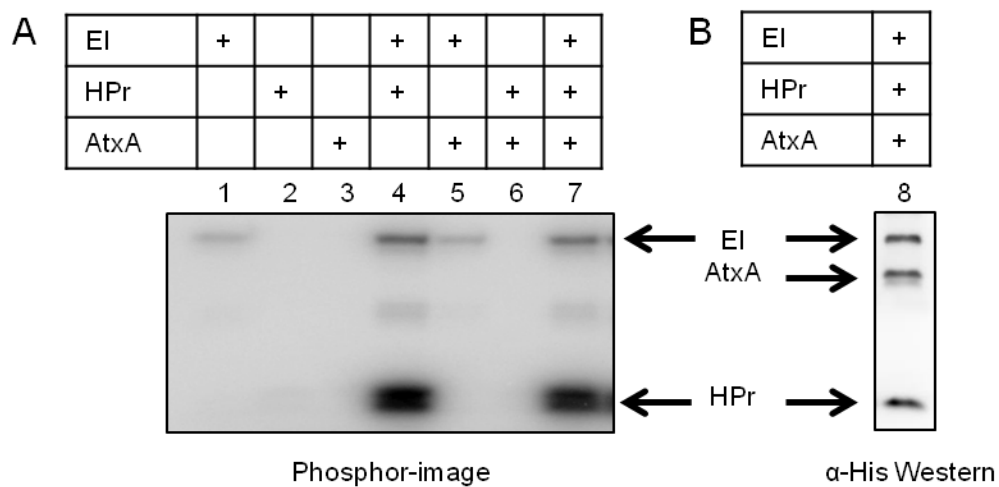
Figure 5-1. Phosphotransferase assay does not produce phosphorylated AtxA. Hexa-His tagged EI, HPr, and AtxA were induced in *B. anthracis* and purified via nickel-affinity purification. A.^{32}P-PEP was mixed with the proteins and incubated at 37° C for 30 min. Samples were separated on 10% poly-acrylamide-SDS gels, dried, and exposed to a phosphor-imaging screen. B. The proteins also were subjected to SDS-PAGE and probed with α-His antibody. Proteins present in each lane are indicated by the table.

5.2.2 The PTS affects transcription of *atxA*

To substantiate the results of the *in vitro* phosphotransferase assay and further investigate the role of EI and HPr on AtxA function, I constructed a markerless mutation of *ptsHI* in *B. anthracis*. When a *B. subtilis* Δ*ptsHI* mutant was tested for AtxA activity, the mutant displayed higher expression of an AtxA-dependent target (*pagA-lacZ*) than the parent strain (59). Given the difference between *B. subtilis* and *B. anthracis* in the effect of glucose on toxin gene expression, it is necessary to determine in *B. anthracis* the relationship between AtxA and the PTS.

The genes encoding HPr and EI were deleted from the chromosome of two strains of *B. anthracis*: a parent strain (ANR-1) and an isogenic strain (UT375) that includes *lacZ* integrated at the native *lef* locus (P*lef-lacZ*). P*lef-lacZ* provides a quantitative reporter of AtxA function *in vivo*. The *lef* gene encodes for the Lethal Factor (LF), one of the anthrax toxin proteins, and transcription of the gene is highly dependent upon AtxA (46, 49). The ANR-1 *ptsHI* mutant (UT405) and the UT375 *ptsHI* mutant (UT408) displayed a slight reduction in replication rate in toxin-inducing medium (CACO$_3$) but had no growth defect in rich medium (LB or BHI media) (data not shown).

To assess *atxA* transcription and AtxA activity, low-copy plasmids carrying transcriptional reporters, P*atxA-lacZ* or P*lef-lacZ*, were inserted into UT405. The *ptsHI* mutant displayed little *lacZ* activity from either promoter fusion when streaked on a CACO$_3$ plate containing X-gal (Fig. 5-2A). In contrast, the parent strain containing the reporter fusions displayed β-galactosidase activity indicating the *atxA* and *lef* promoters were active. These data suggest that *ptsHI* affects *atxA* transcription.

The *ptsHI* mutation was complemented by inducing expression (P*hs*) of His-tagged alleles of *ptsH* or *ptsI* or the native version of the *ptsHI* bicistron. The UT375-derived *ptsHI*-null mutant (UT408) containing the complementation vectors was cultured in toxin-inducing conditions. Induction of HPr and EI began during early exponential phase of growth (2 h,
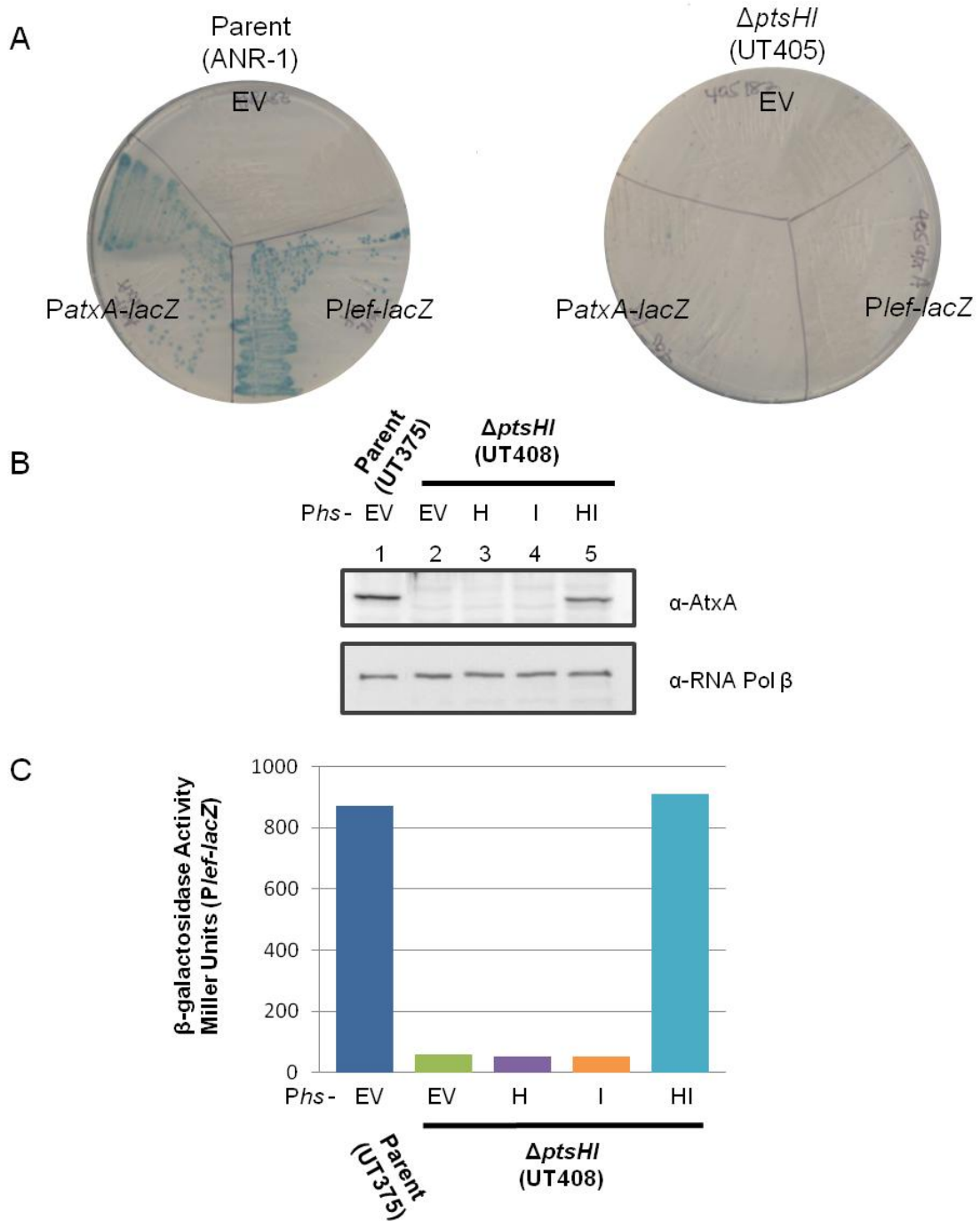
Figure 5-2. *ptsHI* mutation affects expression of *atxA* in *B. anthracis*.

Figure 5-2. *ptsHI* **mutation affects expression of** *atxA* **in** *B. anthracis.* A markerless mutation of *ptsHI* was constructed in the ANR-1 strain of *B. anthracis* producing UT405. A. Plasmid-borne transcriptional reporters of the promoters for *atxA* and a toxin gene (P*atxA-lacZ* and P*lef-lacZ*, respectively) were transformed into the mutant and parent strain. The strains were streaked onto $CACO_3$ plates containing X-gal and incubated at 37° C with 5% CO_2.

      To create UT408, the mutation was made in the ANR-1 derived strain UT375 which contains an integrated *lacZ* gene in the *lef* locus. Plasmids containing *ptsH* (H), *ptsI* (I), or *ptsHI* (HI) controlled by an IPTG-inducible promoter (P*hs*) or the empty vector (EV) were introduced into UT408 and its parent strain, UT375. B. The strains were cultured in $CACO_3$ with added glycerol. After induction of *ptsH*, *ptsI*, or *ptsHI* using 250 μM IPTG (2 h, OD_{600} = 0.202 – 0.302), soluble cell lysates were created at the transition to stationary phase (4 h, OD_{600} = 0.93 – 1.43) and subjected to SDS-PAGE and Western blot analysis using α-AtxA and α-RNA Polymerase β subunit. C. The β-galactosidase activity of *B. anthracis* mutants harboring the P*lef-lacZ* reporter (UT375 and UT408) and IPTG-inducible *ptsH*, *ptsI*, or *ptsHI* was determined as described previously (130). These data are representative of three experiments.

OD_{600} = 0.202 – 0.302) and samples for AtxA westerns and β-galactosidase assays were collected at the transition to stationary phase (4 h, OD_{600} = 0.93 – 1.43). Only the dual expression of HPr and EI restored AtxA protein levels and P*lef-lacZ* activity (Fig. 5-2B, lane 5, and 5-2C).   AtxA was not detected on the Western blot in the *ptsHI* mutant strain containing the empty vector or expressing HPr-His or EI-His alone (lanes 3 and 4). These data support the results from the plate assays (Fig. 5-2A) and indicate that mutation of *ptsHI* abrogates *atxA* transcription which leads to decreased activation of *lef*. It is likely that the mechanism by which *ptsHI* affects *atxA* involves CcpA, which was shown previously to regulate *atxA* (66).

5.2.3 AtxA function is independent of *ptsHI*

It was surprising that mutation of *ptsHI* leads to decreased amounts of *atxA* transcript, because in most instances, PRD-containing proteins are regulated post-translationally via HPr phosphorylation, not by transcriptional control via CcpA/P-Ser-HPr (73, 82).   One exception is a LevR-like protein in *Lactobacillus casei* (161).   LevR, characterized in *B. subtilis*, is a PRD-harboring protein that regulates the fructose-specific PTS (83). In *L. casei*, the activity of the LevR-like protein is regulated via phosphorylation by P~His-HPr, and expression of the LevR-like protein is regulated by CcpA/P-Ser-HPr (161). To determine if the PTS affects AtxA protein function in addition to promoter activity, I investigated if AtxA activity was altered in the Δ*ptsHI* mutant.

The PTS can both positively and negatively regulate PRD-containing proteins (73); therefore, it may decrease or increase AtxA activity. If the PTS induces AtxA function, then the protein's activity may be diminished when the mutant strain is cultured in toxin-inducing conditions ($CACO_3$).   On the other hand, if the PTS decreases AtxA activity, AtxA may display a hyper-active phenotype in the *ptsHI* mutant cultured in a medium that does not produce optimal levels of toxin (LB-air).

To produce AtxA and measure the amount of AtxA activity, I transformed the UT375 ΔptsHI strain (UT408) with the IPTG-inducible Phs-atxA expression vector (pUTE658). The strain was cultured alongside the parent strain (UT375) and a UT375-derived atxA-null strain (UT376) in CACO$_3$ or LB-air. These three strains contain the Plef-lacZ reporter integrated at the lef locus. After induction with IPTG during early exponential phase, samples were collected at the transition to stationary phase for Western blots and Plef-lacZ activity assays. AtxA was present in CACO$_3$ cultures of the parent strain containing the empty vector and the mutant strains inducing Phs-atxA (Fig. 5-3A, lanes 1, 3, and 5). All samples containing detectable amounts of AtxA also exhibited equivalent β-galactosidase activities (Fig. 5-3C). These data indicated that AtxA function was not activated by ptsHI. When culturing in LB-air, AtxA protein was detected only in strains containing Phs-atxA and induced with IPTG (Fig. 5-3B, lanes 8 and 10). The activities of AtxA were over 2-logs lower in strains containing AtxA than the same strains cultured in CACO$_3$ (Fig. 5-3D, compare to Fig. 5-3B). There was little difference between the Plef-lacZ activities in the ΔatxA – Phs-atxA and ΔptsHI – Phs-atxA strains. These data suggested that EI and HPr and the proteins that are phosphorylated by EI and HPr do not negatively impact AtxA protein function.

When data from the in vitro and in vivo assays are analyzed collectively, I conclude that EI and HPr, and by extension, the entire PTS, affect virulence gene regulation via the control of atxA gene expression and the system has no control over AtxA protein function.

5.2.4 Effects of phosphomimetic mutations on AtxA multimerization and function

Although the PTS does not phosphorylate AtxA, data suggest that AtxA is phosphorylated in vivo (59). Using H→A and H→D point mutations within AtxA, the authors conducted experiments suggesting that phosphorylation of H199 promotes AtxA activity and H379 phosphorylation decreases AtxA activity. Alanine substitutions mimic the non-phosphorylated state of a histidine, while H→D mutations are similar to a phosphohistidine. It
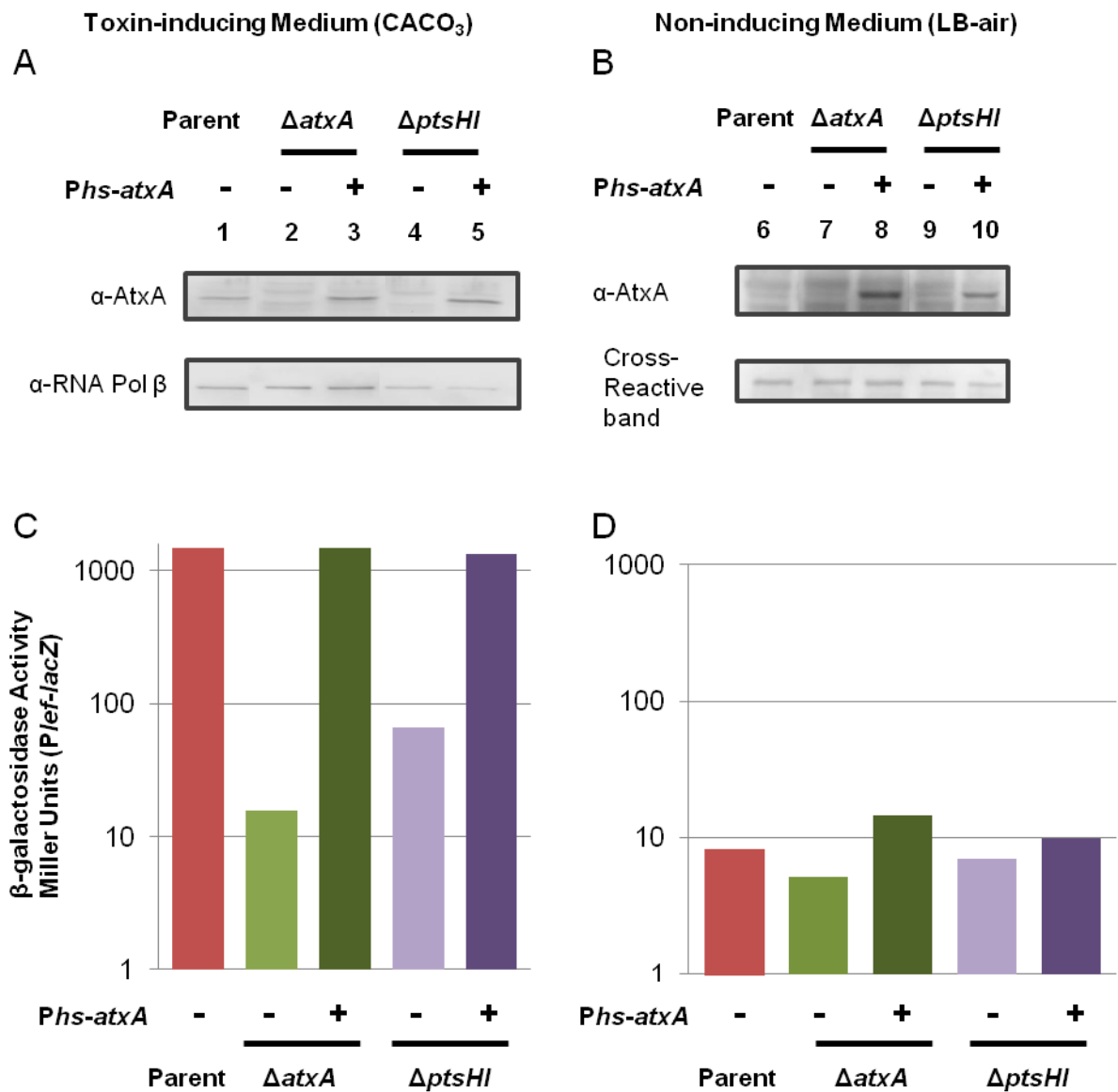
Figure 5-3. Expression of AtxA in *B. anthracis* PTS mutants. UT375-derived *ptsHI* and *atxA* mutant strains (UT408 and UT376, respectively) containing a plasmid-encoded IPTG-inducible *atxA* (P*hs-atxA*) or an empty vector (EV) were cultured in conditions optimal (CACO₃, see A. and C.) or suboptimal (LB-air, see B. and D.) for toxin gene expression. AtxA production was induced during early exponential phase (2 h) and samples were collected for immunoblots or β-galactosidase assays (4 h). Representative data are shown. A. and B. Soluble cell lysates migrated through 10% poly-acrylamide SDS gels and were probed with α-AtxA antibody. RNA Polymerase β subunit or a cross-reactive band are shown as loading controls. C. and D. The β-galactosidase activity of each strain was determined as described previously (130).

is unknown if phosphorylation affects the amount of AtxA multimer, which is proposed to be needed for AtxA to be active (see Chapter 4).

To determine the oligomeric state of AtxA phosphomimetic mutant proteins, I created AtxA H199 and H379 mutations in the P*hs-atxA* expression vector (pUTE658) and expressed the proteins in UT376, an *atxA*-null mutant harboring a transcriptional fusion, P*lef-lacZ*. While culturing in toxin inducing medium, cells were induced with IPTG during early exponential phase (T2), and samples were collected at the transition to stationary phase (T4) to assess the activity and multimeric state of each mutant protein (Fig. 5-4). As seen previously (59), AtxA H199D and AtxA H379A had activity similar to the parent strain in a representative experiment, AtxA H199A had 3-fold less activity, and the activity of AtxA H379D is slightly greater than the empty vector control (Fig. 5-4A).

To detect multimerization of the mutant proteins, I performed co-affinity purification (co-AP) and bis(maleimido) hexane (BMH) cross-linking assays. The co-AP experiment determines if a FLAG-tagged protein interacts with an affinity-purified His-tagged protein. The Load samples (Fig. 5-4B, lanes 1-6) display the proteins induced in each pool of cell lysates. FLAG-tagged proteins which interact with AtxA-His during the NTA-Ni purification were detected via α-FLAG immunoblots of the eluate samples (Fig. 5-4B, lanes 7-12, middle panel). AtxA-FLAG stably interacts with AtxA-His as previously demonstrated (Fig. 5-4B lane 8, and Fig. 4-3). AtxA H199A-FLAG, AtxA H199D-FLAG, and AtxA H379A-FLAG co-affinity purify with AtxA-His. In contrast, AtxA H379D-FLAG was not visible after elution of the proteins from the NTA-Ni resin (Fig. 5-4B, lane 12).

In the BMH cross-linking experiment, BMH reacts specifically with C402 of AtxA to covalently link two AtxA proteins within an AtxA multimer (Fig. 4-5). Cell lysates were created from strains inducing the untagged AtxA mutant proteins. After treatment with BMH, the dominant form of AtxA detected via Western blot after SDS-PAGE was the homodimer at ~100 kDa (Fig. 5-4C, lane 2). Bands with similar mobilities were visible in lanes 3-5,
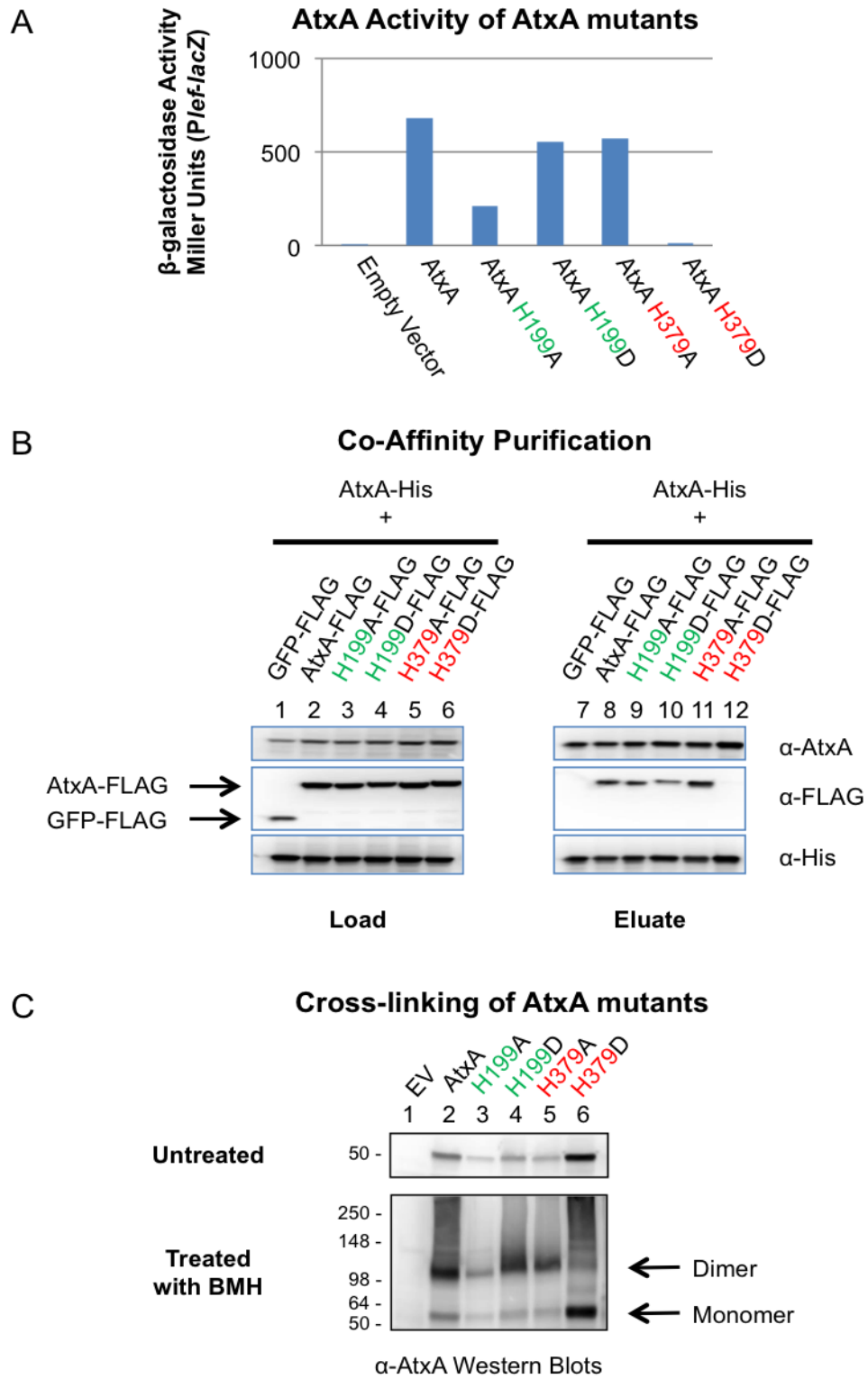
Figure 5-4. Phosphomimetic mutations affect AtxA activity and multimerization.

Figure 5-4. Phosphomimetic mutations affect AtxA activity and multimerization. *B. anthracis atxA*-null strains (UT376) containing pUTE658 (encoding AtxA or mutations in H199 or H379) were induced with 10-40 µM IPTG while culturing in $CACO_3$ and samples were collected for AtxA activity and multimerization assays. A. Activity of P*lef-lacZ* was determined via β-galactosidase assay as described previously (130). B. Lysates from UT376 containing AtxA-His (pUTE991), AtxA-FLAG (pUTE992) with H199 or H379 mutations, or GFP-FLAG (pUTE1013) induced with 40-50 µM IPTG were subjected to co-affinity purification using NTA-Ni resin. Western blots probed with α-AtxA, α-FLAG, and α-His antibodies were performed on soluble cell lysates (Load, lanes 1-6) and purified proteins (Eluate, lanes 7-12). C. Cultures of UT376 containing pUTE658 (encoding AtxA or mutations in H199 or H379) were induced with 40 µM IPTG. Cell lysates were treated with the cross-linking agent BMH. SDS-PAGE (4-15%) and Western blots with AtxA-specific antibody were used to detect various forms of AtxA. EV = empty vector. Molecular weights of the protein standards are listed (SeeBlue Plus2, Invitrogen).

indicating that AtxA H199A, AtxA H199D, and AtxA H379A form a normal AtxA multimer. Conversely, the major band for AtxA H379D was at ~50 kDa, the monomer size of AtxA. As seen for the co-AP experiment, AtxA H379D does not appear to form a multimer. These data indicate that H379D mutation destabilizes the AtxA multimer. From these data, I deduce that phosphorylation of H379 decreases AtxA activity via decreased affinity for AtxA-AtxA binding.

5.3 Discussion

AtxA, the master regulator of virulence of *B. anthracis*, may be controlled via two mechanisms involving HPr. Previous reports suggested that CcpA/P-Ser-HPr affects *atxA* transcription and that AtxA is phosphorylated in a P~His-HPr-dependent manner (59, 66, 157). In the work presented herein, data from biochemical and genetic experiments suggest that the PTS influences *atxA* transcription; however, PTS-mediated phosphorylation of AtxA was not detected.

An *in vitro* phosphotransferase assay provides evidence of protein phosphorylation via EI and HPr. In the phosphotransfer experiment, EI utilizes ^{32}P-PEP as a substrate to phosphorylate HPr at H15. P~His-HPr donates its phosphate to the PRD-containing protein in the reaction. Phosphotransferase assays have demonstrated phosphorylation of several PRD-containing proteins including the *B. subtilis* proteins SacT (158), LicT (153), LevR (160), GlcT (159), and MtlR (82). I expressed and purified amino-terminal His-tagged EI and HPr from *B. anthracis* which display 74% and 73% identity, respectively, to their *B. subtilis* counterparts. AtxA was not phosphorylated in the assay whether it was incubated with EI or HPr alone or with both proteins.

Since AtxA was not phosphorylated in the experiment, it is necessary to ensure the purified proteins (EI, HPr, and AtxA) were functional. EI is a large protein (570 amino acids, 62.9 kDa) which contains two functional domains. The amino terminus contains the site of

phosphorylation when the carboxy terminus catalyzes the conversion of PEP to pyruvate; therefore, both of the domains must be active if the protein is phosphorylated. HPr contains only 87 amino acids and is 9.2 kDa (73). P~His-HPr donates its phosphate to many proteins including sugar-specific EIIAs (up to 15 in a single cell), glycogen phosphorylase, and PRD-containing proteins (73). The same narrow region of HPr is used to interact with EI, EIIAs, or glycogen phosphorylase (162, 163). Thus, like EI, if HPr is phosphorylated it is presumed to be functional. Purified AtxA has been shown to bind DNA (Fig. 3-4) and form multimers in solution (Fig. 4-2), thus it is likely that it is folded correctly. These data suggest that the proteins are functional; however, a protein known to be phosphorylated by HPr is needed to confirm that HPr is active in the assay.

ptsHI mutant strains were constructed in *B. anthracis* to identify if EI and HPr have an indirect role in AtxA protein function. Deleting EI and HPr in *B. subtilis* has pleiotropic effects on carbohydrate utilization and CCR (73, 164, 165). Loss of EI and HPr leads to a defect in PTS-dependent sugar import due to the lack of phosphorylation of the EII complexes which transport and phosphorylate a carbohydrate as it transits the cell membrane. Additionally, disruption of *ptsH* will prevent CcpA/P-Ser-HPr from interacting with its target promoters. *B. subtilis* Δ*ptsHI* strains have reduced growth rates on several PTS sugars. In the conditions used for my experiments, only a slight delay in replication was detected for the *B. anthracis* Δ*ptsHI* strain. However, removal of *ptsHI* resulted in a decreased amount of toxin gene and *atxA* expression and AtxA protein. Loss of *atxA* transcript presumably led to the decrease in the P*lef-lacZ* transcriptional reporter.

HPr and EI may affect *atxA* transcription via CcpA. Chiang *et al.* (66) determined that CcpA indirectly increases *atxA* transcript level. It is also well-established in *B. subtilis* that CcpA requires P-Ser-HPr in order to bind to target promoters (75). Due to the absence of HPr in the *ptsHI* mutant, CcpA would not be able to bind to target promoters and this would lead to misregulation of the *atxA* promoter.

Plasmids harboring IPTG-inducible *ptsH*, *ptsI*, and *ptsHI* were used to complement the *ptsHI* mutation. Only the vector encoding HPr and EI was capable of increasing AtxA protein in the mutant background. Over-expression of *ptsH* was not able to complement the Δ*ptsHI* mutation. These data indicate that both EI and HPr are needed for *atxA* expression. Typically when both EI and HPr are needed for a function, it is due to EI-dependent phosphorylation of HPr H15. However, I propose that HPr is interacting with CcpA and the requirement of EI is related to the physiological state of the bacterium.

I reason that EI is needed for *atxA* expression, because EI increases fructose-1,6-bisphosphate (FBP) levels leading to phosphorylation of HPr S46 by HprK/P. FBP is an intermediate in glycolysis produced only when the PTS is functioning properly (74). In the Δ*ptsHI* strain, glycolysis may not function properly, thus FBP concentrations may be significantly affected. In *B. subtilis* FBP concentrations can range between 1.8 mM to 14.1 mM depending on the carbon source and a Δ*ptsI* strain has 1.8 mM FBP (149). HprK/P phosphorylates HPr in an ATP-dependent manner when there is greater than 5 mM FBP in the cell (166, 167). Low levels of FBP would lead to less HprK/P activity and a lower concentration of P-Ser-HPr. Considering this information, I predict that loss of CcpA-dependent CCA in the Δ*ptsHI* strain was due to the lack of HprK/P phosphorylation of HPr when P*hs-ptsH* was induced. If CcpA/P-Ser-HPr regulates *atxA*, expressing a phosphomimetic version of P-Ser-HPr (HPr S46D, (168)) in the *ptsHI* mutant could bypass the requirement of EI and FBP.

Typically, PRD-harboring proteins are activated by HPr-dependent phosphorylation, and their function is decreased upon phosphorylation via EIIA and/or EIIB. However, in *B. subtilis* Δ*ptsHI* strains, PRD-containing proteins either have no activity (82, 141, 153, 169, 170) or they are constitutively active (171, 172). The PRD proteins LicR, LicT, MtlR, and ManR require phosphorylation by P~His-HPr to be active; therefore in the *ptsHI* mutant their activity is depressed severely. In contrast, LevR and GlcT display constitutive activity in

ptsHI-null strains, because EIIA/B motifs are not able to phosphorylate the proteins to repress the activity of the regulator (82, 159). Given these two scenarios, if AtxA function is regulated by the PTS, an effect on AtxA activity should be detected in a *B. anthracis* Δ*ptsHI* mutant.

Deletion of *ptsHI* does not affect AtxA protein function when AtxA is induced from an IPTG-inducible promoter. The activity of AtxA after induction in the Δ*atxA* and Δ*ptsHI* strains was compared to the parent strain which contains *atxA* controlled by its native promoter. In toxin-inducing conditions (CACO$_3$), all three strains contained AtxA and produced similar levels of AtxA activity. In LB-air, which is not conducive for toxin gene expression, AtxA was only detected when induced from P*hs-atxA* in the Δ*atxA* and Δ*ptsHI* strains. The activity of AtxA in each strain was similar, albeit 100-fold lower than the same strains in CACO$_3$. If regulated by the PTS, AtxA activity should be repressed or constitutive. These data indicate that AtxA function is not regulated by *ptsHI*.

Taken collectively, the data support only one function of the PTS in virulence gene regulation of *B. anthracis*. The phenotype of the *ptsHI*-null strain indicates that CcpA and HPr activate transcription of *atxA*. Due to the lack of a phosphorylated product *in vitro* or an effect on AtxA in the Δ*ptsHI*, I conclude that EI and HPr do not play a role in activation or repression of AtxA activity.

It is quite surprising that AtxA was not phosphorylated in the phosphotransferase assay and that AtxA protein activity was not affected in the Δ*ptsHI* mutant. To date, all PRD-containing proteins tested are phosphorylated via HPr and thus regulated by the PTS. AtxA, which has homology to PRD-containing proteins, would be unique in this sense. However, AtxA contains structural features not found on PRD-containing antiterminators and is missing a motif present in PRD-containing activators. PRD-containing antiterminators, such as LicT and GlcT, contain an RNA-binding domain and two PRDs (73). DNA-binding proteins with PRDs, including MtlR and LicR, have a DNA binding region, two PRDs, an EIIB-like motif,

and an EIIA-like motif (73, 82). The motif structure of AtxA is predicted to be similar to MtlR and LicR; however, the EIIA-like motif is absent.

Before my work, the phosphorylation state of only one protein within the AtxA/Mga protein family has been investigated. Using a phosphotransfer assay, the group A *Streptococcus* virulence gene regulator Mga is phosphorylated via EI and HPr (McIver, personal communication). Results obtained using phosphomimetic mutations indicate that phosphorylation of H204 and H270 decreases Mga activity, whereas phosphorylation of H324 increases the function of the protein.

Due to the lack of evidence that AtxA is phosphorylated by the PTS, it must be considered that AtxA is not phosphorylated *in vivo*. The model proposed by Tsvetanova *et al.* (59) suggests that AtxA is phosphorylated at H199 and H379. The data which support AtxA phosphorylation include ^{32}P-labeled products that are immunoprecipitated by α-AtxA antibody and the activities of point mutations that mimic phosphorylation or dephosphorylation of AtxA (59). After several attempts, I have been unable to immunoprecipitate ^{32}P-labeled AtxA from cells cultured with ^{32}P-phosphate. I have repeated the experiments with the AtxA point mutants and included multimerization assays to gain insight into the structural changes conferred by the point mutations.

Phosphomimetic mutations should simulate the ionic charge and size of the phosphorylated amino acid. NMR studies comparing P-Ser-HPr and HPr S46D show that the proteins have virtually identical structures (173). HPr H15D and HPr H15E have similar affinities as P~His-HPr for HprK/P (174). Exchanging a phosphohistidine for an aspartic acid is the standard mutation used in research of PRD-containing proteins (85, 135, 159). Both aspartic acid residues and phosphohistidines are negatively charged, whereas the histidine side chain is positive when the pH is below 6.0. The carboxyl group in the aspartic acid side change also mimics the P-O bond in the phosphate moiety. These studies suggest that an aspartic acid is an appropriate mimic of a phosphorylated amino acid.

Using an aspartic acid residue to mimic phosphorylation of AtxA H379, I determined that the mutation causes a change in the multimeric properties and activity of AtxA. AtxA H199A, AtxA H199D, and AtxA H379A formed oligomers similar to the native protein. AtxA H379D did not interact with AtxA-His during a co-AP experiment, and it was not susceptible to BMH cross-linking. If it is assumed that AtxA H199D and AtxA H379D represent phosphorylated histidines, then these data are in agreement with the model for LicT dimerization. LicT forms a dimer when sites of positive regulation are phosphorylated. The dimer form of LicT is destabilized when phosphorylated at histidines that lower protein activity (78–80).

Although the AtxA H379D mutation supports the model of PRD-containing proteins, future experiments should be conducted to determine if the size or charge of the amino acid R group is causing the multimerization defect. Asparagine, glutamic acid, glutamine, serine and lysine could be tested instead of aspartic acid. Glutamic acid has a negative similar to aspartic acid and serine contains a polar side chain. Asparagine and glutamine residues contain similar shaped side chains as aspartic acid, except without the charge. Lastly, a lysine would retain the positive charge but increase the size of the histidine side chain. If AtxA H379E and AtxA H379S are the only point mutants to display phenotypes similar to AtxA H379D, then the results would suggest that the mutations are mimicking a phosphohistidine at position 379. The data would also support the model that AtxA is phosphorylated.

In summary, AtxA protein function is not regulated via the PTS; however the transcription rate of *atxA* is affected, presumably via CcpA/P-Ser-HPr. Point mutations at the predicted phosphorylation sites lead to the expected phenotypes when considering the model of PRD-protein function. Future experiments will investigate if AtxA is phosphorylated independent of the PTS.

Chapter VI

<u>Discussion</u>

6.1 Significant findings regarding the structure and function of AtxA

AtxA is a critical virulence gene regulator of *B. anthracis*. A *B. anthracis atxA*–null mutant is highly attenuated in murine models for anthrax (49, 106). The level and activity of AtxA dictate levels of virulence gene transcription within cells. Steady state levels of AtxA protein are impacted by transcriptional regulation of the *atxA* gene and protein stability. Regulation of AtxA activity takes place via post-translational modification and structural changes. Many details are known regarding regulation of the *atxA* promoter and the effect of an *atxA*-null strain on virulence gene expression (46–48). However, before the results conveyed in this dissertation, researchers knew little about the molecular mechanism of AtxA function.

My research has advanced the study of AtxA significantly. Chapter 3 describes my work to characterize the activity of AtxA when induced by a heterologous promoter, to analyze the two large domains within the AtxA protein, and to determine the affinity of AtxA for DNA. In Chapter 4, I describe experiments demonstrating that AtxA forms a homomultimeric structure, possibly a dimer. Formation of the multimer is dependent upon the EIIB-like motif, enhanced by CO_2/bicarbonate, and may be needed for optimal AtxA function. Data presented in Chapter 5 support previous evidence suggesting that CcpA/P-Ser-HPr regulates *atxA* transcription. On the other hand, my data challenged a previously proposed model in which the PTS phosphorylates AtxA. I show that AtxA function is not affected by EI or HPr. Finally, my studies on AtxA demonstrate that AtxA H379D is deficient in multimerization while other H199 and H379 point mutations are able to form oligomers.

Overall, my data support the following model of AtxA function. Oligomers of AtxA associate with specific promoter elements. AtxA activity is increased in response to the host-related signal CO_2/bicarbonate because this signal enhances AtxA multimerization. In contrast, AtxA activity is decreased by phosphorylation at H379 because multimerization is inhibited. Figure 6-1 and the following section detail a comprehensive model of *atxA*-

mediated virulence gene activation based upon previous data and new information generated during my thesis work.

6.2 A comprehensive model of *B. anthracis* virulence gene regulation

Steady state levels of functional AtxA are affected by transcriptional regulation of the *atxA* gene, post-translational covalent modification, and finally AtxA oligomerization. *Trans*-acting factors affect the activity of the *atxA* promoter via activation or repression of transcription. Moreover, the stability of the message is impacted by elements encoded within the *atxA* locus. One global regulator has been shown to affect AtxA protein level indirectly. Finally, post-translational modification and ligand-binding may alter the functional state of the protein.

Multiple proteins and signals affect *atxA* transcription (Fig. 6-1A). Positive regulators include CcpA/P-Ser-HPr and physiological temperature (37° C) (64, 66). AbrB, genes involved in cytochrome *c* biogenesis, and an unidentified repressor protein negatively impact *atxA* transcription (65, 67, 68, 106). These regulators impact *atxA* transcription at the σ^A-dependent P1 promoter and not at the secondary promoter (P2) (49, 63, 106). Additionally, an extended 3' end of the transcript is required for stability (175).

AtxA protein stability is controlled by the pleiotropic regulator CodY in an indirect manner (Fig. 6-1B). A Δ*codY* strain of *B. anthracis* contains normal levels of *atxA* transcription and translation; however the AtxA protein was not detected on Western blots of whole cell lysates (62). The authors of the study suggest that either CodY represses an unidentified protease that degrades AtxA or CodY activates an AtxA-binding protein and/or a chaperone that promotes AtxA stability.

Once the *atxA* gene is transcribed and the protein is stable, AtxA must form the proper structure via protein modification and ligand binding (Fig. 6-1C). The EIIB-like motif
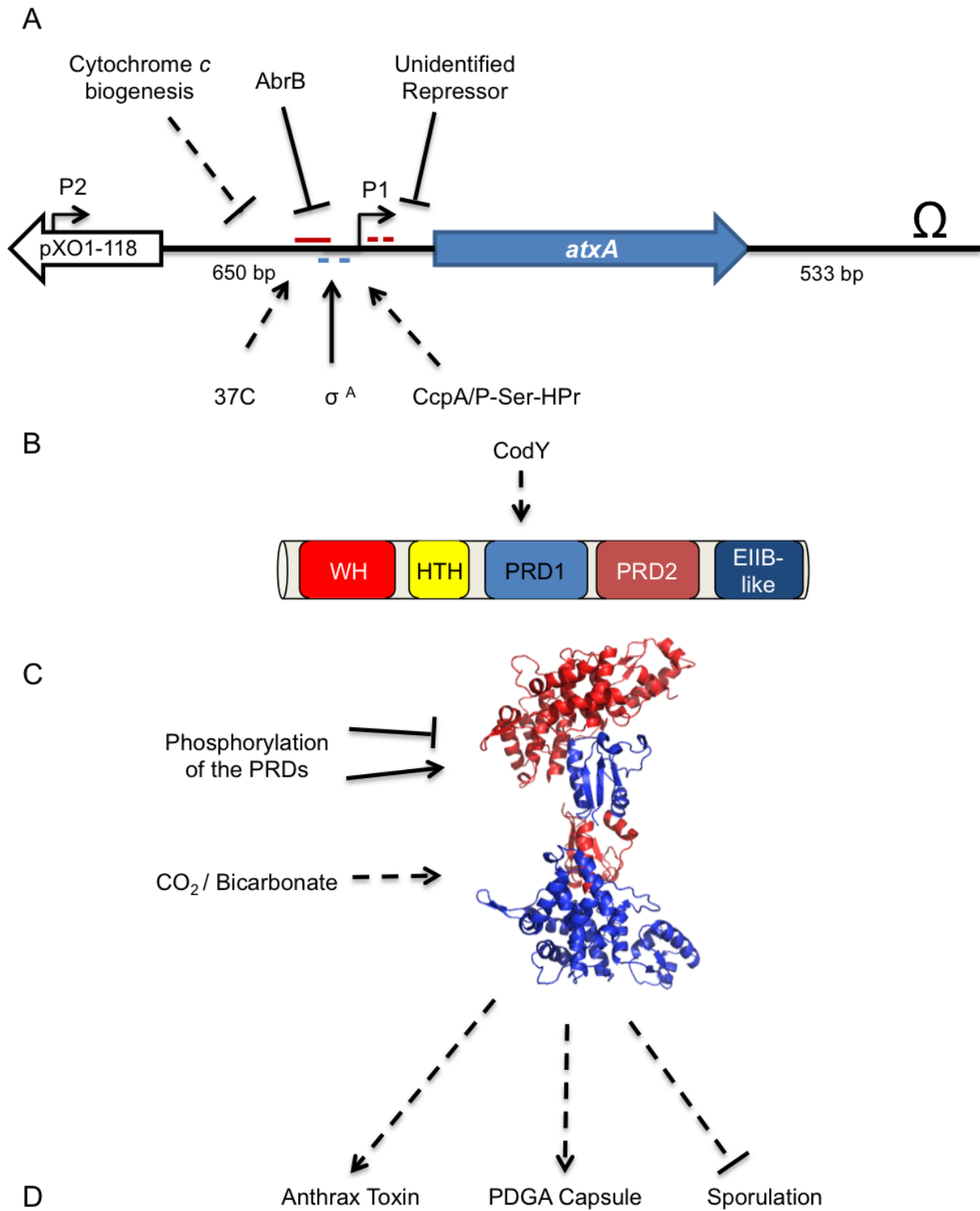
Figure 6-1. A comprehensive model of *atxA*-dependent virulence gene regulation.

Figure 6-1. A comprehensive model of *atxA*-dependent virulence gene regulation. The schematic represents three layers of control governing A. *atxA* transcription, B. AtxA stability, and C. AtxA protein activity. Also presented are the major outcomes of D. AtxA function. See text an explanation of the model. Straight arrows indicate direct regulation, whereas dashed arrows suggest indirect or unknown routes of regulation. A. Upstream of the *atxA* gene are sequences which are bound by repressors (red lines) or an activator (blue line) of transcription.   Transcriptional regulation occurs at the primary promoter (P1), not the promoter located further upstream (P2).   Downstream of the gene is an extended 3' untranslated region and a stem-loop (Ω). B. The cartoon depicts five motifs within AtxA: winged-helix-turn-helix (WH), Mga-like helix-turn-helix (HTH), two PTS regulation domains (PRD1 and PRD2), and an Enzyme IIB-like motif (EIIB-like).   C. A structural model of an AtxA homodimer is shown (one subunit is red and the other is blue).

facilitates formation of a homomultimeric structure and the amount of multimer correlates with AtxA activity. These results suggest that the multimeric form of AtxA is needed for the protein to be active. The mechanisms that induce or inhibit oligomerization are unknown; however, phosphorylation of H379 may inhibit the multimer structure while CO_2/bicarbonate may promote AtxA oligomer formation.

Once all three of these regulatory steps are overcome, *B. anthracis* virulence traits are expressed (Fig. 6-1D). The anthrax toxin genes may be controlled directly by AtxA (46, 47), whereas AtxA activates PDGA capsule biosynthesis indirectly (Bourgogne 2003). AtxA regulates several genes within the *B. anthracis* genome and indirectly inhibits sporulation (57, 176).

For the remainder of my discussion, I will highlight several aspects of this model of AtxA regulation.

6.3 *atxA* control by CcpA/P-Ser-HPr and CodY provides a link between metabolism and *B. anthracis* virulence

Work presented in Chapter 5 provides support for roles of CcpA and HPr in the regulation of the *atxA* gene. *B. anthracis* Δ*ccpA* and Δ*ptsHI* mutants contain a low steady state level of *atxA* transcript compared to the parent strain (66). In a separate study, CodY was shown to mediate AtxA protein stability (62). *B. anthracis* mutants devoid of *codY* exhibit a decrease in AtxA protein level. CcpA/P-Ser-HPr and CodY act indirectly on *atxA* to regulate virulence presumably through different mechanisms. Intriguingly, both CcpA/P-Ser-HPr and CodY activity are influenced by the metabolic state of the bacterium. Therefore, I postulate that the mammalian host provides metabolic signals that prompt *B. anthracis* to induce transcription of *atxA* and stabilize the AtxA protein.

When the local concentration of glucose and other quickly metabolized carbohydrates is high, CcpA/P-Ser-HPr represses and activates genes. Studies in *B. subtilis*

have shown that phosphorylation of HPr S46 is required for the protein to form a heterodimer with CcpA (73). HprK/P is responsible for phosphorylating HPr S46 in an ATP-dependent manner when fructose-1,6-bisphosphate (FBP) concentrations are high. ATP and FBP are abundant in cells growing on carbohydrates the bacteria can import and metabolize quickly, such as glucose.

In *B. subtilis,* metabolism of glucose increases the cellular concentration of GTP, which is an activating ligand of the regulator CodY. Branched-chain amino acids (BCAA; leucine, valine, and isoleucine) also increase activity of CodY. GTP levels are an indicator of the energetic state of the cell while BCAA represent the abundance of nutrients (proteins) in the environment. Either small molecule is able to induce DNA-binding; however there is an additive effect when both interact with CodY (61).

Glucose and BCAA are readily available in the cytoplasm of host cells (177). Glucose is the preferred carbon source for most host cells, and the normal concentration in plasma is 1 mg ml^{-1} (178). BCAA are available in tissue as proteins are broken down due to starvation (179) or proteolytic enzymes, including InhA1 and NprB which are secreted by *B. anthracis* (72, 105).

Signals and conditions associated with replication of *B. anthracis* in mammalian tissue are simulated by toxin-inducing culture medium. When cultured in CACO$_3$ broth incubated at 37° C with 5% atmospheric CO$_2$, *B. anthracis* produces high levels of anthrax toxin compared to other culture media and atmospheric conditions (Fig. 4-8 and 5-3, (47)). CACO$_3$ is a semi-defined medium that contains acid hydrolyzed casein (casamino acids) and glucose among other nutrients (99). Casamino acids contain a mixture of all amino acids, including the BCAA. Since glucose and BCAA promote the activity of CcpA/P-Ser-HPr and CodY, respectively, I propose that the major signals influencing the amount of AtxA protein in CACO$_3$ are glucose and BCAA.

CcpA/P-Ser-HPr and CodY are involved in the production and stability of AtxA. Since these factors are active in the presence of glucose and BCAAs found in the mammalian host, these data show a link between virulence gene activation and the metabolic state of the cell.

6.4 Regulation of AtxA protein function via multimerization

Host-related signals are needed also to promote AtxA protein function. CO_2/bicarbonate and phosphorylation may regulate AtxA activity separately. It would be interesting to study the interplay between CO_2/bicarbonate and phosphorylation with respect to AtxA activity and multimerization. I propose that CO_2/bicarbonate locks AtxA into an active, multimeric state by facilitating rearrangement of the WH and HTH motifs. Without CO_2/bicarbonate, AtxA may still multimerize, but the DNA-binding activity could be reduced. Phosphorylation of H199 may initiate formation of the oligomer via ionic interactions between the phosphohistidine and a basic amino acid. On the other hand, phosphorylation at H379 may deactivate the protein by prohibiting multimerization. This model for AtxA multimerization is similar to the Domain Swing/Lock Mechanism of LicT (79). In this model, AtxA transitions between three functional states: a monomer, an unstable multimer, and a stable, highly active multimer.

The first prediction of the AtxA multimerization model proposes that AtxA has a monomeric form and that the AtxA monomer does not activate target promoters. Experimental evidence suggests that phosphorylation of H379 prevents proper multimer formation. AtxA H379D did not interact with AtxA-His in a co-AP experiment and it was not susceptible to BMH cross-linking (Fig. 5-4). These data suggest that phosphorylation of H379 converts AtxA into a monomer; however, an alternative explanation is that H379 phosphorylation promotes formation of an unstructured aggregate.

The AtxA multimerization model suggests that an unstable oligomeric state for AtxA serves as a transition point between monomeric and highly stable multimeric states. This

stage would occur in the absence of any post-translational modification or CO_2/bicarbonate binding to AtxA. To replicate the non-phosphorylated state of AtxA, I could express AtxA H199A and AtxA H379A. Characterization of the multimeric properties of AtxA H199A and AtxA H379A could provide support for a transient stage of multimerization. AtxA H199A and AtxA H379A are capable of forming normal AtxA multimers (Fig. 5-4). This indicates that multimer formation is not dependent on phosphorylation of H199 or H379. Culturing *B. anthracis* in CA medium in air and the absence of added CO_2/bicarbonate would simulate the ligand-free state of AtxA. In this growth condition, AtxA multimer formation and toxin gene expression are reduced to 50% of the levels observed in the same conditions but with added CO_2/bicarbonate (Fig. 4-8). Since the AtxA multimer was able to form in normal atmospheric conditions, AtxA may form a weak oligomer in the absence of CO_2/bicarbonate or the small molecules may affect AtxA indirectly.

The final form of AtxA suggested by the AtxA multimerization model is a stable, highly active dimer. Ligand-binding and phosphorylation of H199 are the likely modifications needed to lock the AtxA multimer into its active conformation. The relatively low level of toxin gene transcription in strains containing AtxA H199A supports the requirement of H199 phosphorylation for oligomerization. Although the H199A protein displays normal multimers, it produces less than 33% of the activity of native AtxA (Fig. 5-4). Disruption of phosphorylation at H199 may weaken the AtxA multimer resulting in loss of AtxA activity.

I proposed in section 4.3 that CO_2/bicarbonate may bind to AtxA. At the 2011 International Conference on Gram-Positive Microorganisms, data were presented suggesting that N453 of AtxA was involved in binding bicarbonate and had an impact on AtxA solubility (Fouet, personal communication). The carboxy terminus of AtxA (amino acids 438-469) bears weak similarity to the first 32 amino acids of RegA, and within that region, AtxA N453 aligns with RegA N16 suggesting the residues perform similar functions. RegA, an AraC/XylS-type bicarbonate-binding transcription factor of *Citrobacter rodentium*, interacts

with bicarbonate via an amino-terminal motif (144, 145). Mutation of RegA N16 to an alanine results in constitutive activation of RegA-dependent promoters presumably by mimicking the structural changes induced by bicarbonate. The model of RegA activity proposes that two proteins form a dimer via their amino-termini when bicarbonate is present. Activity of AtxA N453A in normal air was similar to AtxA cultured in elevated CO_2/bicarbonate. If AtxA functions similarly to RegA with respect to bicarbonate binding and multimerization, then bicarbonate-binding would lock AtxA proteins together in a multimeric structure. Without bicarbonate, AtxA oligomers could form, but they would not be stable.

Applying the Domain Swing/Lock Mechanism to AtxA, I propose that phosphorylation and bicarbonate affect AtxA function by altering its multimeric structure. Monomers of AtxA are prohibited from forming oligomers when H379 is phosphorylated. When bicarbonate concentrations are low and the protein is not phosphorylated, AtxA is in a transitional form capable of forming weak protein-protein interactions. The AtxA multimer is locked in a highly active state when H199 is phosphorylated and bicarbonate interacts with N453.

Several experiments may be performed to test the model of AtxA homodimer formation. If the energy transfer between two different AtxA-chromophore fusions can be detected *in vivo*, Förster resonance energy transfer (FRET) experiments could detect formation of AtxA multimers. To observe CO_2/bicarbonate enhancement of multimerization, FRET measurements may be collected using cells cultured in the presence or absence of elevated atmospheric CO_2 and dissolved bicarbonate. I would expect to see greater energy transfer when CO_2 and bicarbonate are present. Additional FRET experiments utilizing various culture media (LB and CA) or point mutations within one or both AtxA fusions may provide additional support for the role of AtxA phosphorylation on the stability of AtxA oligomers. Point mutants of AtxA could also be tested *in vitro* by performing size exclusion chromatography, analytical ultracentrifugation, or surface plasmon resonance.

Extensive analysis of an AtxA-bicarbonate interaction has not been done. It may be possible to detect ^{14}C-labeled bicarbonate bound to AtxA. One method would be to affinity-purify AtxA-His expressed in cells cultured in the presence of ^{14}C-bicarbonate. If samples containing AtxA had a higher radioactive signal than control samples (no ^{14}C-bicarbonate and samples without AtxA), the results would indicate that bicarbonate is a ligand of AtxA. A similar experiment can be performed *in vitro* using purified AtxA-His. Adding unlabeled bicarbonate to purified AtxA-His when performing *in vitro* multimerization assays or DNA binding experiments could enhance the activity of AtxA. If AtxA binds bicarbonate and the binding is lost when AtxA N453A is tested, then N453 of AtxA may function similar to RegA N16 and interact with bicarbonate.

6.5 Specific DNA binding by AtxA

The proposed Domain Swing/Lock Mechanism of AtxA multimerization describes the various quaternary structures that may exist for AtxA. Each structure either promotes or prohibits AtxA function *in vivo*. As suggested above, the role of AtxA is to bind to target promoters to enhance transcription of the genes. Work presented in Chapter 3 demonstrates that AtxA can bind to DNA promoters; however, AtxA interacted with the sequences non-specifically. This portion of the discussion will address the reasons why AtxA bound non-specifically to DNA and propose future methodologies to attempt when studying AtxA-DNA interactions.

Filter binding assays were used to assess the interaction between AtxA and promoter sequences. The experiment detects DNA when it has complexed with a protein and subsequently binds to a membrane. In effect, the protein precipitates onto the membrane, and DNA is captured during the precipitation. The protein-DNA affinity is determined using target promoters, whereas other DNA sequences are used to control for non-specific protein-DNA interaction.

The filter binding assay has been used to study many proteins and is a valid technique; however, it may not be the best method to study AtxA-DNA interactions. Precipitation of AtxA, a highly positively charged protein, onto the membrane could indicate falsely that the protein is binding to DNA sequences in the assay. In addition, the interaction of the DNA and protein does not need to be very strong. The method does not require any wash steps and there is little opportunity for DNA and protein to dissociate if they are non-specifically interacting.

During *in vitro* analyses, AtxA may be able to bind DNA independent of its multimeric state. Recently, Hondorp *et al.* described how Mga forms a multimer in solution and that an EIIB-like motif is needed for the protein-protein interaction (180). Interestingly, the authors tested the DNA-binding activity of a derivative of Mga lacking the EIIB-like motif. Although the truncated protein was a monomer in solution and had no detectable activity *in vivo*, it bound to DNA with only a slightly weaker affinity (less than 2-fold change) compared to the full-length protein. These data suggest that Mga, and by extension AtxA, may bind to DNA in these *in vitro* assays as a monomer, whereas a dimeric protein is needed in the cell to bind DNA and activate transcription.

There is some precedence for *in vitro* DNA binding occurring in the absence of the appropriate multimeric state. For example, PhoP, a response regulator involved in Mg^{2+} homeostasis in *Salmonella typhimurium*, typically binds DNA as a dimer after it is phosphorylated (181). However, when present in high concentrations, unphosphorylated PhoP binds DNA as a monomer and then recruits the second monomer to the binding site. The affinity of the first monomer to DNA is ~17-fold higher than the affinity of the second monomer to the binding site. These studies were conducted using biophysical methods including isothermal titration calorimetry, fluorescence titration measurements, analytical ultracentrifugation, and surface plasmon resonance. It would be interesting to see if similar results would be seen using a filter binding assay. I suggest that the binding affinity of the

second monomer of PhoP would be masked by the affinity of the first protein. Once one protein binds to the DNA probe, the probe will stay on the membrane regardless if the second monomer is present or not. If AtxA follows a similar mode of DNA binding where one subunit interacts with DNA with a higher affinity than the second subunit, then I would be detecting only the interaction of the first subunit.

For dimeric DNA binding proteins, interaction of the second monomer provides specificity and optimal affinity of the protein to its cognate DNA (182). In several eukaryotic systems, DNA-binding proteins within the same family have similar recognition sites. The transcription factors achieve specificity by recognizing a predetermined length between the binding sites. *In vitro* several proteins can bind to half sites as a monomer, and full binding by a dimer only occurs when the spacer between the sites is the correct size. AtxA may be similar in this regard. AtxA may bind to a pair or series of specific nucleotide sequences or structural elements. If only one of the sites is present on the non-specific probe used in the filter binding assay, then AtxA will be able to form a complex and an interaction will be detected.

In addition to the methods mentioned above in the study of PhoP, Electrophoretic mobility shift assays (EMSAs), fluorescence polarization, and DNA foot-printing analyses may provide additional information regarding the mechanism and affinity of AtxA to DNA. EMSAs allow the protein-DNA complex to be visualized and if more than one form of the complex is present, they will be detected. EMSAs may be problematic due to the high pI of AtxA (pI = 9.3). At a neutral pH, AtxA is highly positively charged and migrates toward the cathode rather than the anode like the DNA. However, the poly-acrylamide concentration of the gel and pH of the buffer may be optimized to permit analysis of AtxA via this technique. Fluorescence polarization assays allow for protein-DNA interactions to be viewed in real-time as they occur in solution. The assay would not distinguish between a monomer of AtxA and a multimer of AtxA; however, it would remove the precipitation step needed for a filter binding

assay. Lastly, foot-printing experiments could provide sequence-specific information regarding the AtxA-DNA interaction. The size of the region protected in the experiment could indicate the number of AtxA molecules interacting with the DNA element.

The experimental methodology may not be the cause of the non-specific binding of AtxA. It is possible that AtxA is not in the proper form. The dimer form of AtxA may not be the dominant species of the protein in solution. Post-translational modification and ligand-binding may confer structural changes within the protein that allow it to specifically interact with DNA. Point mutations of AtxA could mimic the structural changes needed for DNA-binding.

6.6 A structural model of AtxA

Early attempts to crystallize AtxA or determine the solution structure via NMR spectroscopy were not successful. Nevertheless, obtaining the structure of AtxA remains a worthwhile pursuit. Until a crystal or NMR structure is determined, modeling AtxA against known structures can be informative and guide future experiments. Fortunately, the structure of an AtxA/Mga family member has been solved.

The 2.31 Å-resolution crystal structure of the Mga-like protein from *Enterococcus faecalis* was determined recently (PDB file = 3SQN, (88)). The protein is encoded by the gene EF_3013 and annotated as a "conserved domain protein." No functional information about this protein or gene is known. The structural motifs of the Mga-like protein match those predicted to be in the AtxA/Mga family. Two HTH, two PRDs, and an EIIB-like motif are present producing a structure that is 56% alpha helical and 9% beta sheet. The protein crystallized as a dimer in which the EIIB-like motif of one subunit interacts with the PRDs and HTH motifs of the other subunit (Fig. 1-4). In total, 83 residues are involved in the dimer interface with an area of 3182.8 Å^2 according to the "Protein interfaces, surfaces, and

assemblies" software (PISA, (183)). It is not known if the structure represents an active state of the protein or if the protein forms a homodimer *in vivo*.

I used the protein homology/analogy recognition engine (Phyre2, (137)) and the Swiss-pdb viewer (184) to construct a structural model of an AtxA homodimer using the Mga-like protein as a template (Fig. 6-2 and 6-3A). The Mga-like protein has 19% identity and 39% similarity (total conservation = 58%) to AtxA. The model contains residues 89-474 of AtxA which encompass the Mga-HTH, PRDs, and the EIIB-like motif. The WH motif is not present in the structure generated by Phyre2. I have used the structural model to make predictions about the functions of AtxA motifs as well as locations of specific residues.

Viewing the overall motif organization, I can make two observations. First, the EIIB-like motif is at the center of the homodimer (Fig. 6-2). As is true for the structure of the Mga-like protein, the EIIB-like motif from one chain reaches into a pocket created by the PRDs and EIIB-like motif of the second subunit. If the protein lacked the EIIB-like motif, all contact between the subunits would be lost. In addition, the EIIB-like motifs from each monomer form few contacts with each other; therefore, EIIB-like motifs may not interact if expressed independently. My data suggesting that the EIIB-like motif is necessary, but not sufficient, for dimerization fit this model. The second observation is that HTH motifs from both chains are on the same face of the dimer, and the motifs are extended from the remainder of the protein. Typically, the HTH motifs of dimeric DNA-binding proteins are located on the same side of the complex (126). In addition, the first residues of the recognition helix of each subunit are separated by approximately 98 Å. Since one turn of DNA is 34 Å and encompasses ten nucleotides, the distance between the HTH motifs suggests that AtxA binding sites may be separated by greater than 30 bp. The location of the motifs would allow AtxA to bind DNA.

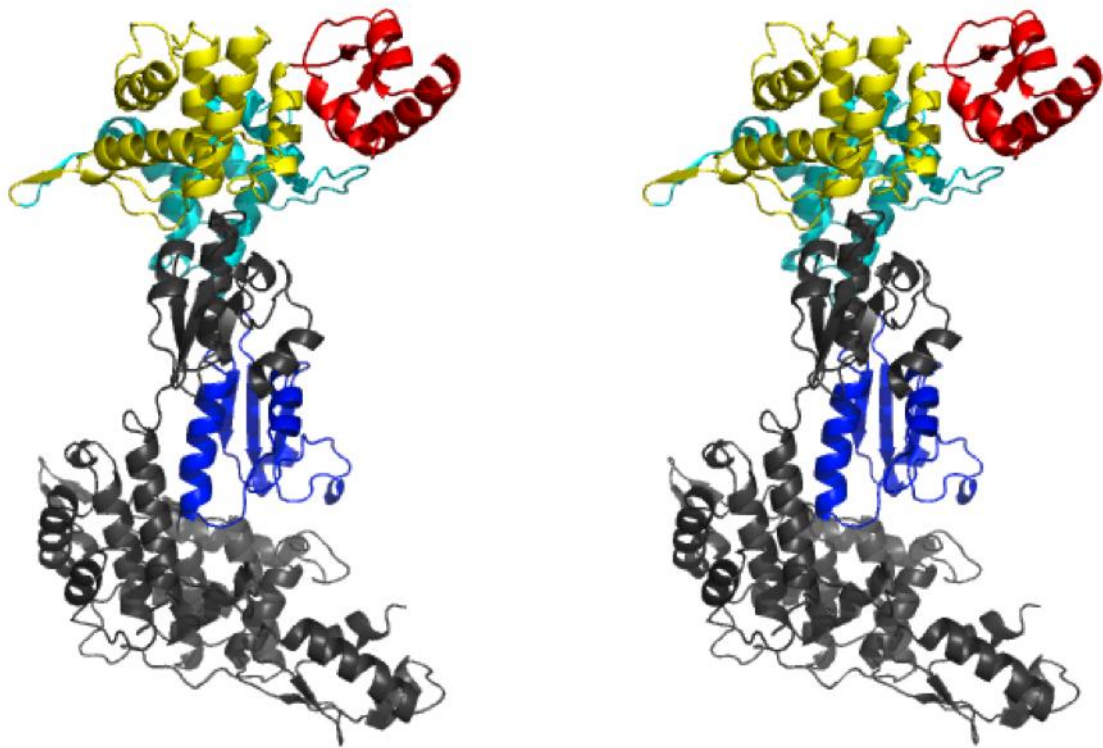**Figure 6-2. A structural model of the AtxA homodimer.** A stereo image of a structural model of AtxA was created using Phrye2 based on the the X-ray crystal structure of the Mga-like protein from *E. faecalis* (PDB = 3SQN, chain B). The motifs of one subunit are colored: HTH is red, PRD1 is yellow, PRD2 is cyan, and EIIB-like motif is blue. The WH motif was not modeled. The second subunit is grey.

After viewing the locations of several key residues, I can provide additional analysis of their roles in AtxA function and their use in my experiments. In section 4.2.3, I described experiments using C→S mutations of AtxA to determine the cysteine required for BMH to cross-link two AtxA proteins. After fixing cell lysates with BMH, AtxA C402S was present only as a monomer, whereas the other C→S mutations, including AtxA C161S and AtxA C202S, were dimers. When native AtxA and AtxA C402S-FLAG were co-expressed in *B. anthracis*, AtxA C402S-FLAG remained as a monomer indicating that it was not able to cross-link with AtxA. These data suggested that C402 cross-linked to the corresponding C402 of the second subunit (C402'). The data clearly indicate that C402 participates in the BMH cross-linking; however, the binding partner of C402 could not be C402' if the structural model is accurate. C402 is located on the opposite side of the dimer interface from C402' (Fig. 6-3B). Using the Swiss-pdb viewer software, the residues are over 46 Å from one another, which is much greater than the size of the spacer arm of BMH (13 Å). When locating the other cysteines in the AtxA model, I detected a region that contained C161, C202, and C402' within 12 Å of each other (Fig. 6-3C). Theoretically, C402' could cross-link to C161 or C202 with equal affinity. However, intermolecular cross-linking of C402' to C161 or C202 may compete with intramolecular BMH bonds between C161 and C202. BMH-mediated cross-linking of C161-C202 of AtxA C402S-FLAG may explain why the mutant protein was not fixed to native AtxA (Fig. 4-5C). To address if C402' cross-links to C161 or C202, I could determine if AtxA C161S/C202S is susceptible to BMH cross-linking.

In addition to C402 being important for the BMH cross-linking experiment, it may have a significant role *in vivo*. As described in section 4.3, C402 resides within the P-loop of the EIIB-like motif which is a conserved region that contains a phosphorylated cysteine in EIIB motifs of the PTS (138). In the AtxA structural model, C402, and thus the P-loop, may contact residues in the adjoining AtxA molecule and phosphorylation of this loop may significantly impact multimerization. Moreover, the pocket containing C402', C161, and C202
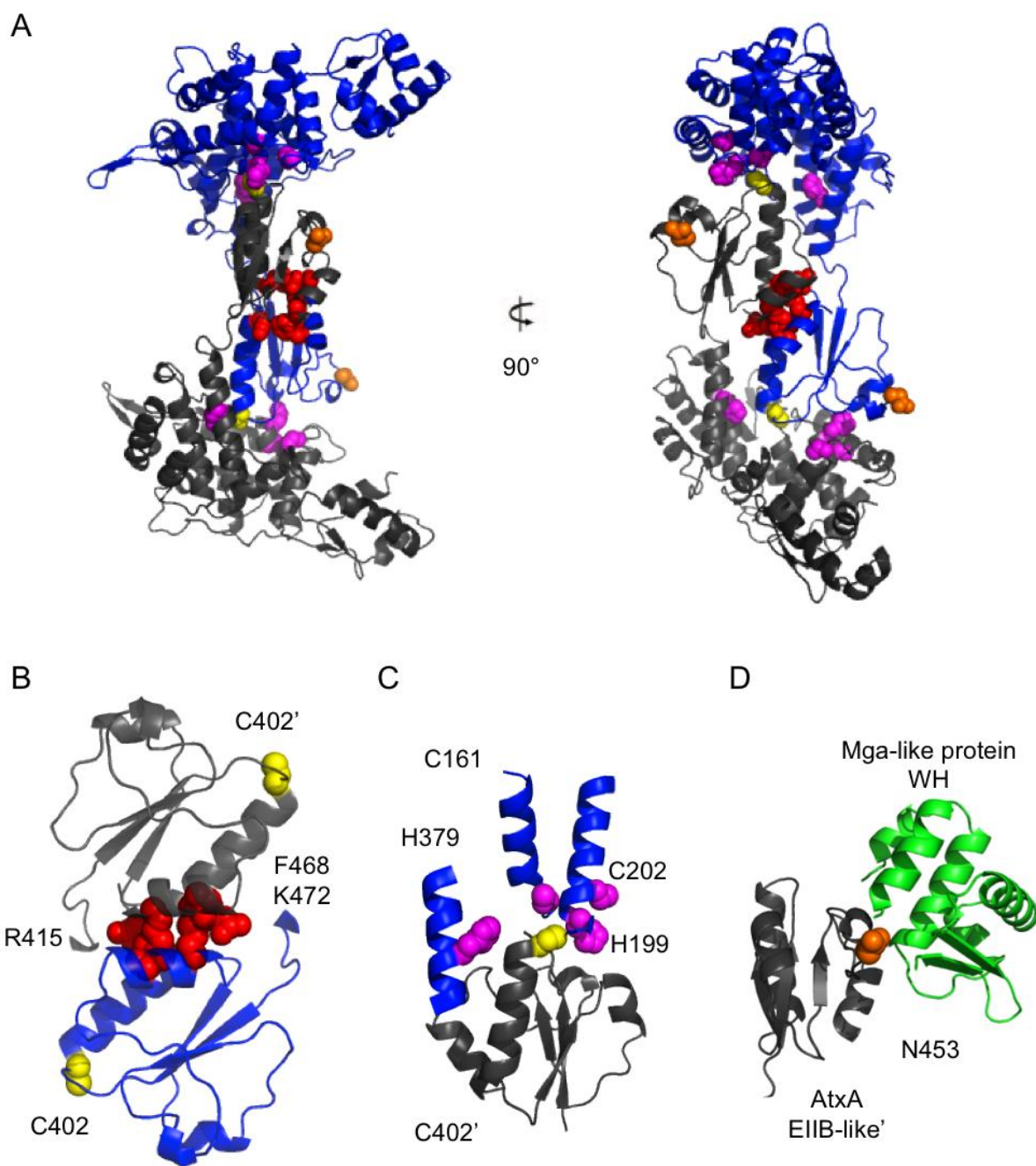
Figure 6-3. Areas of interest in the structural model of the AtxA homodimer.

Figure 6-3. Areas of interest in the structural model of the AtxA homodimer. Three areas of the AtxA homodimer contain residues that have been shown to be important experimentally or *in silico*. A. The model of the homodimer is presented alongside a 90° rotation of the structure. One monomer is colored blue and the other is grey. Side chains of the important residues are depicted as spheres. The color scheme is the same for all panels. B. The EIIB-like motifs from both chains are displayed. The C402 residues (yellow) are on opposite sides of the motifs. Between the motifs, R415, F468, and K472 (red) may form a metal-binding pocket. C. The region surrounding C402 (yellow) from one monomer contains C161, H199, C202, and H379 (magenta) from the second subunit.   D. Depicted is a potential interaction between N453 (orange) of the AtxA EIIB-like motif and the WH motif (green) from the structure of the Mga-like protein (PDB = 3SQN, chain A).

also harbors H199 and H379, the phosphorylation sites of AtxA (Fig. 6-3C). If C402 is phosphorylated, it may present an ionic clash and steric hindrance with a phosphohistidine at H199 or H379.

The AtxA structural model displays residues that may interact with phosphorylated H199 and H379. According to the Domain Swing/Lock Mechanism, phosphohistidine at H199 should increase the stability of an AtxA dimer. The phosphohistidines of LicT interact with arginine residues of the adjacent subunit (135). H199 slightly extends into the adjacent EIIB-like motif suggesting that it forms important contacts. AtxA H199-phosphate may interact with R424' to increase the AtxA-AtxA affinity. Likewise, H379 extends away from the core of PRD2 and toward the interface with the EIIB-like motif of the second AtxA subunit. The helix containing H379 also harbors several non-polar residues (L375, M378, T382, and M385) that face non-polar amino acids on the complementary alpha-helix of the EIIB-like motif (I403', Y406', and L411'). H379 in its non-phosphorylated form may interact with Y406'. When phosphorylated, H379 could disrupt the hydrophobicity of the region and destabilize the dimer. The AtxA multimerization model predicts that H379 inhibits proper multimer formation.

In silico analysis of the AtxA structural model suggests that zinc and magnesium may bind to the protein. The 3DLigandSite Server (185) suggests that R415, F468, and K472 of both AtxA subunits interact with the metal ions. It is significant that these residues form an interface between the EIIB-like motifs of each subunit (Fig. 6-3B). A metal ion may also bind the Mga protein of GAS. McIver and co-authors have suggested that Mga chelates a metal as it is expressed in *E. coli* and *S. pyogenes* (McIver, personal communication). Mutation of R415, F468, and K472 may have a substantial impact on homodimer formation and metal binding.

Another interesting observation was made when constructing a model of a heterodimer of the Mga-like protein and AtxA. In the model, N453 of AtxA resides next to a

loop between the WH and HTH motifs of the Mga-like protein (Fig. 6-3D). The structure of the loop (Mga-like protein residues 76-78) was not detected in the Mga-like protein crystal structure which suggests that it is flexible. As described above, Fouet and colleagues suggest that N453 binds to bicarbonate (Fouet, personal communication). If N453 interacts with a bicarbonate ion, then the loop may become more rigid and alter the conformation of the adjacent WH and HTH motifs. The change in WH and HTH orientation may allow AtxA to bind DNA efficiently and specifically. Bicarbonate binding via N453 may be the final step in AtxA dimerization.

The structural model of the AtxA homodimer has provided support for my experimental data. As with all *in silico* analyses, this structural model provides rationale for many additional experiments.

6.7 Concluding remarks

Future studies of AtxA will answer several lingering questions. Does AtxA bind to bicarbonate? Which proteins phosphorylate AtxA? Does AtxA form a dimer and is that dimer structurally similar to the Mga-like protein? How does AtxA associate with DNA?

Future data will support an emerging model in microbial pathogenesis which suggests that there is a relationship between host signals and virulence gene expression. Many pathogenic bacteria effectively colonize environmental niches that are very different from the conditions within their susceptible host. *Borrelia burgdorferi* inhabits a tick before infecting a mammal, *Vibrio cholerae* is a water-borne bacterium prior to taking up residence in the human intestines, and *B. anthracis* dwells in the soil before rapidly replicating within its host. Signal transduction pathways leading to virulence gene expression must differentiate between the cues in each location. Interestingly, these signals affect basic bacterial physiology. *B. anthracis* senses the temperature, carbohydrate availability, and CO_2/bicarbonate concentration to regulate *atxA* and virulence gene expression. My doctoral

studies have helped to understand the link between these fundamental processes and pathogenesis.

References

1. Bourret, R.B., and R.E. Silversmith. 2010. Two-component signal transduction. Current Opinion in Microbiology. 13: 113–115.

2. Green, B.D., L. Battisti, T.M. Koehler, C.B. Thorne, and B.E. Ivins. 1985. Demonstration of a capsule plasmid in *Bacillus anthracis*. Infect. Immun. 49: 291–297.

3. Kaspar, R.L., and D.L. Robertson. 1987. Purification and physical analysis of *Bacillus anthracis* plasmids pXO1 and pXO2. Biochem. Biophys. Res. Commun. 149: 362–368.

4. Read, T.D., S.N. Peterson, N. Tourasse, L.W. Baillie, I.T. Paulsen, K.E. Nelson, H. Tettelin, D.E. Fouts, J.A. Eisen, S.R. Gill, E.K. Holtzapple, O.A. Okstad, E. Helgason, J. Rilstone, M. Wu, J.F. Kolonay, M.J. Beanan, R.J. Dodson, L.M. Brinkac, M. Gwinn, R.T. DeBoy, R. Madpu, S.C. Daugherty, A.S. Durkin, D.H. Haft, W.C. Nelson, J.D. Peterson, M. Pop, H.M. Khouri, D. Radune, J.L. Benton, Y. Mahamoud, L. Jiang, I.R. Hance, J.F. Weidman, K.J. Berry, R.D. Plaut, A.M. Wolf, K.L. Watkins, W.C. Nierman, A. Hazen, R. Cline, C. Redmond, J.E. Thwaite, O. White, S.L. Salzberg, B. Thomason, A.M. Friedlander, T.M. Koehler, P.C. Hanna, A.B. Kolstø, C.M. Fraser. 2003. The genome sequence of *Bacillus anthracis* Ames and comparison to closely related bacteria. Nature. 423: 81–86.

5. Vodkin, M.H., and S.H. Leppla. 1983. Cloning of the protective antigen gene of *Bacillus anthracis*. Cell. 34: 693–697.

6. Robertson, D.L., and S.H. Leppla. 1986. Molecular cloning and expression in Escherichia coli of the lethal factor gene of *Bacillus anthracis.* Gene. 44: 71–78.

7. Tippetts, M.T., and D.L. Robertson. 1988. Molecular cloning and expression of the *Bacillus anthracis* edema factor toxin gene: a calmodulin-dependent adenylate cyclase. J. Bacteriol. 170: 2263–2266.

8. Makino, S., C. Sasakawa, I. Uchida, N. Terakado, and M. Yoshikawa. 1988. Cloning and CO_2-dependent expression of the genetic region for encapsulation from *Bacillus anthracis*. Mol. Microbiol. 2: 371–376.

9. Hoffmaster, A.R., J. Ravel, D.A. Rasko, G.D. Chapman, M.D. Chute, C.K. Marston, B.K. De, C.T. Sacchi, C. Fitzgerald, L.W. Mayer, M.C. Maiden, F.G. Priest, M. Barker, L. Jiang, R.Z. Cer, J. Rilstone, S.N. Peterson, R.S. Weyant, D.R. Galloway, T.D. Read, T. Popovic, and C.M. Fraser. 2004. Identification of anthrax toxin genes in a *Bacillus cereus* associated with an illness resembling inhalation anthrax. Proc. Natl. Acad. Sci. U.S.A. 101: 8449–8454.

10. Cachat, E., M. Barker, T.D. Read, and F.G. Priest. 2008. A *Bacillus thuringiensis* strain producing a polyglutamate capsule resembling that of *Bacillus anthracis*. FEMS Microbiol. Lett. 285: 220–226.

11. Saile, E., and T.M. Koehler. 2006. *Bacillus anthracis* multiplication, persistence, and genetic exchange in the rhizosphere of grass plants. Appl. Environ. Microbiol. 72: 3168–3174.

12. Schuch, R., and V.A. Fischetti. 2009. The secret life of the anthrax agent *Bacillus anthracis*: bacteriophage-mediated ecological adaptations. PLoS ONE. 4: e6532.

13. Schuch, R., A.J. Pelzek, S. Kan, and V.A. Fischetti. 2010. Prevalence of *Bacillus anthracis*-like organisms and bacteriophages in the intestinal tract of the earthworm Eisenia fetida. Appl. Environ. Microbiol. 76: 2286–2294.

14. Shetron-Rama, L.M., A.C. Herring-Palmer, G.B. Huffnagle, and P. Hanna. 2010. Transport of *Bacillus anthracis* from the lungs to the draining lymph nodes is a rapid process facilitated by CD11c+ cells. Microb. Pathog. 49: 38–46.

15. Russell, B.H., R. Vasan, D.R. Keene, and Y. Xu. 2007. *Bacillus anthracis* internalization by human fibroblasts and epithelial cells. Cell. Microbiol. 9: 1262–1274.

16. Shafazand, S., R. Doyle, S. Ruoss, A. Weinacker, and T.A. Raffin. 1999. Inhalational anthrax: epidemiology, diagnosis, and management. Chest. 116: 1369–1376.

17. Hudson, M.J., W. Beyer, R. Böhm, A. Fasanella, G. Garofolo, R. Golinski, P.L. Goossens, U. Hahn, B. Hallis, A. King, M. Mock, C. Montecucco, A. Ozin, F. Tonello, and S.H. Kaufmann. 2008. *Bacillus anthracis*: balancing innocent research with dual-use potential. Int. J. Med. Microbiol. 298: 345–364.

18. Khajehdehi, P. 2001. Toxemic shock, hematuria, hypokalemia, and hypoproteinemia in a case of cutaneous anthrax. Mt. Sinai J. Med. 68: 213–215.

19. Doğanay, M., M. Bakir, and I. Dökmetaş. 1987. A case of cutaneous anthrax with toxaemic shock. Br. J. Dermatol. 117: 659–662.

20. Swartz, M.N. 2001. Recognition and management of anthrax--an update. N. Engl. J. Med. 345: 1621–1626.

21. 1999. Bioterrorism alleging use of anthrax and interim guidelines for management--United States, 1998. MMWR Morb. Mortal. Wkly. Rep. 48: 69–74.

22. Beall, F.A., M.J. Taylor, and C.B. Thorne. 1962. Rapid lethal effect in rats of a third component found upon fractionating the toxin of *Bacillus anthracis*. J. Bacteriol. 83: 1274–1280.

23. Weiss, S., D. Kobiler, H. Levy, A. Pass, Y. Ophir, N. Rothschild, A. Tal, J. Schlomovitz, and Z. Altboum. 2011. Antibiotics cure anthrax in animal models. Antimicrob. Agents Chemother. 55: 1533–1542.

24. Pomerantsev, A.P., O.M. Pomerantseva, M. Moayeri, R. Fattah, C. Tallant, and S.H. Leppla. 2011. A *Bacillus anthracis* strain deleted for six proteases serves as an effective host for production of recombinant proteins. Protein Expr. Purif. 80: 80–90.

25. Drysdale, M., S. Heninger, J. Hutt, Y. Chen, C.R. Lyons, and T.M. Koehler. 2005. Capsule synthesis by *Bacillus anthracis* is required for dissemination in murine inhalation anthrax. EMBO J. 24: 221–227.

26. Friedman, T.C., V.M. Gordon, S.H. Leppla, K.R. Klimpel, N.P. Birch, and Y.P. Loh. 1995. *In vitro* processing of anthrax toxin protective antigen by recombinant PC1 (SPC3) and bovine intermediate lobe secretory vesicle membranes. Arch. Biochem. Biophys. 316: 5–13.

27. Bradley, K.A., J. Mogridge, M. Mourez, R.J. Collier, and J.A. Young. 2001. Identification of the cellular receptor for anthrax toxin. Nature. 414: 225–229.

28. Mogridge, J., K. Cunningham, D.B. Lacy, M. Mourez, and R.J. Collier. 2002. The lethal and edema factors of anthrax toxin bind only to oligomeric forms of the protective antigen. Proc. Natl. Acad. Sci. U.S.A. 99: 7045–7048.

29. Mogridge, J., K. Cunningham, and R.J. Collier. 2002. Stoichiometry of anthrax toxin complexes. Biochemistry. 41: 1079–1082.

30. Abrami, L., S. Liu, P. Cosson, S.H. Leppla, and F.G. van der Goot. 2003. Anthrax toxin triggers endocytosis of its receptor via a lipid raft-mediated clathrin-dependent process. J. Cell Biol. 160: 321–328.

31. Abrami, L., M. Lindsay, R.G. Parton, S.H. Leppla, and F.G. van der Goot. 2004. Membrane insertion of anthrax protective antigen and cytoplasmic delivery of lethal factor occur at different stages of the endocytic pathway. J. Cell Biol. 166: 645–651.

32. Abrami, L., N. Reig, and F.G. van der Goot. 2005. Anthrax toxin: the long and winding road that leads to the kill. Trends Microbiol. 13: 72–78.

33. Leppla, S.H. 1982. Anthrax toxin edema factor: a bacterial adenylate cyclase that increases cyclic AMP concentrations of eukaryotic cells. Proc. Natl. Acad. Sci. U.S.A. 79: 3162–3166.

34. Golden, H.B., L.E. Watson, H. Lal, S.K. Verma, D.M. Foster, S.R. Kuo, A. Sharma, A. Frankel, and D.E. Dostal. 2009. Anthrax toxin: pathologic effects on the cardiovascular system. Front. Biosci. 14: 2335–2357.

35. Duesbery, N.S., C.P. Webb, S.H. Leppla, V.M. Gordon, K.R. Klimpel, T.D. Copeland, N.G. Ahn, M.K. Oskarsson, K. Fukasawa, K.D. Paull, and G.F. Vande Woude. 1998. Proteolytic inactivation of MAP-kinase-kinase by anthrax lethal factor. Science. 280: 734–737.

36. Vitale, G., R. Pellizzari, C. Recchi, G. Napolitani, M. Mock, and C. Montecucco. 1998. Anthrax lethal factor cleaves the N-terminus of MAPKKs and induces tyrosine/threonine phosphorylation of MAPKs in cultured macrophages. Biochem. Biophys. Res. Commun. 248: 706–711.

37. Collier, R.J., and J.A.T. Young. 2003. Anthrax toxin. Annu. Rev. Cell Dev. Biol. 19: 45–70.

38. Kirby, J.E. 2004. Anthrax Lethal Toxin Induces Human Endothelial Cell Apoptosis. Infection and Immunity. 72: 430 –439.

39. Heffernan, B.J., B. Thomason, A. Herring-Palmer, and P. Hanna. 2007. *Bacillus anthracis* anthrolysin O and three phospholipases C are functionally redundant in a murine model of inhalation anthrax. FEMS Microbiol. Lett. 271: 98–105.

40. Chung, M.-C., T.G. Popova, S.C. Jorgensen, L. Dong, V. Chandhoke, C.L. Bailey, and S.G. Popov. 2008. Degradation of circulating von Willebrand factor and its regulator ADAMTS13 implicates secreted *Bacillus anthracis* metalloproteases in anthrax consumptive coagulopathy. J. Biol. Chem. 283: 9531–9542.

41. Chung, M.-C., S.C. Jorgensen, T.G. Popova, J.H. Tonry, C.L. Bailey, and S.G. Popov. 2009. Activation of plasminogen activator inhibitor implicates protease InhA in the acute-phase response to *Bacillus anthracis* infection. J. Med. Microbiol. 58: 737–744.

42. Chung, M.-C., S.C. Jorgensen, J.H. Tonry, F. Kashanchi, C. Bailey, and S.G. Popov. 2011. Secreted *Bacillus anthracis* proteases target the host fibrinolytic system. FEMS Immunol. Med. Microbiol. 62: 173–181.

43.   Mukherjee, D.V., J.H. Tonry, K.S. Kim, N. Ramarao, T.G. Popova, C. Bailey, S. Popov, and M.C. Chung. 2011. *Bacillus anthracis* protease InhA increases blood-brain barrier permeability and contributes to cerebral hemorrhages. PLoS ONE. 6: e17921.

44.   Shannon, J.G., C.L. Ross, T.M. Koehler, and R.F. Rest. 2003. Characterization of anthrolysin O, the *Bacillus anthracis* cholesterol-dependent cytolysin. Infect. Immun. 71: 3183–3189.

45.   Bishop, B.L., J.P. Lodolce, L.E. Kolodziej, D.L. Boone, and W.J. Tang. 2010. The role of anthrolysin O in gut epithelial barrier disruption during *Bacillus anthracis* infection. Biochem. Biophys. Res. Commun. 394: 254–259.

46.   Uchida, I., J.M. Hornung, C.B. Thorne, K.R. Klimpel, and S.H. Leppla. 1993. Cloning and characterization of a gene whose product is a trans-activator of anthrax toxin synthesis. J. Bacteriol. 175: 5329–5338.

47.   Koehler, T.M., Z. Dai, and M. Kaufman-Yarbray. 1994. Regulation of the *Bacillus anthracis* protective antigen gene: CO2 and a trans-acting element activate transcription from one of two promoters. J. Bacteriol. 176: 586–595.

48.   Fouet, A. 2010. AtxA, a *Bacillus anthracis* global virulence regulator. Research in Microbiology. 161: 735–742.

49.   Dai, Z., J.C. Sirard, M. Mock, and T.M. Koehler. 1995. The atxA gene product activates transcription of the anthrax toxin genes and is essential for virulence. Mol. Microbiol. 16: 1171–1181.

50.   Fouet, A., and M. Mock. 1996. Differential influence of the two *Bacillus anthracis* plasmids on regulation of virulence gene expression. Infect. Immun. 64: 4928–4932.

51.   Uchida, I., S. Makino, T. Sekizaki, and N. Terakado. 1997. Cross-talk to the genes for *Bacillus anthracis* capsule synthesis by atxA, the gene encoding the trans-activator of anthrax toxin synthesis. Mol. Microbiol. 23: 1229–1240.

52.   Guignot, J., M. Mock, and A. Fouet. 1997. AtxA activates the transcription of genes harbored by both *Bacillus anthracis* virulence plasmids. FEMS Microbiol. Lett. 147: 203–207.

53.   Sirard, J.C., C. Guidi-Rontani, A. Fouet, and M. Mock. 2000. Characterization of a plasmid region involved in *Bacillus anthracis* toxin production and pathogenesis. Int. J. Med. Microbiol. 290: 313–316.

54.   Mignot, T., M. Mock, and A. Fouet. 2003. A plasmid-encoded regulator couples the synthesis of toxins and surface structures in *Bacillus anthracis*. Mol. Microbiol. 47: 917–927.

55.   Hoffmaster, A.R., and T.M. Koehler. 1997. The anthrax toxin activator gene atxA is associated with CO2-enhanced non-toxin gene expression in *Bacillus anthracis*. Infect. Immun. 65: 3091–3099.

56.   Hoffmaster, A.R., and T.M. Koehler. 1999. Autogenous regulation of the *Bacillus anthracis* pag operon. J. Bacteriol. 181: 4485–4492.

57.   Bourgogne, A., M. Drysdale, S.G. Hilsenbeck, S.N. Peterson, and T.M. Koehler. 2003. Global effects of virulence gene regulators in a *Bacillus anthracis* strain with both virulence plasmids. Infect. Immun. 71: 2736–2743.

58.   Hadjifrangiskou, M., and T.M. Koehler. 2008. Intrinsic curvature associated with the coordinately regulated anthrax toxin gene promoters. Microbiology (Reading, Engl.). 154: 2501–2512.

59.   Tsvetanova, B., A.C. Wilson, C. Bongiorni, C. Chiang, J.A. Hoch, and M. Perego. 2007. Opposing effects of histidine phosphorylation regulate the AtxA virulence transcription factor in *Bacillus anthracis*. Mol. Microbiol. 63: 644–655.

60.   Koehler, T.M. 2009. *Bacillus anthracis* physiology and genetics. Molecular Aspects of Medicine. 30: 386–396.

61. Sonenshein, A.L. 2005. CodY, a global regulator of stationary phase and virulence in Gram-positive bacteria. Current Opinion in Microbiology. 8: 203–207.

62. van Schaik, W., A. Château, M.-A. Dillies, J.-Y. Coppée, A.L. Sonenshein, and A. Fouet. 2009. The global regulator CodY regulates toxin gene expression in *Bacillus anthracis* and is required for full virulence. Infect. Immun. 77: 4437–4445.

63. Bongiorni, C., T. Fukushima, A.C. Wilson, C. Chiang, M.C. Mansilla, J.A. Hoch, and M. Perego. 2008. Dual promoters control expression of the *Bacillus anthracis* virulence factor AtxA. J. Bacteriol. 190: 6483–6492.

64. Dai, Z., and T.M. Koehler. 1997. Regulation of anthrax toxin activator gene (atxA) expression in *Bacillus anthracis*: temperature, not CO2/bicarbonate, affects AtxA synthesis. Infect. Immun. 65: 2576–2582.

65. Wilson, A.C., J.A. Hoch, and M. Perego. 2009. Two small c-type cytochromes affect virulence gene expression in *Bacillus anthracis*. Mol. Microbiol. 72: 109–123.

66. Chiang, C., C. Bongiorni, and M. Perego. 2011. Glucose-dependent activation of *Bacillus anthracis* toxin gene expression and virulence requires the carbon catabolite protein CcpA. J. Bacteriol. 193: 52–62.

67. Saile, E., and T.M. Koehler. 2002. Control of anthrax toxin gene expression by the transition state regulator *abrB*. J. Bacteriol. 184: 370–380.

68. Strauch, M.A., P. Ballar, A.J. Rowshan, and K.L. Zoller. 2005. The DNA-binding specificity of the *Bacillus anthracis* AbrB protein. Microbiology (Reading, Engl.). 151: 1751–1759.

69. Bartkus, J.M., and S.H. Leppla. 1989. Transcriptional regulation of the protective antigen gene of *Bacillus anthracis*. Infect. Immun. 57: 2295–2300.

70. Cataldi, A., A. Fouet, and M. Mock. 1992. Regulation of pag gene expression in *Bacillus anthracis*: use of a pag-lacZ transcriptional fusion. FEMS Microbiol. Lett. 77: 89–93.

71. Sirard, J.C., M. Mock, and A. Fouet. 1994. The three *Bacillus anthracis* toxin genes are coordinately regulated by bicarbonate and temperature. J. Bacteriol. 176: 5188–5192.

72. Chitlaru, T., O. Gat, Y. Gozlan, N. Ariel, and A. Shafferman. 2006. Differential proteomic analysis of the *Bacillus anthracis* secretome: distinct plasmid and chromosome CO_2-dependent cross talk mechanisms modulate extracellular proteolytic activities. J. Bacteriol. 188: 3551–3571.

73. Deutscher, J., C. Francke, and P.W. Postma. 2006. How phosphotransferase system-related protein phosphorylation regulates carbohydrate metabolism in bacteria. Microbiol. Mol. Biol. Rev. 70: 939–1031.

74. Fujita, Y. 2009. Carbon catabolite control of the metabolic network in *Bacillus subtilis*. Biosci. Biotechnol. Biochem. 73: 245–259.

75. Deutscher, J., E. Küster, U. Bergstedt, V. Charrier, and W. Hillen. 1995. Protein kinase-dependent HPr/CcpA interaction links glycolytic activity to carbon catabolite repression in gram-positive bacteria. Mol. Microbiol. 15: 1049–1053.

76. Almengor, A.C., T.L. Kinkel, S.J. Day, and K.S. McIver. 2007. The catabolite control protein CcpA binds to Pmga and influences expression of the virulence regulator Mga in the Group A streptococcus. J. Bacteriol. 189: 8405–8416.

77. Schnetz, K., J. Stülke, S. Gertz, S. Krüger, M. Krieg, M. Hecker, and B. Rak. 1996. LicT, a *Bacillus subtilis* transcriptional antiterminator protein of the BglG family. J. Bacteriol. 178: 1971–1979.

78. Tortosa, P., N. Declerck, H. Dutartre, C. Lindner, J. Deutscher, and D. Le Coq. 2001. Sites of positive and negative regulation in the *Bacillus subtilis* antiterminators LicT and SacY. Mol. Microbiol. 41: 1381–1393.

79. Graille, M., C.-Z. Zhou, V. Receveur-Bréchot, B. Collinet, N. Declerck, and H. van Tilbeurgh. 2005. Activation of the LicT transcriptional antiterminator involves a domain

swing/lock mechanism provoking massive structural changes. J. Biol. Chem. 280: 14780–14789.

80. Ben-Zeev, E., L. Fux, O. Amster-Choder, and M. Eisenstein. 2005. Experimental and computational characterization of the dimerization of the PTS-regulation domains of BglG from *Escherichia coli*. J. Mol. Biol. 347: 693–706.

81. Tobisch, S., J. Stülke, and M. Hecker. 1999. Regulation of the *lic* operon of *Bacillus subtilis* and characterization of potential phosphorylation sites of the LicR regulator protein by site-directed mutagenesis. J. Bacteriol. 181: 4995–5003.

82. Joyet, P., M. Derkaoui, S. Poncet, and J. Deutscher. 2010. Control of *Bacillus subtilis mtl* operon expression by complex phosphorylation-dependent regulation of the transcriptional activator MtlR. Molecular Microbiology. 76: 1279–1294.

83. Débarbouillé, M., I. Martin-Verstraete, A. Klier, and G. Rapoport. 1991. The transcriptional regulator LevR of *Bacillus subtilis* has domains homologous to both sigma 54- and phosphotransferase system-dependent regulators. Proc. Natl. Acad. Sci. U.S.A. 88: 2212–2216.

84. Henstra, S.A., M. Tuinhof, R.H. Duurkens, and G.T. Robillard. 1999. The *Bacillus stearothermophilus* mannitol regulator, MtlR, of the phosphotransferase system. A DNA-binding protein, regulated by HPr and EIICB^{mtl}-dependent phosphorylation. J. Biol. Chem. 274: 4754–4763.

85. Henstra, S.A., R.H. Duurkens, and G.T. Robillard. 2000. Multiple phosphorylation events regulate the activity of the mannitol transcriptional regulator MtlR of the *Bacillus stearothermophilus* phosphoenolpyruvate-dependent mannitol phosphotransferase system. J. Biol. Chem. 275: 7037–7044.

86. Hondorp, E.R., and K.S. McIver. 2007. The Mga virulence regulon: infection where the grass is greener. Mol. Microbiol. 66: 1056–1065.

87. Bourgogne, A., K.V. Singh, K.A. Fox, K.J. Pflughoeft, B.E. Murray, and D.A. Garsin. 2007. EbpR Is Important for Biofilm Formation by Activating Expression of the Endocarditis and Biofilm-Associated Pilus Operon (*ebpABC*) of *Enterococcus faecalis* OG1RF. Journal of Bacteriology. 189: 6490 –6493.

88. Osipiuk, J., R. Wu, R. Jedrzejczak, S. Moy, and A. Joachimiak. 2011. Putative Mga family transcriptional regulator from *Enterococcus faecalis*. To be Published. : -.

89. Ribardo, D.A., and K.S. McIver. 2006. Defining the Mga regulon: Comparative transcriptome analysis reveals both direct and indirect regulation by Mga in the group A streptococcus. Mol. Microbiol. 62: 491–508.

90. McIver, K.S., A.S. Heath, B.D. Green, and J.R. Scott. 1995. Specific binding of the activator Mga to promoter sequences of the *emm* and *scpA* genes in the group A streptococcus. J. Bacteriol. 177: 6619–6624.

91. McIver, K.S., and R.L. Myles. 2002. Two DNA-binding domains of Mga are required for virulence gene activation in the group A streptococcus. Mol. Microbiol. 43: 1591–1601.

92. Vahling, C.M., and K.S. McIver. 2006. Domains required for transcriptional activation show conservation in the *mga* family of virulence gene regulators. J. Bacteriol. 188: 863–873.

93. Vietri, N.J., R. Marrero, T.A. Hoover, and S.L. Welkos. 1995. Identification and characterization of a trans-activator involved in the regulation of encapsulation by *Bacillus anthracis*. Gene. 152: 1–9.

94. Drysdale, M., A. Bourgogne, S.G. Hilsenbeck, and T.M. Koehler. 2004. *atxA* controls *Bacillus anthracis* capsule synthesis via *acpA* and a newly discovered regulator, *acpB*. J. Bacteriol. 186: 307–315.

95. Drysdale, M., A. Bourgogne, and T.M. Koehler. 2005. Transcriptional analysis of the *Bacillus anthracis* capsule regulators. J. Bacteriol. 187: 5108–5114.

96. Bourgogne, A., L.C. Thomson, and B.E. Murray. 2010. Bicarbonate enhances expression of the endocarditis and biofilm associated pilus locus, *ebpR-ebpABC*, in *Enterococcus faecalis*. BMC Microbiol. 10: 17.

97. Bertani, G. 1951. Studies on Lysogenesis I. J Bacteriol. 62: 293–300.

98. Haden, R.L. 1923. Elective Localization in the Eye of Bacteria from Infected Teeth. Arch Intern Med. 32: 828–849.

99. Thorne, C.B., and F.C. Belton. 1957. An agar-diffusion method for titrating *Bacillus anthracis* immunizing antigen and its application to a study of antigen production. J. Gen. Microbiol. 17: 505–516.

100. Hadjifrangiskou, M., Y. Chen, and T.M. Koehler. 2007. The alternative sigma factor *sigmaH* is required for toxin gene expression by *Bacillus anthracis*. J. Bacteriol. 189: 1874–1883.

101. Britton, R.A., P. Eichenberger, J.E. Gonzalez-Pastor, P. Fawcett, R. Monson, R. Losick, and A.D. Grossman. 2002. Genome-Wide Analysis of the Stationary-Phase Sigma Factor (Sigma-H) Regulon of *Bacillus subtilis*. J. Bacteriol. 184: 4881–4890.

102. Hammerstrom, T.G., J.H. Roh, E.P. Nikonowicz, and T.M. Koehler. 2011. *Bacillus anthracis* virulence regulator AtxA: oligomeric state, function and CO_2-signalling. Mol. Microbiol. 82: 634–647.

103. Welkos, S., S. Little, A. Friedlander, D. Fritz, and P. Fellows. 2001. The role of antibodies to *Bacillus anthracis* and anthrax toxin components in inhibiting the early stages of infection by anthrax spores. Microbiology. 147: 1677–1685.

104. Agaisse, H., and D. Lereclus. 1994. Expression in *Bacillus subtilis* of the *Bacillus thuringiensis cryIIIA* toxin gene is not dependent on a sporulation-specific sigma factor and is increased in a *spo0A* mutant. Journal of Bacteriology. 176: 4734–4741.

105. Pflughoeft, K.J., P. Sumby, and T.M. Koehler. 2011. *Bacillus anthracis sin* Locus and Regulation of Secreted Proteases. J. Bacteriol. 193: 631–639.

106. Dale, J.L., M.J. Raynor, P. Dwivedi, and T.M. Koehler. 2012. *cis*-acting control regions of the *Bacillus anthracis* virulence gene regulator *atxA*. In preparation. .

107. Marrero, R., and S.L. Welkos. 1995. The transformation frequency of plasmids into *Bacillus anthracis* is affected by adenine methylation. Gene. 152: 75–78.

108. Chaffin, D.O., L.M. Mentele, and C.E. Rubens. 2005. Sialylation of group B streptococcal capsular polysaccharide is mediated by *cpsK* and is required for optimal capsule polymerization and expression. J. Bacteriol. 187: 4615–4626.

109. Arantes, O., and D. Lereclus. 1991. Construction of cloning vectors for *Bacillus thuringiensis*. Gene. 108: 115–119.

110. Horton, R.M., H.D. Hunt, S.N. Ho, J.K. Pullen, and L.R. Pease. 1989. Engineering hybrid genes without the use of restriction enzymes: gene splicing by overlap extension. Gene. 77: 61–68.

111. Cormack, B.P., R.H. Valdivia, and S. Falkow. 1996. FACS-optimized mutants of the green fluorescent protein (GFP). Gene. 173: 33–38.

112. Dunn, A.K., and J. Handelsman. 1999. A vector for promoter trapping in *Bacillus cereus*. Gene. 226: 297–305.

113. O'Gorman, R.B., M. Dunaway, and K.S. Matthews. 1980. DNA binding characteristics of lactose repressor and the trypsin-resistant core repressor. Journal of Biological Chemistry. 255: 10100 –10106.

114. Eswaramoorthy, P., T. Guo, and M. Fujita. 2009. *In vivo* domain-based functional analysis of the major sporulation sensor kinase, KinA, in *Bacillus subtilis*. J. Bacteriol. 191: 5358–5368.

115. Rasband, W.S. 1997. ImageJ. Bethesda, Maryland, USA: U. S. National Institutes of Health.

116. Cortay, J.C., D. Nègre, M. Scarabel, T.M. Ramseier, N.B. Vartak, J. Reizer, M.H. Saier, and A.J. Cozzone. 1994. *In vitro* asymmetric binding of the pleiotropic regulatory

protein, FruR, to the ace operator controlling glyoxylate shunt enzyme synthesis. J. Biol. Chem. 269: 14885–14891.

117. Galinier, A., J. Haiech, M.C. Kilhoffer, M. Jaquinod, J. Stülke, J. Deutscher, and I. Martin-Verstraete. 1997. The *Bacillus subtilis crh* gene encodes a HPr-like protein involved in carbon catabolite repression. Proc. Natl. Acad. Sci. U.S.A. 94: 8439–8444.

118. Studier, F.W. 2005. Protein production by auto-induction in high-density shaking cultures. Protein Expression and Purification. 41: 207–234.

119. Mattoo, R.L., and E.B. Waygood. 1983. An enzymatic method for [^{32}P]phosphoenolpyruvate synthesis. Analytical Biochemistry. 128: 245–249.

120. Santos, C.L., F. Tavares, J. Thioulouse, and P. Normand. 2009. A phylogenomic analysis of bacterial helix–turn–helix transcription factors. FEMS Microbiology Reviews. 33: 411–429.

121. Kohn, W.D., C.T. Mant, and R.S. Hodges. 1997. α-Helical Protein Assembly Motifs. Journal of Biological Chemistry. 272: 2583 –2586.

122. Brennan, R.G., and B.W. Matthews. 1989. Structural basis of DNA-protein recognition. Trends in Biochemical Sciences. 14: 286–290.

123. Gajiwala, K.S., and S.K. Burley. 2000. Winged helix proteins. Current Opinion in Structural Biology. 10: 110–116.

124. Clark, K.L., E.D. Halay, E. Lai, and S.K. Burley. 1993. Co-crystal structure of the HNF-3/fork head DNA-recognition motif resembles histone H5. Nature. 364: 412–420.

125. Finnin, M.S., M.P. Cicero, C. Davies, S.J. Porter, S.W. White, and K.N. Kreuzer. 1997. The activation domain of the MotA transcription factor from bacteriophage T4. EMBO J. 16: 1992–2003.

126. Huffman, J.L., and R.G. Brennan. 2002. Prokaryotic transcription regulators: more than just the helix-turn-helix motif. Curr. Opin. Struct. Biol. 12: 98–106.

127. Sullivan, D.M., B.G. Bobay, D.J. Kojetin, R.J. Thompson, M. Rance, M.A. Strauch, and J. Cavanagh. 2008. Insights into the Nature of DNA Binding of AbrB-like Transcription Factors. Structure. 16: 1702–1713.

128. Declerck, N., H. Dutartre, V. Receveur, V. Dubois, C. Royer, S. Aymerich, and H. van Tilbeurgh. 2001. Dimer stabilization upon activation of the transcriptional antiterminator LicT. J. Mol. Biol. 314: 671–681.

129. Declerck, N., F. Vincent, F. Hoh, S. Aymerich, and H. van Tilbeurgh. 1999. RNA recognition by transcriptional antiterminators of the BglG/SacY family: functional and structural comparison of the CAT domain from SacY and LicT. J. Mol. Biol. 294: 389–402.

130. Miller, J.H. 1972. Experiments in molecular genetics. New York, New York: Cold Spring Harbor Laboratory. pp. 352–355.

131. Fontana, A., P.P. de Laureto, B. Spolaore, E. Frare, P. Picotti, and M. Zambonin. 2004. Probing protein structure by limited proteolysis. Acta Biochim. Pol. 51: 299–321.

132. Deleeuw, L., A.V. Tchernatynskaia, and A.N. Lane. 2008. Thermodynamics and Specificity of the Mbp1−DNA Interaction†. Biochemistry. 47: 6378–6385.

133. Friedmann, D.R., and R.A. Kovall. 2010. Thermodynamic and structural insights into CSL-DNA complexes. Protein Science. 19: 34–46.

134. Fux, L., A. Nussbaum-Shochat, and O. Amster-Choder. 2003. Interactions between the PTS regulation domains of the BglG transcriptional antiterminator from *Escherichia coli*. J. Biol. Chem. 278: 46203–46209.

135. van Tilbeurgh, H., D. Le Coq, and N. Declerck. 2001. Crystal structure of an activated form of the PTS regulation domain from the LicT transcriptional antiterminator. EMBO J. 20: 3789–3799.

136. Marchler-Bauer, A., J.B. Anderson, M.K. Derbyshire, C. DeWeese-Scott, N.R. Gonzales, M. Gwadz, L. Hao, S. He, D.I. Hurwitz, J.D. Jackson, Z. Ke, D. Krylov, C.J.

Lanczycki, C.A. Liebert, C. Liu, F. Lu, S. Lu, G.H. Marchler, M. Mullokandov, J.S. Song, N. Thanki, R.A. Yamashita, J.J. Yin, D. Zhang, and S.H. Bryant. 2007. CDD: a conserved domain database for interactive domain family analysis. Nucleic Acids Res. 35: D237–240.

137. Kelley, L.A., and M.J.E. Sternberg. 2009. Protein structure prediction on the Web: a case study using the Phyre server. Nat Protoc. 4: 363–371.

138. Evans, B., P.A. Tishmack, C. Pokalsky, M. Zhang, and R.L. Van Etten. 1996. Site-directed mutagenesis, kinetic, and spectroscopic studies of the P-loop residues in a low molecular weight protein tyrosine phosphatase. Biochemistry. 35: 13609–13617.

139. Nobelmann, B., and J.W. Lengeler. 1996. Molecular analysis of the *gat* genes from *Escherichia coli* and of their roles in galactitol transport and metabolism. J. Bacteriol. 178: 6790–6795.

140. Volpon, L., C.R. Young, A. Matte, and K. Gehring. 2006. NMR structure of the enzyme GatB of the galactitol-specific phosphoenolpyruvate-dependent phosphotransferase system and its interaction with GatA. Protein Sci. 15: 2435–2441.

141. Sun, T., and J. Altenbuchner. 2010. Characterization of a Mannose Utilization System in *Bacillus subtilis*. J. Bacteriol. 192: 2128–2139.

142. Zeng, L., and R.A. Burne. 2009. Transcriptional Regulation of the Cellobiose Operon of *Streptococcus mutans*. J Bacteriol. 191: 2153–2162.

143. Watanabe, S., M. Hamano, H. Kakeshita, K. Bunai, S. Tojo, H. Yamaguchi, Y. Fujita, S.L. Wong, and K. Yamane. 2003. Mannitol-1-Phosphate Dehydrogenase (MtlD) Is Required for Mannitol and Glucitol Assimilation in *Bacillus subtilis*: Possible Cooperation of *mtl* and *gut* Operons. J. Bacteriol. 185: 4816–4824.

144. Yang, J., E. Hart, M. Tauschek, G.D. Price, E.L. Hartland, R.A. Strugnell, and R.M. Robins-Browne. 2008. Bicarbonate-mediated transcriptional activation of divergent

operons by the virulence regulatory protein, RegA, from *Citrobacter rodentium*. Mol. Microbiol. 68: 314–327.

145. Yang, J., C. Dogovski, D. Hocking, M. Tauschek, M. Perugini, and R.M. Robins-Browne. 2009. Bicarbonate-mediated stimulation of RegA, the global virulence regulator from *Citrobacter rodentium.* J. Mol. Biol. 394: 591–599.

146. Badger, M.R., and G.D. Price. 2003. CO_2 concentrating mechanisms in cyanobacteria: molecular components, their diversity and evolution. Journal of Experimental Botany. 54: 609 –622.

147. Jiang, M., M. Chen, Z.-F. Guo, and Z. Guo. 2010. A bicarbonate cofactor modulates 1,4-dihydroxy-2-naphthoyl-coenzyme a synthase in menaquinone biosynthesis of *Escherichia coli*. J. Biol. Chem. 285: 30159–30169.

148. Poncet, S., E. Milohanic, A. Mazé, J. Nait Abdallah, F. Aké, M. Larribe, A.E. Deghmane, M.K. Taha, M. Dozot, X. De Bolle, J.J. Letesson, and J. Deutscher. 2009. Correlations between carbon metabolism and virulence in bacteria. Contrib Microbiol. 16: 88–102.

149. Singh, K.D., M.H. Schmalisch, J. Stülke, and B. Görke. 2008. Carbon Catabolite Repression in *Bacillus subtilis*: Quantitative Analysis of Repression Exerted by Different Carbon Sources. Journal of Bacteriology. 190: 7275 –7284.

150. Deutscher, J., B. Bauer, and H. Sauerwald. 1993. Regulation of glycerol metabolism in *Enterococcus faecalis* by phosphoenolpyruvate-dependent phosphorylation of glycerol kinase catalyzed by enzyme I and HPr of the phosphotransferase system. J. Bacteriol. 175: 3730–3733.

151. Charrier, V., E. Buckley, D. Parsonage, A. Galinier, E. Darbon, M. Jaquinod, E. Forest, J. Deutscher, and A. Claiborne. 1997. Cloning and Sequencing of two Enterococcal *glpK* Genes and Regulation of the Encoded Glycerol Kinases by Phosphoenolpyruvate-dependent, Phosphotransferase System-catalyzed

Phosphorylation of a Single Histidyl Residue. Journal of Biological Chemistry. 272: 14166 –14174.

152. Krüger, S., and M. Hecker. 1995. Regulation of the putative *bglPH* operon for aryl-beta-glucoside utilization in *Bacillus subtilis*. J. Bacteriol. 177: 5590–5597.

153. Lindner, C., A. Galinier, M. Hecker, and J. Deutscher. 1999. Regulation of the activity of the *Bacillus subtilis* antiterminator LicT by multiple PEP-dependent, enzyme I- and HPr-catalysed phosphorylation. Mol. Microbiol. 31: 995–1006.

154. Aung-Hilbrich, L.M., G. Seidel, A. Wagner, and W. Hillen. 2002. Quantification of the influence of HPrSer46P on CcpA-cre interaction. J. Mol. Biol. 319: 77–85.

155. Moreno, M.S., B.L. Schneider, R.R. Maile, W. Weyler, and M.H. Saier Jr. 2001. Catabolite repression mediated by the CcpA protein in *Bacillus subtilis*: novel modes of regulation revealed by whole-genome analyses. Mol. Microbiol. 39: 1366–1381.

156. Deutscher, J., R. Herro, A. Bourand, I. Mijakovic, and S. Poncet. 2005. P-Ser-HPr--a link between carbon metabolism and the virulence of some pathogenic bacteria. Biochim. Biophys. Acta. 1754: 118–125.

157. Stülke, J. 2007. Regulation of virulence in *Bacillus anthracis*: the phosphotransferase system transmits the signals. Mol. Microbiol. 63: 626–628.

158. Arnaud, M., M. Débarbouillé, G. Rapoport, M.H. Saier, and J. Reizer. 1996. *In Vitro* Reconstitution of Transcriptional Antitermination by the SacT and SacY Proteins of *Bacillus subtilis*. Journal of Biological Chemistry. 271: 18966 –18972.

159. Schmalisch, M.H., S. Bachem, and J. Stülke. 2003. Control of the *Bacillus subtilis* Antiterminator Protein GlcT by Phosphorylation. Journal of Biological Chemistry. 278: 51108 –51115.

160. Martin-Verstraete, I., V. Charrier, J. Stülke, A. Galinier, B. Erni, G. Rapoport, and J. Deutscher. 1998. Antagonistic effects of dual PTS-catalysed phosphorylation on the *Bacillus subtilis* transcriptional activator LevR. Mol. Microbiol. 28: 293–303.

161. Mazé, A., G. Boël, S. Poncet, I. Mijakovic, Y. Le Breton, A. Benachour, V. Monedero, J. Deutscher, and A. Hartke. 2004. The *Lactobacillus casei ptsH*I47T mutation causes overexpression of a LevR-regulated but RpoN-independent operon encoding a mannose class phosphotransferase system. J. Bacteriol. 186: 4543–4555.

162. Wang, G., M. Sondej, D.S. Garrett, A. Peterkofsky, and G.M. Clore. 2000. A Common Interface on Histidine-containing Phosphocarrier Protein for Interaction with Its Partner Proteins. Journal of Biological Chemistry. 275: 16401 –16403.

163. Chen, Y., J. Reizer, M.H. Saier Jr, W.J. Fairbrother, and P.E. Wright. 1993. Mapping of the binding interfaces of the proteins of the bacterial phosphotransferase system, HPr and IIA^{glc}. Biochemistry. 32: 32–37.

164. Darbon, E., A. Galinier, D. Le Coq, and J. Deutscher. 2001. Phosphotransfer functions mutated *Bacillus subtilis* HPr-like protein Crh carrying a histidine in the active site. J. Mol. Microbiol. Biotechnol. 3: 439–444.

165. Martin-Verstraete, I., A. Galinier, E. Darbon, Y. Quentin, M.-C. Kilhoffer, V. Charrier, J. Haiech, G. Rapoport, and J. Deutscher. 1999. The Q15H mutation enables Crh, a Bacillus subtilis HPr-like protein, to carry out some regulatory HPr functions, but does not make it an effective phosphocarrier for sugar transport. Microbiology. 145: 3195 – 3204.

166. Jault, J.M., S. Fieulaine, S. Nessler, P. Gonzalo, A. Di Pietro, J. Deutscher, and A. Galinier. 2000. The HPr kinase from *Bacillus subtilis* is a homo-oligomeric enzyme which exhibits strong positive cooperativity for nucleotide and fructose 1,6-bisphosphate binding. J. Biol. Chem. 275: 1773–1780.

167. Reizer, J., C. Hoischen, F. Titgemeyer, C. Rivolta, R. Rabus, J. Stülke, D. Karamata, M.H. Saier Jr, and W. Hillen. 1998. A novel protein kinase that controls carbon catabolite repression in bacteria. Mol. Microbiol. 27: 1157–1169.

168. Deutscher, J., J. Reizer, C. Fischer, A. Galinier, M.H. Saier Jr, and M. Steinmetz. 1994. Loss of protein kinase-catalyzed phosphorylation of HPr, a phosphocarrier protein of the phosphotransferase system, by mutation of the *ptsH* gene confers catabolite repression resistance to several catabolic genes of *Bacillus subtilis*. J. Bacteriol. 176: 3336–3344.

169. Gorke, B., and B. Rak. 1999. Catabolite control of *Escherichia coli* regulatory protein BglG activity by antagonistically acting phosphorylations. EMBO J. 18: 3370–3379.

170. Tobisch, S., P. Glaser, S. Krüger, and M. Hecker. 1997. Identification and characterization of a new beta-glucoside utilization system in *Bacillus subtilis*. J. Bacteriol. 179: 496–506.

171. Stülke, J., I. Martin-Verstraete, M. Zagorec, M. Rose, A. Klier, and G. Rapoport. 1997. Induction of the *Bacillus subtilis ptsGHI* operon by glucose is controlled by a novel antiterminator, GlcT. Molecular Microbiology. 25: 65–78.

172. Martin-Verstraete, I., J. Stülke, A. Klier, and G. Rapoport. 1995. Two different mechanisms mediate catabolite repression of the *Bacillus subtilis* levanase operon. J. Bacteriol. 177: 6919–6927.

173. Wittekind, M., J. Reizer, J. Deutscher, M.H. Saier, and R.E. Klevit. 1989. Common structural changes accompany the functional inactivation of HPr by seryl phosphorylation or by serine to aspartate substitution. Biochemistry. 28: 9908–9912.

174. Casabon, I., M. Couture, K. Vaillancourt, and C. Vadeboncoeur. 2009. Kinetic Studies of HPr, HPr(H15D), HPr(H15E), and HPr(His~P) Phosphorylation by the *Streptococcus salivarius* HPr(Ser) Kinase/Phosphorylase. Biochemistry. 48: 10765–10774.

175. Bertin, M., A. Château, and A. Fouet. 2010. Full expression of *Bacillus anthracis* toxin gene in the presence of bicarbonate requires a 2.7-kb-long *atxA* mRNA that contains a terminator structure. Res. Microbiol. 161: 249–259.

176. Dale, J.L., M.C. Ty, M. Hadjifrangiskou, and T.M. Koehler. 2012. Altered *atxA* expression and its impact on *Bacillus anthracis* virulence gene expression and development. In preparation. .

177. Eisenreich, W., T. Dandekar, J. Heesemann, and W. Goebel. 2010. Carbon metabolism of intracellular bacterial pathogens and possible links to virulence. Nat. Rev. Microbiol. 8: 401–412.

178. Sherwood, L. 2004. Human Physiology: From Cells to Systems. Fifth. Thomson Brooks/Cole.

179. Valerio, A., G. D'Antona, and E. Nisoli. 2011. Branched-chain amino acids, mitochondrial biogenesis, and healthspan: an evolutionary perspective. Aging (Albany NY). 3: 464–478.

180. Hondorp, E.R., S.C. Hou, A.D. Hempstead, L.L. Hause, D.M. Beckett, and K.S. McIver. 2012. Characterization of the Group A Streptococcus Mga virulence regulator reveals a role for the C-terminal region in oligomerization and transcriptional activation. Molecular Microbiology. 83: 953–967.

181. Singh, V., M.K. Ekka, and S. Kumaran. 2012. Second Monomer Binding Is the Rate-Limiting Step in the Formation of the Dimeric PhoP–DNA Complex. Biochemistry. 51: 1346–1356.

182. Georges, A.B., B.A. Benayoun, S. Caburet, and R.A. Veitia. 2010. Generic Binding Sites, Generic DNA-Binding Domains: Where Does Specific Promoter Recognition Come From? FASEB J. 24: 346–356.

183. Krissinel, E., and K. Henrick. 2007. Inference of Macromolecular Assemblies from Crystalline State. Journal of Molecular Biology. 372: 774–797.

184. Guex, N., and M.C. Peitsch. 1997. SWISS-MODEL and the Swiss-PdbViewer: an environment for comparative protein modeling. Electrophoresis. 18: 2714–2723.

185. Wass, M.N., L.A. Kelley, and M.J.E. Sternberg. 2010. 3DLigandSite: predicting ligand-binding sites using similar structures. Nucleic Acids Res. 38: W469–473.

Vita

Troy G. Hammerstrom was born September 10, 1982 in Austin, Texas to Douglas L. Hammerstrom and Lynn D. Hammerstrom. He graduated from Samuel Clemens High School (Schertz, Texas) in 2001 before attending Texas A&M University (College Station, Texas). In 2005, he received the Bachelors of Science degree with a major in microbiology and a minor in chemistry. Starting the fall of 2005, he attended the University of Texas Health Science Center at Houston Graduate School of Biomedical Sciences.

Permanent address:

4501 Horseshoe Cove

Schertz, Texas 78154